A Comparison between Stall Prediction Models for Axial Flow Compressors

by

Andrew Gill

Thesis presented in partial fulfilment of the requirements for the degree of Master of Science in Mechanical Engineering at Stellenbosch University

Department of Mechanical Engineering,
University of Stellenbosch,
Private Bag X1, 7602 Matieland, South Africa.

Supervisors:

Prof. T.W. Von Backström Prof. G.D. Thiart

April 2006

Declaration

I, the undersigned, hereby declare that the work contained in this thesis is my own original work and that I have not previously in its entirety or in part submitted it at any university for a degree.

Signature: .....

A. Gill

Date: .....

Abstract

The Stellenbosch University Compressor Code (SUCC) has been developed for the purpose of predicting the performance of axial flow compressors by means of axisymmetric inviscid throughflow methods with boundary layer blockage and empirical blade row loss models. This thesis describes the process of the implementation and verification of a number of stall prediction criteria in the SUCC. In addition, it was considered desirable to determine how certain factors influence the accuracy of the stall prediction criteria, namely the nature of the computational grid, the choice of throughflow method used, and the use of a boundary layer blockage model and a radial mixing model. The stall prediction criteria implemented were the diffusion factor limit criterion, de Haller's criterion, Aungier's blade row criterion, Aungier's boundary layer separation criterion, Dunham's, Aungier's and the static-to-static stability criteria. The compressors used as test cases were the Rofanco 3-stage low speed compressor, the NACA 10-stage subsonic compressor, and the NACA 5-stage and 8-stage transonic compressors. Accurate boundary layer blockage modelling was found to be of great importance in the prediction of the onset of stall, and that the matrix throughflow Method provided slightly better accuracy than the streamline curvature method as implemented in the SUCC by the author. The ideal computational grid was found to have many streamlines and a small number of quasi-orthogonals which do not occur inside blade rows. Radial mixing modelling improved the stability of both the matrix throughflow and streamline curvature methods without significantly affecting the accuracy of the stall prediction criteria. De Haller's criterion was over-conservative in estimating the stall line for transonic conditions, but more useful in subsonic conditions. Aungier's blade row criterion provided accurate results on all but the Rofanco compressor. The diffusion factor criterion provided over-optimistic predictions on all machines, but was less inaccurate than de Haller's criterion on the NACA 5-stage transsonic machine near design conditions. The stability methods performed uniformly and equally badly, supporting the claims of other researchers that they are of limited usefulness with throughflow simulations. Aungier's boundary layer separation method failed to predict stall entirely, although this could reflect a shortcoming of the boundary layer blockage model.

Opsomming

Die Stellenbosch University Compressor Code (SUCC) is ontwikkel om die prestasie van aksiaalvloei kompressors te voorspel met behulp van aksisimmetriese nie-viskeuse deurvloeimetodes met grenslaagblokkasie en empiriese modelle vir die verliese binne lemrye. Hierdie tesis beskryf die proses waarmee sekere staakvoorspellingsmetodes in die SUCC geïmplementeer en geverifieer is. Dit was ook nodig om die effek van sekere faktore, naamlik die vorm van die berekeningsrooster, die keuse van deurvloeimetode en die gebruik van 'n grenslaagblokkasiemodel en radiale vloeivermengingsmodel op die akuraatheid van die staakvoorspellingsmetodes te bepaal. Die staakvoorspellingsmetodes wat geïmplementeer is, is die diffusie faktor beperking metode, de Haller se metode, Aungier se lemrymetode, Aungier se grenslaagmetode en die Dunham, Aungier en die statiese-tot-statiese stabiliteitsmetodes. Die kompressors wat gebruik is om die metodes te toets is die Rofanco 3-stadium lae-spoed kompressor, die NACA 10-stadium subsoniese kompressor en die NACA 5- en 8-stadium transsoniese kompressors. Daar is vasgestel dat akkurate grenslaagblokkasie modelle van groot belang was om 'n akkurate aanduiding van die begin van staking te voorspel, en dat, vir die SUCC, die Matriks Deurvloei Metode oor die algemeen 'n bietjie meer akkuraat as die Stroomlyn Kromming Metode is. Daar is ook vasgestel dat die beste berekeningsrooster een is wat baie stroomlyne, en die kleinste moontlike getal quasi-ortogonale het, wat nie binne lemrye geplaas mag word nie. Die numeriese stabiliteit van beide die Matriks Deurvloei en die Stroomlyn Kromming Metode verbeter deur gebruik te maak van radiale vloeivermengingsmodelle, sonder om die akkuraatheid van voorspellings te benadeel. De Haller se metode was oorkonserwatief waar dit gebruik is om die staak-lyn vir transsoniese vloei toestande, maar meer nuttig in die subsoniese vloei gebied. Aungier se lemrymetode het akkurate resultate gelewer vir alle kompressors getoets, behalwe die Rofanco. Die diffusie faktor metode was oor die algemeen minder akuraat as Aungier se metode, maar meer akkuraat as de Haller se metode vir transsoniese toestande. Die stabiliteitsmetodes het almal ewe swak gevaar. Dit stem ooreen met die bevindings van vorige navorsing, wat bewys het dat hierdie metodes nie toepaslik is vir simulasies wat deurvloeimetodes gebruik nie. Aungier se grenslaagmetode het ook baie swak gevaar. Waarskynlik is dit as gevolg van tekortkomings in die grenslaagblokkasiemodel.

Acknowledgements

I would like to thank my two supervisors, Professor T.W. von Backström and Professor G.D. Thiart for their constant guidance, advice and support, and the innumerable ways in which they have helped me to complete this project. I would also like to thank Thomas Roos for his advice and encouragement and his assistance in obtaining geometric data. I am also indebted to Adriaan Steenkamp, who also assisted me greatly in obtaining geometric data. I would also like to thank my family and friends for their emotional support and prayers. Finally, I am most grateful to Armscor, who provided me with financial support.

Contents

List of Figures

List of Tables

Nomenclature

a	blade profile dependent parameter for calculating D_{eq}
a_s	Speed of sound
c	blade profile chord length
c_p	non-dimensional pressure coefficient
h	static enthalpy
i	blade cascade incidence angle
l_c	length of compressor in Moore and Greitzer (1986a)
m	meridional coordinate
$\dot{m}$	massflow rate
r	radial coordinate
s	entropy
t	blade profile thickness
t_b	maximum blade profile thickness
w	work input or output into a turbomachine
x	axial coordinate in Moore and Greitzer (1986a)
y	quasi-normal (quasi-orthogonal) coordinate
z	axial coordinate
A_c	frontal area of compressor in Moore and Greitzer (1986a)
B	Mach-number dependent parameter in Moore and Greitzer (1986a)
C	absolute velocity
DF	diffusion factor
D_{eq}	equivalent diffusion factor
H	stagnation enthalpy, boundary layer shape factor
I	rothalpy
M	Mach-number
P	pressure
T	temperature
U	blade velocity
V	absolute velocity
V_p	plenum chamber volume in Moore and Greitzer (1986a)
W	relative velocity
W_{RE}	square-root of the relative outlet and inlet dynamic pressure ratio across a blade row, used by Aungier (2003)

α	angle of attack for blade cascade
β	blade profile relative leading or trailing edge flow angle, radial mixing parameter
γ	blade cascade stagger angle
ϵ	angle between quasi-normal and true normal
θ	camber angle, wheel angle in Moore and Greitzer (1986a)
η	non-dimensional axial coordinate in Moore and Greitzer (1986a)
ξ	non-dimensional time unit in Moore and Greitzer (1986a)
ρ	density
κ	blade cascade metal angle
κ_m	streamline curvature
λ	quasi-normal angle
ϕ	angle between meridional vector and axial direction, flow coefficient
ψ	stream function, load coefficient
σ	blade row solidity
ω	angular velocity, blade row total pressure loss coefficient

Subscripts

m	meridional component of quantity
θ	circumferential component of quantity
rel	relative property
0	total or stagnation thermodynamic conditions
1	blade row inlet property
2	blade row outlet property
TT	total-to-total
TS	total-to-static
SS	static-to-static

Superscripts

$*$	design condition

Chapter 1

Introduction

This chapter presents some of the background information necessary to understand the significance this project. A brief history of the axial compressor research conducted at the University of Stellenbosch is presented, so as to explain the origins and need for this project. The scope for this project is then defined, and the questions which this project has addressed are presented.

1.1 Background

This section will briefly explain the importance of stall prediction in the general field of axial flow compressor simulation, and in South Africa today. The origins of this project are also described.

1.1.1 General background

With the increasing speed of computer hardware and the increasing power of Computational Fluid Dynamics (CFD) software, it has become possible to simulate the flow phenomena within an axial flow compressor in three dimensions, taking viscous effects into account, as in Pratap *et al.* (2005), or in a time dependent effects, such as in Grüber and Carstens (2001). However, the amount of labour and computational time required for such a project is still rather large, as was commented on by Pratap *et al.* (2005). Furthermore, a large amount of experience and a high level of training is required of the researcher operating the software if meaningful results are to be obtained. For these reasons the author believes that simpler simulation methods are often more suitable for many purposes. Finally, it is often considerably easier to make use of empirical relations and data in a custom written simulation than to try to incorporate them into a standard commercial CFD package.

One family of methods that is frequently dealt with in literature such as Novak (1967), Cumpsty (1989), Gannon and von Backström (2000) and Aungier (2003), are the so-called throughflow methods. These typically make use of axisymmetric, inviscid flow approximations in which viscous effects such as endwall boundary layers are corrected for by blockage modelling. All blade-related phenomena and other loss mechanisms must also be simulated by means of separate models. Compressor stall is one such phenomenon.

Stall is a potentially dangerous mode of operation which should be prevented if possible as it can lead to damage of the compressor. This is because a compressor operating in a state of stall experiences significant fatigue loadings, which can damage or destroy the rotor and stator blades of the machine. Because of the assumptions made in the throughflow methods and the complex nature of flow in a stalled compressor, it is not apparent from the results whether a compressor being simulated would be undergoing stall or not. Thus separate stall criteria must be developed, so as to ensure that the results are realistic. The stall criteria also provide a constraint or limit in the design of a compressor. However, the phenomenon of stall in axial flow compressors is still not fully understood.

Although there is some similarity between the phenomenon of stalling on an aircraft wing and stall in an axial flow compressor, the latter phenomenon is considerably more complicated. This is emphasised in most of the works read by the author containing a description of stall phenomena in compressors, especially Cumpsty (1989) and Pampreen (1993). Unlike an aircraft wing, the relative flow velocity seen by a rotor blade varies across its span in an axial flow compressor, because it is rotating relative to the flow and because of hub and shroud boundary layers. In addition, the entry conditions for a compressor stage are dictated by the nature of flow from the previous stage, and a stalled stage in a compressor will thus adversely affect the performance of stages following it, although not necessarily to the point where they too will begin to develop stall cells.

Many of the phenomena associated with the propagation of stall after its inception are thus highly three-dimensional in nature. This is made very clear in explanations of stall provided by researchers such as Day (1993). For this reason, they cannot be modelled effectively using axisymmetric methods. Furthermore, the main motivation behind the attempt to predict the onset of stall is so that it can be avoided. The stall prediction methods to be investigated here therefore aim to predict the range of operating conditions under which stall or surge will occur in a given compressor, while much of the research into the three-dimensional propagation of stall within a machine is conducted by means of practical testing of experimental compressor rigs.

1.1.2 Background to this project

The South African Air Force requires the ability to predict the performance and life-expectancy of the various gas-turbine engines of the aircraft it operates. This is necessary for a number of reasons: the manufacturers of the aircraft engines are not always willing to provide the necessary information, performance data for the engine operating under South African conditions may not exist, or the engines may be very old, and nearing the end of their operational life. An important prerequisite to the development of this ability is that it should be possible to accurately predict the performance map for the axial flow compressors used in these engines. The development of this aspect of gas-turbine engine modelling and research has been entrusted to the University of Stellenbosch.

The University of Stellenbosch possesses a Rofanco 3-stage low-speed compressor test bench. At some point, the blades of this machine were destroyed during testing. Bernadé (1986) describes the development of a computer software package which was used to design new blades. The new blades gave the machine a higher reaction ratio, and eliminated the need for inlet guide vanes.

The new blades were dully manufactured by the Atomic Energy Corporation. Lewis (1989) began the process of recommissioning the test bench, and used the machine to provide experimental data for the stability-based stall model which was developed. However, only the first rotor row and the last stator row were fitted to the machine for this experimental work.

Full reblading and recommissioning of the Rofanco test bench was performed by Roos (1990). The performance of the compressor with the new blading was determined, and compared reasonably well with the predictions of Bernadé (1986).

The next developments were in the field of axisymmetric througflow simulations. A new method, the streamline throughflow Method (STFM) was developed to overcome the flaws in the existing throughflow methods, namely the streamline curvature method (SCM) and the matrix throughflow method (MTFM). The first version of this method was developed and described in Roos (1995), and a slightly differently formulated version was compared to the SCM in Gannon and von Backström (2000).

As a result of these efforts, a computer software package implementing the STFM for the axisymmetric simulation of axial flow compressors was written. Thomas (2005) added blade row and boundary layer blockage modelling to this package.

At the same time, another computer software package, the Stellenbosch University Compressor Code (SUCC) was being developed. This package contained an implementation of the MTFM, but made allowance for the implementation of alternative throughflow methods. Both packages were lacking any sort of stall prediction

capability. The importance of this capability has already been discussed, therefore it was considered necessary to implement a stall prediction model in at least one of the codes. On considering the codes, it was decided to implement the model in the SUCC, as it was written in a modular fashion that simplified this, and was better documented. This project was born of that requirement.

1.2 Problem statement

The Stellenbosch University Compressor Code (SUCC) is a software package intended to allow the axisymmetric simulation of axial flow compressor operation for the purposes of performance prediction. A stall prediction model is required for use with SUCC. This model must provide an accurate prediction of the operating conditions which will lead to the onset of compressor stall. This requires that the methods used are able to predict the onset of stall in any of its various forms, such as tip stall or rotating stall, as well as the operational conditions under which a compressor may begin to stall, or experience surge. The resulting stall prediction models should provide a high degree of accuracy in prediction of flow under conditions identical to those for which experimentally or practically obtained data is available. It is therefore necessary to determine which of the existing stall prediction models is most accurate, and under which conditions of simulated compressor operation it is most applicable.

1.3 Objectives of this thesis

The main objective of this thesis is:

1 To investigate and evaluate existing stall prediction models for various types of compressor.

The secondary objectives are:

2 To determine what effect the choice of throughflow method has on the accuracy of each stall prediction criterion.

3 To determine the effect of the use of blockage and mixing models, or their omission, on the accuracy of stall prediction for the various criteria.

4 To determine the effect that the layout and coarseness of the computational grid have on the the accuracy of each stall prediction criterion.

5 To determine which aspects of stall in an axial flow compressor require full three-dimensional treatment. In other words: to determine which aspects of compressor stall cannot be accurately modelled or simulated by use of a two-dimensional blade cascade, and meridional throughflow methods.

1. Evaluation of existing stall prediction models

A number of stall prediction criteria that have been found in literature were implemented in the SUCC and used to obtain stall predictions for a variety of compressor test cases.

2. Effect of choice of throughflow method

Stall prediction methods were applied to simulations of test cases using the matrix throughflow method and the streamline curvature method to solve the meridional flow field. The stall predictions for each criterion and each throughflow method were then compared to experimental data from previous researchers to determine the accuracy of the results. It was necessary to implement the streamline curvature method in the SUCC to perform this comparison.

3. Effect of blockage and mixing models

Simulations of the test cases were performed with and without the modelling of effects such as boundary layer blockage and radial mixing. The stall prediction results from these simulations were then compared with experimental results. It was necessary to implement a radial mixing model to perform this comparison.

4. Effect of layout and coarseness of computational grid

An attempt was made to discover the sensitivity of the the stall prediction methods to the number of streamlines in the grid. The effect of the number and placement of quasi-orthogonals was also noted.

5. Limitations of stall prediction in axisymmetric throughflow simulations

Literature describing the various models for the mechanisms involved in the inception and propagation of stall cells, and the experimental investigation of stall in compressor test benches, was examined. The conclusions and insight drawn from this were useful for the selection or rejection of stall criteria and models for implementation in the SUCC.

1.4 Concluding remarks

This thesis required the adaptation and understanding of various stall prediction models based upon the work of previous researchers in the field, and the implementation of these models as FORTRAN subroutines in the SUCC. It focuses mainly on flow phenomena involving the rotor blades of axial flow compressors. The investigation was thus largely restricted to blade row and stall related subjects, although it was necessary for the author to become familiar with many other aspects of axial flow compressor analysis and simulation to better understand the workings of the SUCC. Chapter 2 contains descriptions and discusssions of these subjects. Chapter 3 describes the implementation of the stall criteria, giving further theoretical background and describing the algorithms used to implement them. Chapter 4 introduces the four test cases used to evaluate these stall criteria. The results of the evaluation for each test case, a comparison with experimental data and the simulation results of Aungier (2003) and a discussion thereof, are then presented. Chapter 5 provides contains interpretation of the significance of the results obtained and attempts to draw useful conclusions from them. Subjects requiring further research are also described.

Chapter 2

Axial flow compressor theory

This chapter begins by explaining some terminology and theory which is generally applicable to turbomachinery. It then briefly describes some of the axisymmetric throughflow methods used to predict flow in such machinery. Stall is then defined and differentiated from similar phenomena such as surge. Various models for the inception of stall are explained and discussed, and methods for the prediction of the stall limit for a compressor are introduced to the reader. The chapter concludes with a brief overview of the use of CFD analysis in stall prediction and simulation.

2.1 General turbomachinery theory and terminology

The field of axial flow compressor analysis has been extensively explored, and it is not the intention of this author to provide a detailed explanation of the turbomachine theory relating to this type of machine. Readers requiring such a treatment are directed to the many excellent books written on this subject. Those used most extensively by the author were Aungier (2003) and Cumpsty (1989). However, it is desirable to include a very brief examination of some of the more important concepts and definitions from the field in this work, as all subsequent work in this document is somewhat dependent upon them.

Both Aungier (2003) and Cumpsty (1989) use Euler's turbine equation (2.1) as a starting point for their introduction to basic compressor theory. This equation represents the work done by an idealised turbomachine on the flow passing through it, on a single stream surface.

$$w = \dot{m}\omega \left(r_2 V_{\theta 2} - r_1 V_{\theta 1} \right) \tag{2.1}$$

Equation (2.1) relates the work performed on the flow, w, to the inlet and outlet

radii of the stream surface (r_1 and r_2) and the corresponding velocity components in the tangential direction (V_{θ_1} and V_{θ_2}).

Aungier (2003) and Cumpsty (1989) also both present definitions for the flow coefficient ϕ (2.2) and the stage loading, or stage work coefficient ψ (2.3).

$$\phi = \frac{V_x}{U} \tag{2.2}$$

$$\psi = \frac{\Delta H}{U^2} = \frac{\Delta P_0}{\rho \omega^2 D^2} \tag{2.3}$$

The stage loading relates the pressure change across a stage of a compressor to the approximate kinetic energy of the flow relative to the blade, while the flow coefficient is the ratio of the axial component flow rate to the blade tip speed. Another important quantity which is defined in both Cumpsty (1989) and Aungier (2003), is the reaction ratio, R, defined in Equation(2.4), which is a measure of the portion of the static pressure rise for a compressor stage which occurs in the rotor of the stage, i.e.

$$R = \frac{W_1^2 - W_2^2}{2U\left(W_{\theta 1} - W_{\theta 2}\right)} \tag{2.4}$$

in which W_1 and W_2 are the inlet and outlet velocities relative to the rotor blades, and $W_{\theta 1}$ and $W_{\theta 2}$ are the tangential components of the relative velocities. Both Cumpsty (1989) and Aungier (2003) state that it is generally accepted that the optimal value of the reaction ratio is $R = 0.5$, which indicates an equal pressure rise across stator and rotor of a stage. However Cumpsty (1989) provides examples of compressors for which the reaction ratio does not correspond to this value. This is also the case with two of the test cases used in this project, namely the Rofanco 3-stage low speed compressor and the NACA 5-stage transonic compressor, both of which have a comparatively higher degree of reaction.

A useful quantity which Cumpsty (1989) deals with considerably earlier than Aungier (2003) is rothalpy, I, defined in equation (2.6). The quantity is arrived at by substituting the expression for work performed by the turbomachine according to Euler's turbomachine equation (2.1) into the energy equation along a streamline crossing a blade row in an adiabatic turbomachine, shown in equation (2.5). This equation is then manipulated and the absolute velocities rewritten in terms of blade speeds and relative flow velocities, so as to reflect the conservation of a quantity that is conserved along a streamline crossing blade rows. For a rotating frame of reference, this quantity is analogous to enthalpy in a static frame of reference, and is thus named rothalpy. It can also be seen that the rothalpy will equal the stagnation

enthalpy for a static blade row.

$$h_1 + V_1^2 + w = h_2 + V_2^2 \tag{2.5}$$

(2.6).

$$I = h + \frac{W^2}{2} - \frac{U^2}{2} \tag{2.6}$$

The diffusion factor, DF, shown in Equation (2.7), is of considerable importance in several stall prediction theories, and is thus of importance in this text. Cumpsty (1989) defines it as follows:

> "... Essentially this relates empirically the peak velocity on the suction surface of the blade to the velocity at the trailing edge ..."

The significance of the diffusion factor is that it gives an indication of the thickness of the boundary layer and likelihood of boundary layer separation occurring on the suction surface of a blade, which would dramatically increase blade profile losses, and could also indicate that the blade (but not necessarily the compressor) was operating in a state of stall.

$$DF = \frac{1}{W_1}\left(W_1 - W_2 + \frac{\Delta W_\theta}{2\sigma}\right) \approx \frac{W_{max} - W_2}{W_1} \tag{2.7}$$

Cumpsty (1989) provides a virtually identical expression, but substitutes absolute velocities for the relative velocities used by Aungier (2003). In the approximate equality, given by Aungier (2003), W_1 and W_2 are the relative inlet and exit velocities for the blade row, and W_{max} is the maximum relative velocity attained in the blade row ΔW_θ is the change in relative swirl velocity across the blade row. The symbol σ represents the solidity of the blade row, or the ratio of blade chord to circumferential blade pitch for the rotor. Cumpsty (1989) and other sources state that for most axial flow compressors, σ is generally greater than 1 but rarely exceeds a value of 2.

In the early days of axial flow compressor design, it was considered inconvenient to calculate the diffusion factor, as this required the value of W_{max}, which was difficult to obtain. This led to the development of the equivalent diffusion factor, D_{eq}, which was based upon the geometric properties of the blade row. The equivalent diffusion factor is defined in equation (2.8):

$$D_{eq} = \frac{W_{max}}{W_2} \tag{2.8}$$

Cumpsty (1989) provides equation (2.9) for the calcualtion of D_{eq}:

$$D_{eq} = \frac{\cos\kappa_2}{\cos\kappa_1}\left[1.12 + a\,(\Delta i)^{1.43} + 0.61\frac{\cos^2\kappa_1}{\sigma}\,(\tan\kappa_1 - \tan\kappa_2)\right] \tag{2.9}$$

The formulation presented by Aungier (2003) is virtually identical, except that it is written in terms of flow angles β_1 and β_2 instead of blade metal angles κ_1 and κ_2. The diffusion factor will be discussed further when the associated stall prediction method is explained in the next chapter.

2.2 Numerical simulation of compressor operation

2.2.1 Introduction

As was mentioned in chapter 1, the increasing power of computer hardware, coupled with advances in the field of CFD make it theoretically possible to perform a full three-dimensional simulation of the operation of an axial flow compressor. However, such simulations are still rather costly in terms of the time required to prepare them, the simulation execution time, and the actual financial cost of the software. Because of their speed and relative simplicity, the meridional analysis methods are therefore still widely used for purposes where they offer sufficiently accurate results.

Three meridional analysis methods will be discussed. All are inviscid flow approximations which assume axisymmetric flow in the compressors which they are used to simulate. They generally make use of boundary layer assumptions and smoothing mixing models to approximate endwall blockage and radial mixing, which are not accounted for by inviscid flow methods.

Another important simplifying assumption which can be made is that the effects of the various blade rows can be approximated by one or more actuator disks per blade row. Actuator disks can be regarded as infinitely thin rotors having no frictional losses across them, with an infinite number of blades, which impart or remove energy and angular momentum to or from the flow. An improvement of the accuracy of the simulation can be obtained by calculating the exit angle of the flow from the blade row based upon blade row geometry and the deviation angle for the blade row obtained from empirical relations, usually obtained from experimental blade cascades. The relative outlet velocity vector for the blade row can then be determined. Finally, the blade row speed is subtracted so as to yield the absolute flow velocity vector. Because the phenomenon of stall is strongly linked to blade row geometry by almost all researchers, the latter model was the one used in all simulations in this project.

Of the three throughflow methods, the streamline curvature method (SCM) will be discussed in the greatest detail, as it was necessary to implement it in order to complete this project. The matrix throughflow Method (MTFM) will also be discussed in some detail, as it was the throughflow method originally implemented in the SUCC. The streamline throughflow method (STFM) will be briefly discussed as it was locally developed, and will almost certainly be implemented in the SUCC by future researchers.

2.2.2 Streamline curvature method

The first method to be discussed streamline curvature method (SCM). This method appears to be by far the most popular, judging by comments made in Cumpsty (1989), the fact that no other throughflow method is described by Aungier (2003), and that it is used as a standard against which to measure other throughflow methods, as in Gannon and von Backström (2000). In this method, the meridional flow field is divided up into a computational grid by a number of quasi-normal lines (i.e. lines approximately normal to the streamlines for the flow field within the compressor), and streamlines, the positions of which are initially estimated based on equal fractions of the annulus radius or some similar crude method, and change as the simulation progresses. The quasi-normals, or quasi-orthogonals are usually oriented approximately radially. They are often positioned on the leading and trailing edges of the blade rows, and their position remains fixed throughout the simulation. The intersections between the quasi-normals and the streamlines form the computational grid for the streamline curvature method. Starting with the first quasi-normal at the compressor inlet, and moving towards the exhaust, the meridional flow field on each quasi-normal is solved at each grid point by iteratively performing a mass-balance and a momentum-balance on the meridional flow across the quasi-normal. The momentum-balance is performed by solving a discretized form of equation (2.10), which is the axisymmetric, time-steady, normal momentum equation for flow in the compressor. This requires that the curvature for each streamline be calculated at each grid point on the quasi-normal, giving the method its name. The swirl component of the velocity is calculated using either actuator disk models, or from empirical blade row models based on experimental cascade data. The other properties of the flow, for instance the temperature and entropy of the gas, are then calculated at each grid point on the quasi-normal. Finally, once the meridional flow field has been solved on all quasi-normals, new values for the positions of the streamlines on the quasi-normals are calculated. The change in streamline position must be under-relaxed in order to ensure stability of the method. The entire process is repeated

until the position of the streamlines change less than a certain desired tolerance.

Equation(2.10), the momentum equation for the normal direction as given by Cumpsty (1989), is thus the basis of the streamline curvature method:

$$\frac{1}{2}\frac{\partial}{\partial y}V_m^2 = \frac{\partial H}{\partial y} - T\frac{\partial s}{\partial y} + V_m\frac{\partial V_m}{\partial m}\sin(\phi+\gamma) + \frac{V_m^2}{r_m}\cos(\phi+\gamma) - \frac{1}{2r^2}\frac{\partial}{\partial y}\left(r^2V_\theta^2\right) + \frac{V_m}{r}\frac{\partial}{\partial m}(rV_\theta)\tan\epsilon \tag{2.10}$$

In Equation (2.10) ϕ is the angle subtended by a vector in the axial direction, x, and the vector m, which is tangential to the streamline. The angle γ is the angle subtended by the radial direction r vector and the quasi-normal q. The angle ϵ is the angle between the meridional plane and the curved surface upon which the streamlines are to be found. The symbol H is the stagnation enthalpy of the flow. This information is derived from a description of the method in Cumpsty (1989). A similar explanation is provided by Aungier (2003), who bases his version of the SCM on that of Novak (1967). Cumpsty (1989) and Roos (1995) explain that an advantage of the SCM over stream function based throughflow methods such as the MTFM and the STFM is that it can handle areas of supersonic meridional flow, which would imply two possible solutions for the flow field for a stream function based method. The main disadvantage is its inherent instability, which requires the use of numerical damping. A more detailed explanation of the SCM, as described in Aungier (2003) and implemented during this project, is included in appendix B.

2.2.3 Matrix throughflow method

The second method to be discussed is derived from a similar theoretical basis to the SCM. It is called the matrix throughflow method (MTFM). The method makes use of the concept of the stream function, represented by the symbol ψ. By definition, this function has a constant value along a streamline or stream surface. The velocity component along a direction vector at a given point in a flow field can also be determined if the gradient of the stream function with respect to the direction vector is known. Thus, if the value of the stream function is known at various points of a flow field (for instance, in a relatively evenly distributed grid across the entire flow field), the flow velocity and direction can be determined at any point in the flow field by means of interpolation and numerical differentiation. Thus the meridional flow field is divided up by streamlines and quasi-normals to form a computational grid in the same way as is done for the streamline curvature method. An important difference between the two methods is that for the matrix throughflow method, the positions of the streamlines used to define the computational grid are not adjusted

from their initial estimated positions during computation. For this reason they are called quasi-streamlines. The position of the true streamlines may be calculated by interpolating in terms of the stream function between the grid points on the computational grid.

The value of the stream function at various points in the flow field can be solved by discretizing equation (2.11) and solving the resulting system of equations in ψ at each point on the computational grid by means of a matrix inversion. Equation (2.11), also given by Cumpsty (1989), is derived from the same momentum and energy equations which give rise to equation(2.10) of the streamline curvature method, but it is reformulated in terms of the stream function.

$$\frac{\partial^2\psi}{\partial p^2} + \frac{\partial^2\psi}{\partial y^2} = \rho\frac{rB}{V_p}\left(\frac{\partial H}{\partial y} - T\frac{\partial s}{\partial y} - \frac{V_\theta}{r}\frac{\partial}{\partial y}\left(rV_\theta\right) + a_\theta \tan\epsilon\right) + \frac{\partial\psi}{\partial p}\frac{\partial}{\partial p}\ln\left(\rho rB\right) + \frac{\partial\psi}{\partial y}\frac{\partial}{\partial y}\ln\left(\rho rB\right) \tag{2.11}$$

Thus the values of the stream function at each point on the computational grid are obtained at once. However, examination of equation (2.11) will reveal that the solution requires the values of the velocity components and thermodynamic properties on the computational grid. It is therefore necessary to begin with estimated values and improve these values by successive applications of the method. In the SUCC, the process is stabilised somewhat by beginning the simulation at lower rotational speed and a correspondingly low massflow rate, or a solution for a previous simulation with similar operating conditions, and slowly increasing it to the desired simulation conditions.

This information is derived from the description of the matrix throughflow Method given in Cumpsty (1989). A far more complete explanation of the matrix througflow Method and its derivation is to be found in Thiart (2005), which is included as appendix A.

2.2.4 Streamline throughflow method

The third method of determining the shape of the streamlines within the compressor is known as the streamline throughflow method. This axisymmetric method is the most recent of the three methods discussed here, as it was developed at the University of Stellenbosch in the 1990's. The development of this method, and the advantages that it offers over the SCM and MTFM are described in detail in Roos (1995) and Gannon and von Backström (2000). Here follows a brief description of this method, as gleaned from these two sources.

The method begins with the fundamental equations which give rise to the MTFM.

Boadway's transformation is then applied to the fundamental equations to yield the partial differential equation of the form shown in (2.12):

$$\left(1+\left(\frac{\partial r}{\partial z}\right)^2\right)\frac{1}{\rho r}\frac{\partial}{\partial \psi}\left(\rho r\frac{\partial r}{\partial \psi}\right)+\left(\frac{\partial r}{\partial \psi}\right)^2\rho r\frac{\partial}{\partial z}\left(\frac{1}{\rho r}\frac{\partial r}{\partial z}\right)= 2\frac{\partial r}{\partial z}\frac{\partial r}{\partial \psi}\frac{\partial^2 r}{\partial z\partial \psi}-(\rho r)^2\left(\frac{\partial r}{\partial \psi}\right)^3\left[\frac{\partial h_0}{\partial \psi}-T\frac{\partial s}{\partial \psi}-\frac{C_\theta}{r}\frac{\partial\left(rC_\theta\right)}{\partial \psi}\right] \tag{2.12}$$

This equation is then solved numerically for a radius, r, in terms of the known quantities stream function ψ and axial position z by means of a matrix inversion. In other words, instead of calculating the value of the stream function at various points on a computational grid, then interpolating between points to find the position of the streamlines, as in the MTFM, the STFM assumes certain values for the stream function, then calculates the radial positions of streamlines at each axial position.

Gannon and von Backström (2000) provides a good summary of the advantages of the streamline throughflow method over the older streamline curvature method. Perhaps the most important advantage is that it inherently satisfies the mass-conservation criterion, which eliminates the need for an iterative process to ensure this. As a consequence, a computational solution utilising this method converges to a solution in an order of magnitude less time than an equivalent SCM computational solution, Other advantages are that this method is somewhat more numerically stable and more tolerant of distorted computational grids. It produces results of a level of accuracy very similar to that achieved by the streamline curvature method and the matrix throughflow method.

2.2.5 Blade cascade modelling

An approximation often used in modelling of axial flow turbomachines is to regard the flow along a stream surface through the blades in a blade row as a two-dimensional flow. Such an arrangement is termed a *blade cascade*.

Figure 2.1, copied from a very similar figure in Aungier (2003), shows the most important geometric properties for blade calculations. The *mean camber line* is a line connecting the origins of the set of all inscribed circles between the blade row surfaces. The *blade chord line* is a line joining the points where the leading and trailing edges intersect the mean camber line. The angles κ_1 and κ_2 are termed the inlet and outlet blade metal angles, and are the mean leading and trailing edge angles of the blade profile relative to the axial direction. Under design conditions, flow relative to the blade row would enter and leave the cascade at these respective angles, if there were no flow deviation. The actual relative velocities, W_1 and W_2,

at which the flow enters and leaves the cascade make relative angles of β_1 and β_2 with the axial direction. The difference between the blade metal inlet and the flow inlet angles, κ_1 and β_1, is termed the *angle of incidence*, i. This is usually used as a parameter in blade cascade models, although some require the angle of attack, α, which is defined as the angle between the flow and the blade chord line. The difference between the outlet metal and flow angles is termed the *deviation angle*, δ, and must be accounted for by a blade cascade correlation, usually empirically based, to be described shortly. The difference between κ_1 and κ_2 is termed the *camber angle*, θ, and the angle between the line joining the leading and trailing edges and the axial direction is termed the *stagger angle*, γ.

Aungier (2003) provides a method for calculating blade cascade losses, loadings and deviation angles. The first step is to calculate the design angles of attack (α^*) and incidence (i^*). using an iterative scheme, since both are dependent on one another. Aungier (2003) provides correlations that are obtained by fitting curves to the data obtained by Johnsen and Bullock (1954). Aungier then calculates the design deviation angle, δ^*, using correlations developed by Lieblein, described in Johnsen and Bullock (1954). Following this, Aungier (2003) presents a method to calculate the pressure loss coefficient for flow at the design incidence angle, ω, once again developed by Lieblein. This requires the calculation of the equivalent diffusion factor, D_{eq}. The loss coefficient thus calculated only accounts for profile losses, so additional loss models must be used to account for other losses due to blade tip leakage, Mach-number related effects, endwall boundary layer effects, and leakage through seals. The originator of the method which Aungier (2003) advocates

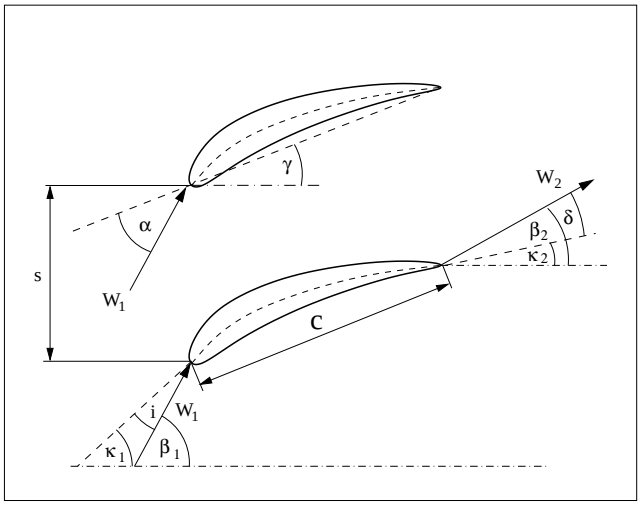

Figure 2.1: Blade cascade nomenclature

was Howell (1945). The loss coefficient is then adjusted to represent off design conditions. Once all the loss-coefficients have been calculated, they can be added together. Aungier (2003) recommends that the limit $\omega \leq 0.5$ be applied to all loss coefficients. The loss coefficient is used to calculate the pressure loss over the blade row on each stream-surface examined by use of equation(2.13):

$$(\Delta P_{t,rel}) = \omega \left(P_t - P\right)_{in} \tag{2.13}$$

Finally, for a compressor operating in transonic conditions, shock losses must be accounted for.

The details of the method presented here in overview are to be found in Aungier (2003), and a similar but alternative method was implemented by Thomas (2005). Some details of the implementation of these models in SUCC are given by Thiart (2004).

2.2.6 Radial mixing modelling

An assumption inherent in all the meridional throughflow methods discussed is that no flow occurs along quasi-normals, or, in other words, no mixing of flow occurs between stream surfaces. Cumpsty (1989) and Aungier (2003) state that this assumption will lead to an unrealistic loss or entropy distribution along quasi-normals in blade rows, as mixing does occur between stream sheets in a real compressor. As quasi-normals are usually approximately radially aligned for an axial flow compressor, the mixing between stream sheets is often referred to as *radial mixing*. Both Aungier (2003) and Cumpsty (1989) agree that the omission of some correction to allow for radial mixing in throughflow methods can cause numerical instability in the throughflow method to the extent that the method will not converge to a solution. Aungier (2003) adds that the errors resulting from the omission of a mixing model will be most severe when the simulation is being performed for conditions close to that of the surge limit of the real machine. Cumpsty (1989) provides an explanation for radial mixing based on that of Gallimore and Cumpsty (1986) which accounts for this. In this model, mixing is equated to turbulence, which Cumpsty (1989) defines for this purpose as any non-deterministic, unsteady flow occurring within the machine. Now the onset of surge is determined by the stability of the compressor system, according to Pampreen (1993) and Cumpsty (1989), as will be discussed in the next section. As the real compressor approaches the point of surge, the stability of the flow will break down, and more and more unsteadiness will be observable in the flow, thus a greater degree of mixing will occur.

Cumpsty (1989) also provides an alternative model for radial mixing based upon the work of Adkins and Smith (1982). In this model, the mixing is assumed to be caused by secondary flows in a radial direction, due to effects such as non-uniform blade circulation, radial flow in the boundary layers, tip leakage, and leakage from the suction to the pressure surface of a blade near the endwalls. In other words, the mixing is assumed to be caused by secondary flow patterns of deterministic (and thus predictable) origin. This model for the smoothing of of a general thermodynamic property P. The mixing is simulated by solution of equation(2.14):

$$\frac{\partial P}{\partial z} = \beta \frac{\partial^2 P}{\partial r^2} \tag{2.14}$$

In equation(2.14, the value of the mixing parameter β is given by:

$$\beta = \frac{x}{a} \int_0^a \frac{V_r^2}{V_z^2} da$$

Aungier (2003) suggests that radial mixing be approximated by applying smoothing to the total pressure losses calculated for each blade row, $(\Delta P_t')_i$, according to the weighted averaging scheme described in equations (2.15) to (2.17). The principle behind this scheme is that the value of a numerical approximation of the hub-to-tip integral of the property will be identical for the original and smoothed values. The symbol i denotes the number of the streamline on which the smoothing is applied, with 1 at the hub, and N at the tip.

$$(\Delta P_t')_{i,smooth} = \left[(\Delta P_t')_{i-1} + 2\,(\Delta P_t')_i + (\Delta P_t')_{i+1}\right]/4; 1 < i < N \tag{2.15}$$

$$(\Delta P_t')_{1,smooth} = 2\,(\Delta P_t')_{2,smooth} - (\Delta P_t')_{3,smooth} \tag{2.16}$$

$$(\Delta P_t')_{N,smooth} = 2\,(\Delta P_t')_{N-1,smooth} - (\Delta P_t')_{N-2,smooth} \tag{2.17}$$

This method of modelling radial mixing is rather crude, as it is not based upon a specific explanation of the mechanism leading to radial mixing. It merely seeks to mimic the effects of radial mixing to some degree. Another criticism is that the degree of smoothing is dependent to some extent on the number of iterations, as the smoothing is applied for each iteration of the throughflow method. Of course, the properties which are smoothed are recalculated during each iteration, but these new values will be based partially on the old values of the various properties, which

have already been smoothed. The chief advantage of this method is that it is very easy to implement.

2.3 The nature of stall

2.3.1 Stall, surge and choke

The terms "stall" and "surge" are often confused or used interchangeably when used in the study of axial flow compressors, although they are rather different in nature. Generally, one attempts to predict the conditions under which stall will occur, as it will usually precede surge, and is slightly less dangerous to compressor hardware. It is possible for a compressor to operate within its design envelope with minor stall, or small stall cells occurring in some blade rows. Once a compressor enters a state of surge, however, all normal, steady operation ceases. Here follows a brief explanation of these two phenomena, deriving from the explanations provided by Cumpsty (1989) and Pampreen (1993).

In axial flow compressors, stall is a condition whereby flow through the machine is partially blocked by one or more pockets of the working fluid not moving in the intended direction through the blade passages in one or more rotor or stator rows. Such a pocket of fluid is referred to as a stall cell. boundary layer separation on the hub or shroud can influence the formation of stall cells and the onset of stall. A compressor will experience a large drop in discharge pressure when entering stall, but may continue operating in a relatively stable fashion in this new condition. However, the performance is thus obviously degraded, and the stall cell rotates relative to the blade row it affects, at a significant fraction of the rotational speed of the compressor. This, coupled with the unsteady nature of flow within the stall cell can cause the individual blades in the blade row to vibrate, which can lead to fatigue-related failures, which can have catastrophic results. It is thus highly undesirable for an axial flow compressor to operate stalled. There is also the danger that if an axial flow compressor is sufficiently badly stalled, and a sufficiently large difference in pressure exists between the discharge end and the inlet, surge may occur.

Compressor surge is defined as a total breakdown of stable compressor operation. Whereas most of the fluid in a stalled compressor will still be travelling from the inlet to the exit, this is not the case for a machine suffering from surge. Under this condition, the flow and pressure gradient within the compressor may change rapidly and unexpectedly, and flow conditions within the machine bear no resemblance to those for which it was designed. The condition is thus highly undesirable, as the

various components are exposed to conditions for which they were not designed. Surge is a system phenomenon; that is to say that it is dependent not only upon the properties of the compressor, but of the entire flow system to which the compressor is coupled. The frequency of the surge fluctuations is dependent on both the compressor and the volume of the ducts or chambers from which the compressor receives and to which it exhausts working fluid.

It is simpler to predict stall than surge, as it is necessary to know something of the system of which the compressor forms a part in order to arrive at an accurate surge prediction, as surge is a system-dependent phenomenon, while it is only necessary to know the operating conditions and geometry of the compressor being considered in order to predict stall.

At the opposite extreme to surge and stall, a compressor may operate in a choked condition. Choke in a compressor is very similar to choke in a duct; that is to say that it represents the maximum flow rate attainable by the working fluid through the blade row passages, and generally implies that the average throughflow velocity is equal to the local speed of sound in the fluid based upon the relative stagnation properties of the fluid upstream of the choke location.

2.3.2 Cumpsty's discussion of compressor stall

Cumpsty (1989) and Pampreen (1993) differentiate between progressive and abrupt stall, and full-span or part-span stall. Progressive stall is normally part span, and occurs near the tips of the stalled blade row, while abrupt stall is usually full-span. Abrupt, full-span stall is an extremely serious condition, which can do significant damage to a compressor because although the pressure rise and gas flow rate are generally low, the work input to the compressor is high under such a condition, and this work is transformed into heat energy, causing the compressor to become dangerously hot, and possibly suffer thermally-related damage.

Cumpsty (1989) provides a simplified explanation of how a stall cell forms and grows. Excessive flow separation occurs in one or more blade passages in the rotor, leading to the formation of a small stall cell in that passage. The separation may be caused by a tiny imperfection in the surface or alignment of one of the blades. Whatever agency causes the separation to occur, it increases in severity until it effectively blocks the flow through this passage, which affects the flow through neighbouring passages. The blades ahead of the stalled blade in the direction of rotation of the rotor are subjected to flow at a lower angle of incidence than they were designed for, which takes the stalled blade passage out of stall, while the angle of incidence of those following increases, causing them to stall as well. This causes the stall cell to

grow somewhat, and rotate around the axis of the machine, in the same direction as the rotor, only more slowly, once it has grown as much as it can. This means that the stall cell rotates backwards relative to the rotor. This is illustrated in figure 2.2

Cumpsty (1989) also mentions the phenomenon of hysteresis, which a compressor will exhibit while stalling and recovering from stall. A compressor which has been throttled to the point of stall inception and beyond will not recover from stall until the throttle has been opened significantly further than the position at which it was set when stall initiated. In other words, the compressor leaves the stalled condition at a considerably higher massflow rate than that at which it enters the stalled condition. This can have serious implications on stall-recovery in compressors, particularly in aero-engines, where the hysteresis effect has been known to make it necessary for an engine to be shut down and restarted in order to recover from stall.

Cumpsty (1989) explains that a compressor with low aspect ratio, long chord blades stalls at a much lower flow coefficient than one with high aspect ratio blades, as the former are less badly affected by the pressure and velocity gradients near the endwalls of the compressor. The former are also more resistant to vibration than the latter.

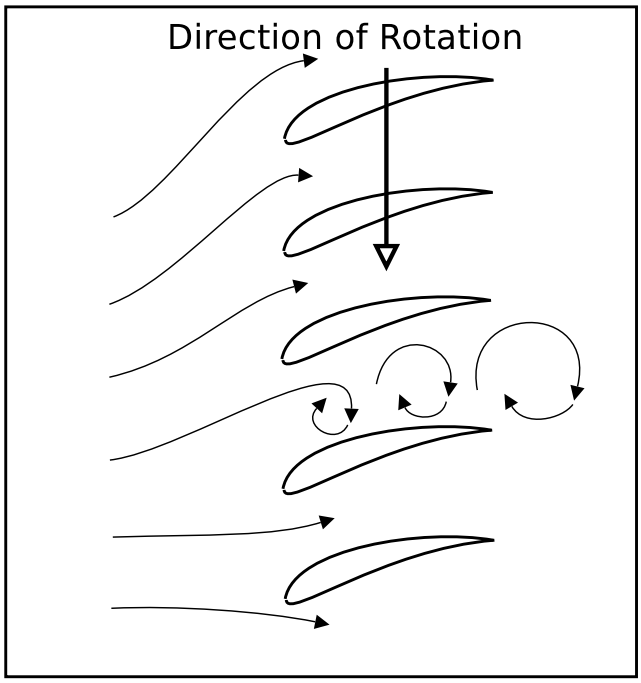

Figure 2.2: A simplified diagram of stall inception in a rotor blade row

2.3.3 Day's findings on stall inception mechanisms

I. J. Day is a researcher who has made an important contribution to the current understanding of rotating stall phenomena in axial flow compressors. In Day (1993) he discusses two of the most common flow models used to explain the inception of rotating stall in an axial flow compressor. The first he discussed is essentially the same as the explanation given by Cumpsty (1989) in the previous section, involving the separation of flow from a single blade, the resulting blockage of the blade passage, and the resulting alteration of the angle of incidence of the blades to either side of the blocked passage, causing the stall cell to move around the blade row. This explanation dates back to the 1950's. He then draws attention to the fact that a stall cell generated by this mechanism will only affect a few blades at a time, and will thus be small. Such a stall cell will also only affect one blade row. For this reason he refers to this type of stall inception mechanism as a *short length scale disturbance*.

The second flow model which Day (1993) discusses is of more recent vintage, and was first developed by Moore and Greitzer (1986*a*) and applied in Moore and Greitzer (1986*b*). This model supposes a sinusoidal velocity variation about the annulus of the compressor, affecting flow throughout its entire length, which rotates and has a wavelength equal to the circumferential distance around the annulus. The speed at which the velocity-variation rotates is smaller than that of the blade rotation, but it occurs in the same direction. This velocity variation is initially very small, but grows rapidly in amplitude as the stability limit of the compressor is approached, and would, according to the theory, thus bring about stalling in the machine in an apparently instantaneous fashion. Some practical measurements, particularly by McDougall *et al.* (1990), indicate that these *modal perturbations*, as Day calls them, do indeed exist and play a role in stall inception.

By experimental techniques described in the next section, Day demonstrated that modal velocity disturbances are not a mechanism leading to the inception of stall, but rather an indication that the compressor is nearing its region of unstable operation. An alternative indication is the formation of a small, but finite sized stall cell. He explains that while a modal disturbance is a relatively reversible type of disturbance, which need not seriously affect the compressor performance, the formation of a small finite stall cell is highly irreversible, and will precipitate stall in a comparatively short time. He adds that coupling can only occur if the modal disturbances are well established by the time of the formation of the finite sized stall cell.

Day concluded that stall cells can either be restricted to a small portion of the

circumference of the annulus, or occur around a larger portion of the circumference, giving rise to the perception that there are 'small' and 'large' stall cells, although in fact stall cells could occur in any intermediate size. He states that the smaller, more restricted stall cells move faster around the annulus than the larger, less restricted ones, and that their onset is more sudden and violent. The formation of a finite sized stall cell destroys any modal disturbance that is not already well established, and interacts with those that are. Finally, Day (1993) states that the smaller, short length scale stall cells appear to be the most common cause of stall inception in the compressor.

Day continued his research into short length scale and modal disturbance phenomena, and in Day and Camp (1997) presented further findings obtained in conjunction with Camp. His findings were that a modal disturbance of sufficiently large amplitude could result in a breakdown of flow through the compressor in the part of the compressor annulus affected by the velocity trough. This could lead to the gradual, slow formation of a large, slowly rotating stall cell, although usually a spike-disturbance, or short length scale stall cell, developed first.

2.4 Experimental investigation of stall

Many important experimental investigations into the onset of stall, and its causes, were performed by I. J. Day, and was described in Day (1993). A brief account of his experimental approach and subsequent findings are included below, as they provided a considerable insight into the nature of stall, particularly the phenomenon of rotating stall.

Day conducted a practical experimental investigation into the role played by modal disturbances by measuring flow velocities as a function of time at various angular positions at a constant radius and axial position ahead of the first rotor row in two different axial compressors entering stall; one a single-stage machine, and the other a multi-stage machine. From the time-dependent data gathered, the inception, growth and speed of rotation of an instability about the axis of the machine in an angular direction could be determined.

Day then conducted a series of tests in which he artificially created modal disturbances by injecting high speed air jets into the compressor inlet at various radial positions while the machine was running at the lowest throughflow velocity possible without initiating premature stalling. The frequency of the induced disturbance was varied by control of these jets, and the amplitude of the variation of the velocity at a later stage in the compressor was recorded and plotted against the frequency of the induced disturbance. The range of frequencies in which a maximum variation of

flow velocity was recorded corresponded remarkably well with the rotational speed of the disturbance measured in the previously described test.

Day then proceeded to investigate short length scale stall cells and their formation. His eventual findings were that short length scale stall cells move considerably faster around the compressor annulus than larger ones, and generally prevent stall cells due to modal disturbances from forming, as they destroy the axisymmetric nature of the modal oscillations. He also concluded that short length scale disturbances were a more common cause of stall inception than modal disturbances.

A number of researchers have since attempted to find indicators for the onset of stall of various types in axial flow compressors. Many of the stall prediction criteria which have now achieved general acceptance had their basis in correlations drawn from experimental data rather than theoretical flow analysis.

Many recent researchers have resorted to sophisticated measuring devices, and the development of new methods of practically obtaining stall measurement is a rich field of development and research.

Both Inoue *et al.* (2001) and Bernd Höss and Fottner (2000) adopted an approach involving the use of Fourier-transforms and Wavelet-transforms on pressure fluctuations in axial flow compressors. The latter was interesting in that the experimental data was obtained from an entire working turbofan engine, rather than a compressor operating as an isolated test bench.

Ottavy *et al.* (2001) presented a two-part paper that described the analysis of flow fields between the blade rows of a transonic axial flow compressor. The first part describes the experimental method employed to obtain a velocity distribution, using the technique of Laser 2-Focus anemometry. This measurement technique is described at some length, followed by a description of the moving shock observed within the compressor under investigation. The second part of the paper consisted of an explanation of an unsteady flow analysis performed on the compressor which was tested. The analysis compared data obtained experimentally for inlet guide vane wakes and rotor leading edge shocks with those obtained from an analytical model, with good agreement reported between the two.

Locally, Lewis (1989) made use of the Rofanco 3-stage low pressure compressor test bench at Stellenbosch University to validate a small perturbation stability stall inception model. The stall model in which the experimental data was used was based upon a stability analysis of the flow field between the trailing edge of a rotor blade row and the leading edge of the stator in the same stage. As a result, only the first stage rotor blade row and the last stage stator blade row were present in the machine during experimental testing, so as to provide a large blade free region. A 3-hole cobra probe was used to measure flow properties within the compressor, as it

provided adequate temporal and spatial resolution, as well as introducing a small but desirable amount of averaging of measured properties, and allowing measurement of static and dynamic pressures using one instrument. The instrument was mounted on a traversing mechanism to allow measurements at various radial stations. A hot-wire probe, and static pressure tappings at various points along the machine in the axial direction were also used to confirm the results obtained from the cobra probe, and provide supplementary data respectively. The results thus obtained provided reasonable agreement with theoretically predicted values obtained by application of the stall model. It was also observed that at all radii investigated (hub, tip and mid-span), the diffusion factor was close to or in excess of 0.6 at the point of stall, which is in accordance with the diffusion factor stall criterion, as described in the next section.

The stall model developed was not capable of calculating the number of stall cells present, thus separate predictions had to be made for cases with one, two and three cells respectively. Even more importantly it relies on time-dependent, non-axisymmetric instabilities, making it unsuitable for implementation in the SUCC.

2.5 Stall prediction methods

2.5.1 Introduction

A widely quoted and oft-used method of predicting the onset of stall is that it coincides with the increase of the diffusion factor beyond a certain value, for instance $DF > 0.6$. This criterion dates back to the work of Howell in the 1940's. Although it is still of some use, Cumpsty (1989) is critical of it, as this is merely indicative of large wake thicknesses on some of the blades and blade rows in some stages. This is not an optimal state for the operation of the compressor, but does not of itself imply that the compressor as a whole is stalling, and the machine may continue to operate in a stable fashion for considerably higher diffusion factor values.

2.5.2 Cumpsty's discussion of stall prediction criteria

Cumpsty (1989) appears to prefer de Haller's 1953 proposal that $c_p < 0.44$ or $V_2/V_1 > 0.72$ for a blade row if stall is to be avoided. He also cites the method of Koch (1981), which regards the rotor and stator blades as a two-dimensional diffuser, after making allowances for factors such as tip clearance.

Cumpsty (1989) also describes methods of determining overall compressor stability. He first presents a linearised one-dimensional model in which a compressor is connected to a plenum chamber with a throttle via a duct. With the appropriate

assumptions, the model reduces to a second-order linear equation, analogous to the classic mass-spring-damper system model. The task of finding the point of instability of the compressor then becomes a matter of finding the natural frequency of the system. Such a system has the advantage that it can take into account effects resulting from the interaction with the compressor of the other components of the system of which the compressor is a part, if they can be modelled as described, and the assumptions made, for instance the linearisations, are reasonable.

A second, two-dimensional model for the prediction of the point of instability is also presented by Cumpsty (1989). In this model, first proposed by Dunham in 1965, the derivative of the non-dimensional static pressure rise across a single stage of a compressor, $\psi_{TS} = (p_3 - p_{02}) / (\rho U^2)$ with respect to the local flow coefficient, $\phi = V_{x2}/U$ is used as a criterion for the determination of the range of unstable operation, as presented in Equation (2.18):

$$\frac{d\psi_{TS}}{d\phi} = \frac{1}{\rho U} \frac{d}{dV_x} (p_3 - p_{02}) > 0 \tag{2.18}$$

The stall point according to this criterion on a nondimensionalised compressor characteristic is shown in figure 2.3

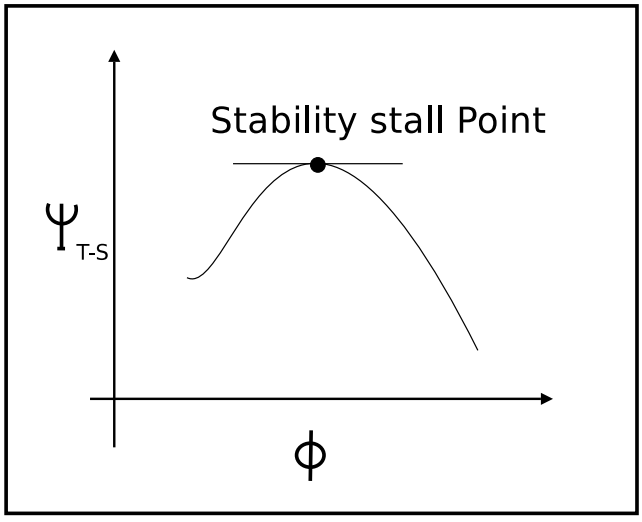

Figure 2.3: A fictitious total-to-static compressor characteristic with the 2-dimensional stability stall point indicated

2.5.3 Aungier's discussion of stall prediction criteria

Aungier (2003) begins his discussion on stall prediction techniques by referring to the method of Dunham, as described in the previous section. He states that this method is not very well suited to axisymmetric simulation of a compressor, as such methods can often not resolve the gradient with sufficient accuracy near the point of instability.

He then mentions the diffusion factor based stall criteria, and briefly explains that the weakness of such methods is that they predict blade stall, which does not necessarily lead to unstable compressor operation (i.e. full compressor stall).

He then briefly describes de Haller's criterion, stating that it is now generally accepted as an indicator of stall related to boundary layer separation, but adding that it is nonetheless a more accurate or reliable indicator of the onset of compressor stall. His descriptions of and comments on the diffusion factor and de Haller's stall criteria are very much in agreement with those made by Cumpsty (1989).

For prediction of the onset of compressor surge or stall, Aungier (2003) suggests the application of the following three criteria:

1. The gradient of the discharge pressure as a function of the flow coefficient approaches zero. This is very similar to the two-dimensional compressor stability criterion advocated in Cumpsty (1989), which has already been described.

2. The ratio between the displacement-thickness and momentum-thickness for the casing endwall boundary layer exceeds a certain value ($H_1 = 2.4$). This is referred to as *endwall boundary layer stall* in Aungier (2003), as it signifies that separation has occurred on the endwall boundary layer.

3. Stall is indicated by the blade row stall criterion developed by Aungier (2003). This method is described in some detail in section 3.3 on page 34 [see equations (3.4) and (3.5)], where its implementation is also explained. For now, it is sufficient to say that it is similar to Koch's criterion in that it uses blade row geometry to create an equivalent diffuser geometry, for which the peak pressure recovery rate (a condition which Aungier associates with blade row stall) can be determined. Aungier's correlation also makes allowance for blade loading effects by using the equivalent diffusion factor D_{eq} to adjust the limiting values for the correlation.

2.5.4 The transient compressor stability model of Moore and Greitzer

E. M. Greitzer and F. K. Moore have performed a large amount of research in the field of axial flow compressors, particularly compressor instabilities.
In Moore and Greitzer (1986*a*) they presented a model for the analysis of instabilities in a compressor system. This model has, as its basis, the one-dimensional model as presented by Cumpsty (1989), described in section 2.3, but incorporates elements of the two-dimensional model described by the same source. Although it will be seen that this model is not applicable to the present work, because of its transient, non-axisymmetric nature, it is important because it represents an attempt to unify the one- and two-dimensional models for compressor surge and stall as described by Cumpsty (1989). It also provides an indication of the sort of effects which are neglected by a steady-state, axisymmetric simulation technique such as the SCM or the MTFM.

The model consists of a compressor operating in a duct, which discharges into a large plenum chamber via the duct. The fluid in the plenum chamber is throttled to the environment via another duct. Because the plenum chamber is large relative to the volume of the duct, the pressure in the chamber is assumed to be uniform throughout the entire volume, and the flow velocity is assumed to be negligible at all points within the chamber. Where this model differs from the previous one-dimensional model is in the compressor model used. Variations are assumed to occur in fluid properties in both the axial and the circumferential or angular direction. This is based upon the assumption that the hub-to-tip ratio of the compressor is small, and allows some two-dimensional disturbances to be taken into account. Variations of fluid properties are, of course, also taken into account.

The set of equations used to model the compressor system thus has three parameters, namely the wheel angle θ, the nondimensionalised axial coordinate η, as defined in equation (2.19), and the nondimensionalised time unit, ξ, which is defined as shown in equation (2.20).

$$\eta = x/R \tag{2.19}$$

$$\xi = \frac{Ut}{R} \tag{2.20}$$

In these definitions, x is the axial distance, R is the compressor mean radius, U is the wheel speed at the mean radius, and t is the time.

After these quantities are defined, expressions for various types of disturbance in various parts of the compressor and the related system are derived, as well as expressions for properties such as the pressure rise across the compressor. Eventually

three equations are derived, a sufficient number for the system to be solved, namely the pressure rise equation for the system, given in equation(2.21), the mass balance equation for the plenum, given in equation(2.22), and the overall pressure balance of the compressor, given in equation 2.23:

$$\Psi(\xi) + l_c \frac{d\Phi}{d\xi} = \Psi_c(\Phi - Y_{\theta\theta})\, d\theta - mY_\xi + \frac{1}{2a}(2Y_{\xi\theta\theta} + Y_{\theta\theta\theta}) \tag{2.21}$$

$$l_c \frac{d\Psi}{d\xi} = \frac{1}{4B^2}\left[\Phi(\xi) - F_t^{-1}(\Psi)\right] \tag{2.22}$$

$$\Psi(\xi) + l_c \frac{d\Phi}{d\xi} = \frac{1}{2\pi}\int_0^{2\pi} \Psi_c(\Phi - Y_{\theta\theta})\, d\theta \tag{2.23}$$

In these equations, $\Phi(\xi)$ is the pressure rise coefficient. B is a parameter dependent upon the speed of sound, a_s, the average blade speed, U, the volume of the plenum chamber V_p and the volume of the compressor, $A_c L_c$:

$$B \equiv \frac{U}{2a_s}\sqrt{\frac{V_p}{A_c L_c}}$$

$F_T^{-1}(\Psi)$ is merely an expression for Φ_T, the flow coefficient for the throttling duct. l_c is the nondimensionalised form of the length of the compressor, obtained by dividing the actual length by the compressor mean diameter. Finally, $Y(\xi, \theta)$ is an unknown function in terms of two of the nondimensionalised parameters, and subscripts denote partial derivatives in terms of whichever nondimensional variable is used as the subscript.

A sufficient number of equations having been derived for the model to be solvable, Moore and Greitzer then go on to consider the cases of pure rotating stall and pure surge. For surge, they assume that there is no circumferential variation, that is no variation with respect to the wheel angle θ. This causes equations (2.21) and (2.23) to simplify to the form shown in equation (2.24).

$$\Psi(\xi) + l_c \frac{d\Phi}{d\xi} = \psi_c(\Phi) \tag{2.24}$$

For rotating stall, it is assumed that the plenum chamber pressure and the throughflow as averaged around the annulus of the compressor do not vary with time. In other words, $d\Psi/d\xi = 0$ and $d\Phi/d\xi = 0$. This simplifies equation (2.22) to the expression $\Phi = \Phi - T$. The function $Y(\xi, \theta)$ can then be assumed to be a wave function, dependent only upon the variable $\theta^* \equiv \theta - f\xi$, in which f is the frequency of the wave. After some manipulation, this yields new forms of equations (2.21) and

(2.23), as given in equations (2.25) and (2.26):

$$\mu \frac{d^3Y}{d\theta^{*3}} + mf\frac{dY}{d\theta^*} - \left[\Psi - \psi_c\left(\Phi - \frac{d^2Y}{d\theta * 2}\right)\right] = 0 \tag{2.25}$$

$$\Psi = \frac{1}{2\pi}\int_0^{2\pi} \Psi_c\left(\Phi - \frac{d^2Y}{d\theta^{*2}}\right) d\theta^* \tag{2.26}$$

In order to then obtain an actual stall prediction, a cubic compressor characteristic in terms of the dimensionless groups ϕ and ψ was assumed by the researchers.

The stall-simulation model presented in Moore and Greitzer (1986a) has now been described in brief. The model is highly complex, and requires that the details of the entire compressor system be known (such as the dimensions of ducts and plenum chambers), and not merely the the compressor geometry.

Furthermore, it makes a large number of assumptions about the nature of that system. It does not, however, make use of the axisymmetric flow assumption necessary for the use of throughflow methods. For these reasons it does not appear to be suitable for use in this project, although it does provide valuable additional insight into the mechanisms associated with surge and stall in an axial flow compressor. It is also the basis for much of the work being performed in the field of active stall control.

2.6 Numerical simulation of stalling

Perhaps because of the complex nature of flow within a stall cell, and possible difficulty in setting suitable boundary conditions, until fairly recently not as much work has been done on modelling stall phenomena by means of computational fluid dynamics software (CFD) as has been done by measuring flow conditions directly in actual physical compressors during operation. Much of the early work was done in areas such as cascade simulation research where two-dimensional simulations could be used.

This has, however changed considerably in the last few years, and an attempt to adequately describe all the research into stalling conducted with CFD would require considerably more space than is available in this document. It would also be somewhat beyond the scope of this work, as the techniques used for CFD simulation of stall inception are not generally applicable to use with axisymmetric inviscid throughflow methods. For this reason, only two examples are presented, chosen so as to provide examples of what can be accomplished using CFD.

Although the research described in Grüber and Carstens (2001) does not relate

specifically to the simulation of stall, the article gives a good idea of some of the complexities and problems which are associated with the use of CFD techniques in analysing flow in an axial flow compressor. The two researchers attempted to obtain a numerical, time dependent solution for the full Navier-Stokes equations describing flow around a vibrating 2-dimensional blade cascade. The researchers commented that the simulation was very sensitive to choice of initial conditions, and the choice of the parameter value in the turbulence model which they chose. They further found that the turbulence model required some minor modification in order to obtain good results. Another comment, made specifically about the Baldwin-Lomax turbulence model, but applicable to the entire field of CFD simulation is that the model

> ...cannot be used as a "black box" and that the results obtained with the model have to be interpreted very carefully.

A large portion of the research into the CFD simulation of stall is performed in conjunction with practical tests, and the data obtained from each was compared so as to verify the simulation results. This was the case in Pratap *et al.* (2005), who made use of a three-dimensional Navier-Stokes based CFD package to improve the design of a three-stage transonic compressor so as to try to predict and improve the surge margin. The approach used was to model the entire flow path, with multiple blades from each blade row, in three dimensions. Attention was paid to most of the important loss mechanisms, including shocks in the blade rows, tip leakage, boundary layers on end walls and corner-related losses at the hub and tip.

Performance predictions for the compressor agreed reasonably well with an experimentally determined performance map, and Pratap *et al.* (2005) states that much insight was gained in the redesign process through the use of three-dimensional simulation, but estimation of the surge margin was less accurate than was considered desirable. Interestingly, the inception of stall was judged by means of de Haller's criterion, which has already been described briefly. De Haller's criterion is, of course, easily implemented in axisymmetric throughflow simulation methods, but Aungier (2003) shows it to be unsuitable for prediction of stall in some transonic compressors, such as the NACA 5-stage machine.

Chapter 3

Implementation of stall prediction methods

The purpose of this chapter is to describe the implementation of the stall prediction criteria described in section 2.5. The models implemented were the diffusion factor criterion, de Haller's criterion, Aungier's blade row, boundary layer and system stability criterion, a simplified version of Dunham's stability criterion, and a similar static-to-static stability criterion. Each method is described mathematically, explained, and the algorithm used to implement it in the SUCC is presented.

With the exception of Aungier's boundary layer separation method, the criteria or models can be divided into two distinct families: those that consider each compressor blade row individually and determine whether it is stalled, and those that consider the overall compressor stability. The diffusion factor criterion, Aungier's blade row criterion and de Haller's criterion belong to the former group, while Dunham's stability criterion, Aungier's stability criterion and the static-to-static stability criterion belong to the latter group.

3.1 Diffusion factor criterion

This method is the oldest being used. It has generally been agreed that is is not a good indication of the onset of stall, and it has been superceded by prediction methods such as de Haller's method, or Koch's method. It has been included in the code primarily as a datum, or (perhaps more accurately) as a worst-case against which to compare newer prediction methods.

The diffusion factor, DF, and the equivalent diffusion factor, D_{eq}, are useful for the calculation of loss coefficients for blade cascades, and also provide indications as to whether or not a blade row is operating at its maximum loading or not. This

condition is considered to be achieved when $DF = 0.6$ or $D_{eq} = 2.2$. This condition was associated with the onset of stall by early turbomachinery researchers. From this, the diffusion factor stall criterion was derived.

Equation (2.7) is repeated here for convenience.

$$DF = \frac{1}{W_1}\left(W_1 - W_2 + \frac{\Delta W_\theta}{2\sigma}\right) \approx \frac{W_{max} - W_2}{W_1} \tag{3.1}$$

The equivalent diffusion factor was defined in equation (2.8), and is also presented again for convenience, together with Lieblein's correlation for it, as provided by Cumpsty (1989):

$$D_{eq} = \frac{W_{max}}{W_2} = \frac{\cos\kappa_2}{\cos\kappa_1}\left[1.12 + a\,(\Delta i)^{1.43} + 0.61\frac{\cos^2\kappa_1}{\sigma}\,(\tan\kappa_1 - \tan\kappa 2)\right] \tag{3.2}$$

This expression is dependent upon the parameter a, the value of which is dependent upon the blade profile type. The author, having some difficulty implementing this in a satisfactory way, elected to implement the diffusion factor limit stall criterion and not the equivalent diffusion factor limit. However, the value of D_{eq} is needed for the application of Aungier's blade row stall criterion, to be described in detail later. The author therefore used both expressions in equation(3.1) to arrive at an approximate expression for W_{max}. It was then a simple matter to substitute this expression into equation (3.2), providing an expression for D_{eq} shown in equation (3.3).

$$D_{eq} \approx \frac{W_1}{W_2}\left(W_1 - W_2 + \frac{\Delta W_\theta}{2\sigma}\right) + 1 = DF\left(\frac{W_1}{W_2}\right) + 1 \tag{3.3}$$

This equation, although approximate, appears to give results within the expected range for D_{eq}, where a value of approximately 2.2 indicates the limit of stable operations, which was sometimes exceeded near stall.

The weakness of the diffusion factor limit criterion is that what the method essentially predicts is the degree of separation of flow from a blade, or blade cascade, while flow separation on the surface of a compressor blade is not, in itself, sufficient indication of stall. Cumpsty (1989) and Aungier (2003) state that it has been experimentally demonstrated that a compressor can run with a significant amount of separation occurring on its blades without experiencing a seriously negative effect on its performance.

For the software package being developed, the diffusion factor method was implemented as follows:

1. Each blade row is examined in turn.

2. On each blade row, the diffusion factor is calculated from simulation data at a number of radii. These radii correspond with the position of the nodes on the computational grid used for simulating flow through the compressor.

3. The criterion is applied.

4. If the criterion indicates stall at a specific radius, then the radial position and the blade row for which stall occurred are recorded, and a message is printed indicating that stall has been predicted, and the position at which it has occurred.

5. If a certain percentage of the total area of a blade row is indicated to be in a state of stall, then the blade row is deemed to have stalled.

6. If a certain number of blade rows are deemed to have stalled by the process described described in the preceding steps, then the compressor as a whole is deemed to have stalled.

For the purposes of this investigation, it was found that one occurrence of stall on one blade row was sufficient to indicate the stall limit for all the test cases.

3.2 De Haller's criterion

De Haller's method for the prediction of the onset of stall in axial flow compressors is applied by comparing the pressure coefficients at the leading and trailing edges of a given blade with a known critical value. Because the total pressure coefficient is proportional to the velocity of the flow passing over the blade, this can be rewritten as a ratio between the leading and trailing edge relative velocities. This results in the expression found in Cumpsty (1989), Aungier (2003) and a host of other works touching on the subject of compressor stall: $W_2/W_1 > 0.72$.

Aungier (2003) and Cumpsty (1989) claim that this criterion is primarily of use for prediction of endwall boundary layer stall. Numerous researchers including Day (1993) have indicated that stall frequently occurs in this region, and most also agree that this method is a significant improvement over the older stall prediction methods based on a critical value of the diffusion factor. For the purposes of compressor design, this method has gained widespread popularity, probably because it combines simplicity with a generally acceptable level of accuracy.

For the software package being developed, de Haller's method was implemented in the same way as the preceding diffusion factor criterion, with de Haller's limit subtituted for the diffusion factor limit.

For the purposes of this investigation, it was found that one occurrence of stall on one blade row was sufficient to indicate the stall limit for all the test cases.

3.3 Aungier's blade row criterion

A number of stall prediction methods exist which attempt to regard the passage between blades in a compressor blade row as a diffuser. De Haller's criterion might be regarded as an early example of such thinking, while Koch's method attempted use the diffuser analogy more directly while making allowances for the effects of blade geometry.

Due to deficiencies in the existing methods, Aungier (2003) developed his own method based upon the work of Reneau *et al.* (1967) on straight two-dimensional diffusers. The latter source presents a graphical correlation between velocity ratios, area ratios and geometry for peak static pressure recovery in diffusers, a condition which corresponds to the onset of stall in axial flow compressor blade rows. Aungier obtained curve-fitted equations for this correlation. He then expressed the diffuser velocity and area ratios in terms more appropriate to the description of a compressor blade row and the flow passing through it. This is essentially how this criterion works, although Aungier found it necessary to adapt the method somewhat when the equivalent diffusion factor for the blade row has a value higher than 2.2, and a number of other corrections and limits were necessary.

According to Aungier's stall criterion, compressor stall will occur when the conditions described by equation (3.4) and (3.5) are fulfilled, and the ratio between the blade thickness and chord length $t_b/c \approx 0.1$.

$$W_{RE} < \begin{cases} \left[(0.15 + 11t_b/c) \,/\, (0.25 + 10t_b/c)\right] \,/ \\ \left[1 + 0.4\left[\theta\sigma/\left[2\sin(\theta/2)\cos\gamma\right]\right]^{0.65}\right] & \text{if } D_{eq} \leq 2.2 \\ \\ \left(\left[(2.2/D_{eq})^{0.6}\right](0.15 + 11t_b/c) \,/\, (0.25 + 10t_b/c)\right) \,/ \\ \left(1 + 0.4\left[\theta\sigma/\left(2\sin(\theta/2)\cos\gamma\right)\right]^{0.65}\right) & \text{if} D_{eq} > 2.2 \end{cases} \tag{3.4}$$

$$\theta\sigma/\left[2\sin(\theta/2)\cos\gamma\right] \geq 1.1 \tag{3.5}$$

Reneau *et al.* (1967) originally developed a graphical correlation between the geometry and performance of two-dimensional diffusers. Aungier (2003) obtained an equivalent numerical correlation, and adapted it to application to an axial compressor blade row. In other words, Aungier (2003) provides a method for obtaining a two-dimensional diffuser geometry that is equivalent to the blade row for which

the stall prediction is required. This criterion is thus in very much the same spirit as that of Koch as described in Cumpsty (1989), but is apparently more generally applicable, as Koch's criterion is said to require some adjustment to be applicable to a specific compressor. Aungier (2003) does, however, caution that this criterion does not provide an accurate indication as to whether stalling will occur if the rotational speed of the compressor is smaller than approximately 85% of the design speed. At lower speeds, the method may apparently predict stall under conditions for which an actual compressor may operate normally.

Figure 3.1 shows the most important blade row properties from which an equivalent diffuser geometry can be generated.

For the software package being developed, Aungier's blade row stall prediction method was implemented as follows:

1. Each blade row is examined in turn.

2. On each blade row, the equivalent diffusion factor is calculated from simulation data at a number of radii. These radii correspond with the position of the nodes on the computational grid used for simulating flow through the compressor.

3. The value of the equivalent diffusion factor, D_{eq}, is determined.

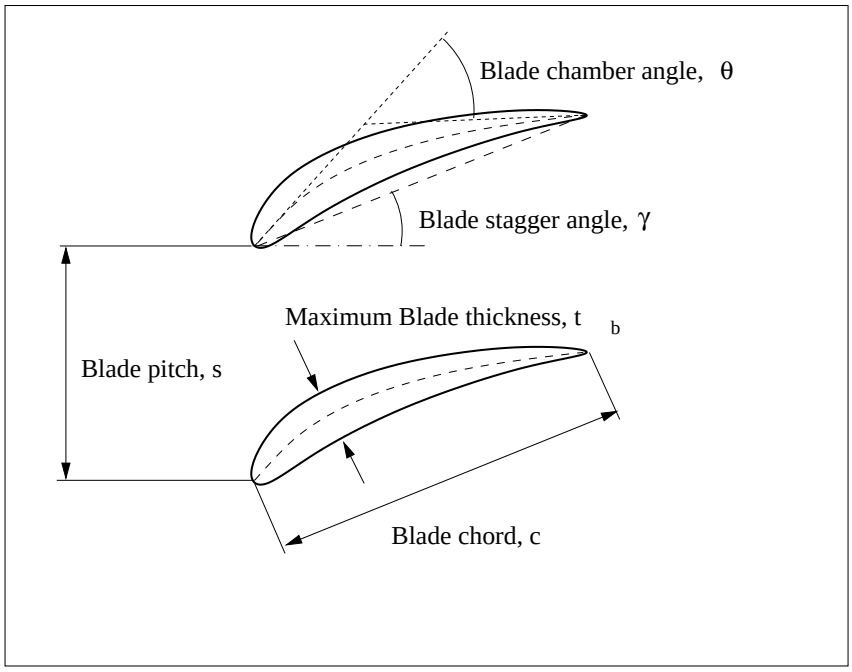

Figure 3.1: Some blade row geometry factors used for Aungier's blade row criterion

4. The value of the blade geometry denominator expression is calculated according to the left hand side of equation (3.5).This expression is equivalent to the ratio of the length to the inlet width of a two-dimensional diffuser.

5. If the value of the equivalent length-to-inlet-width ratio is less than 1.1, it is limited to 1.1 so that errors do not occur due to extrapolation of the curve fits used being too far outside the curve-fitted range.

6. The entire geometry-dependent expression with which the relative velocity ratio is to be compared is now calculated.

7. If the equivalent diffusion factor has a value higher than 2.2, then the equivalent length-to-inlet-width ratio to the left of the inequality (3.5) is multiplied by a correction-factor which is a function of the diffusion factor.

8. The criterion [equation(3.4)] is applied.

9. If the criterion indicates stall at a specific radius, then the radial position and the blade row for which stall occurred are recorded, and a message is printed indicating that stall has been predicted, and the position at which it has occurred.

10. If a certain percentage of the total area of a blade row is indicated to be in a state of stall, then the blade row is deemed to have stalled.

11. If a certain number of blade rows are deemed to have stalled by the process described in the preceding steps, then the compressor as a whole is deemed to have stalled.

For the purposes of this investigation, it was found that one occurrence of stall on one blade row was sufficient to indicate the stall limit for all the test cases.

3.4 Aungier's boundary layer separation criterion

Aungier (2003) describes three criteria which can be used to predict the onset of stall or surge in an axial flow compressor. This particular criterion is used for predicting endwall boundary layer stall. The mechanism leading to this type of stall is the separation of the boundary layer on the endwalls (often the casing because the flow speeds are higher there). Now a number of well-known criteria exist to determine when boundary layer separation occurs for various geometries. Aungier has chosen one involving the boundary layer shape factor. When the shape factor for

the boundary layer exceeds a certain value, (Aungier uses 2.4), the method indicates stall.

For the software package being developed, Aungier's boundary layer separation method was implemented as follows:

1. Each quasi-orthogonal on the computational grid is examined in turn.
2. The boundary layer shape factor value is extracted from the boundary layer model.
3. The criterion is applied on the hub and casing wall boundary layers at each quasi-orthogonal.

3.5 Dunham's characteristic gradient method

Dunham's method for stall and surge prediction is a method that relies on examining the overall performance of a compressor rather than that of one blade row at a time. It is described in some detail by Cumpsty (1989), and some of the work by Moore and Greitzer (1986*a*) was heavily influenced by it. As implemented, the method utilises a compressor characteristic obtained when the total-to-static load coefficient ψ_{TS} is plotted against the flow coefficient for a given compressor. The point on this characteristic where the gradient is equal to zero is found, and the conditions of compressor operation at that point are then those under which stall or surge might be expected to occur.

For the purposes of the software package being developed, Dunham's characteristic gradient method was implemented as follows:

1. For each speed, a new node is added to a link-list containing all the speeds, and a pointer to a link-list which will contain the flow coefficients and corresponding total-to-static load coefficients for all the different massflow rates at that speed.
2. If the simulation at a given speed and massflow rate yield results, then the flow and total-to-static load coefficients are calculated, and added to the link-list for the current speed.
3. Once the simulations for all the speeds and massflow rates are complete, the flow coefficients, total-to-static load coefficients and total-to-total pressure ratios for all the characteristics are extracted from the link-list and written to 1-dimensional arrays.
4. The arrays are then sorted using the Quicksort Algorithm.

5. A curve-fit is then performed on the data in the three arrays, for the purposes of determining the point of zero gradient on the total-to-static load coefficient versus flow coefficient characteristic. If more than one point of zero gradient exist, then the point corresponding to the higher flow coefficient is used, as this should correspond to the point at which stall is initiated.

6. Having determined the flow coefficient, total-to-static load coefficient and total-to-total pressure ratio at the stall point, the percentage of the design massflow rate at the stall-point is calculated from the flow coefficient. The stall massflow rate percentage and pressure ratio are calculated as these are the output of the SUCC in its present form, and also because these values are somewhat more useful than the nondimensionalised coefficients when considering a real compressor, and comparing experimentally determined and numerically simulated values.

Two types of curve-fit have been implemented:

1. A quadratic curve-fit approximation is applied to each possible group of three consecutive points on the characteristic, starting from those corresponding to the highest flow coefficient, until a point of zero gradient is found which corresponds to a flow coefficient within the region across which the interpolation was performed. In other words, the final point of zero gradient must occur between the highest and the lowest of the three points used for the curve-fit. If no such point is found, then a message is displayed stating this. If such a point is found, then a second quadratic interpolation between the flow coefficient and the total-to-total pressure ratio is used to obtain a value for the pressure ratio at that point.

   The point of zero gradient for a quadratic equation of the form $f(x) = ax^2 + bx + c$ is, of course, obtained from elementary algebra as $x = -b/2a$ at the point of zero gradient for a parabola. This value was then substituted back into the quadratic equation to obtain the value of the fitted function.

2. A parametric three-dimensional cubic spline-fit is applied to the flow coefficient, total-to-static load coefficient and pressure ratio. The gradient is once again determined in terms of the flow and load coefficients; the pressure ratio is only included in the spline to facilitate interpolation of the corresponding value of this quantity. In order to determine the point at which the gradient of this parametric curve is equal to zero, it should be remembered that for a curve defined by the parametric equations in t, $x = f(t)$ and $y = g(t)$, $\frac{dy}{dx} = \frac{dy}{dt} / \frac{dx}{dt}$. This implies that the gradient of the the parametric curve is equal

to zero when the numerator is equal to zero, that is when $dy/dt = 0$, or the denominator tends toward positive or negative infinity, that is $\lim dx/dt \rightarrow \infty$. Now, because a cubic spline is being used, the forms of $x = f(t)$ and $y = y(t)$ are cubic polynomials of the form $f(t) = b_1 + b_2 t + b_3 t^2 + b_4 t^3$. Thus the expression for the derivative of both x and y is a quadratic polynomial in t. Since dx/dt is a quadratic polynomial in t, it has a finite value for any finite value of t, and the possibility that $\lim dx/dt \rightarrow \infty$ can be discarded, and it is only necessary to calculate the roots of the derivative of y, if they exist, to find all the possible points of zero gradient on the curve. As stated previously, for the cubic spline fit used, $y = b_1 + b_2 t + b_3 t^2 + b_4 t^3$, so the derivative is $dy/dt = b_2 + 2b_3 t + 3b_4 t^2$. The roots of this quadratic equation are

$$t = \frac{-2b_3 \overset{+}{-} \sqrt{4b_3^2 - 12b_2 b_4}}{6b_4} \tag{3.6}$$

The discriminant of this equation is first evaluated to ensure that the quadratic equation has real roots. The absolute value of the coefficient b_4 is also checked to ensure that it is not close to zero, as this would adversely affect the accuracy of the solution. If this coefficient has a value which is smaller than the threshold, the third-order term in the polynomial is ignored, and the polynomial is treated as a parabola with only one point of zero gradient.

The points of zero gradient are calculated for each successive chord segment from that corresponding to the highest flow coefficient to the lowest, until a zero-point is found which lies within the chord segment bounds. As the derivative is of quadratic form, there are potentially two zero-points, as indicated in equation (3.6). If both zero-points are real, then the point corresponding to the higher flow coefficient is evaluated first. If no suitable points are found, the a message is displayed stating this.

Details of the cubic spline fit used can be found in Rogers and Adams (1976).

3.6 Static-to-static characteristic gradient method

This method differs from Dunham's method, described in section 3.5, only in that the static-to-static load coefficient is used in lieu of the total-to-static coefficient which Dunham suggests. In all other ways, including the method of implementation in the software, it is identical to the aforementioned method.

3.7 Aungier's gradient method

Aungier (2003) describes three methods for stall and surge prediction. Two have already been described. The remaining method is very similar to Dunham's method, described in section 3.5. The principle difference is that Aungier's method makes use of the characteristic formed by the discharge pressure verses the flow coefficient. As in Dunham's method, the point on the characteristic at which the gradient is zero is taken as an indication of the conditions under which stall or surge will occur. The method for the implementation of this method in the software software is also virtually identical.

Chapter 4

Results

Four test cases were used in verifying stall prediction results. These consisted of NACA 5-stage, 8-stage and 10-stage compressors used as test cases by Aungier (2003), as well as the Rofanco low pressure compressor. All test cases were simulated using both the streamline curvature method (SCM) and the matrix throughflow Method (MTFM), as implemented in the SUCC. The results for all test cases are presented and points of interest discussed. The effect of various factors such as the layout of the computational grid, boundary layer calculation, and radial loss smoothing are also presented and discussed.

4.1 Convergence criteria, relaxation factors and computational times

The convergence criteria applied to the MTFM and SCM were similar in principle, but different in detail. For the MTFM, the convergence criterion used was that the normalised maximum change in the stream function at all points on the computational grid, should not exceed the convergence tolerance. For the SCM, the convergence criterion used is that the maximum value of the change in position of a streamline on any quasi-normal, normalised by the length of that quasi-normal, should be less than the convergence tolerance at all points on the computational grid. For all test cases, the convergence tolerance for both throughflow methods was set to 10^{-5}. This value was chosen after some experimentation showed that it offered no noticeable loss in accuracy over the value initially used, 10^{-8}, but allowed an appreciable saving in computation time. Furthermore, the former value was identical to the smallest tolerance used for the simulations conducted using the SCM described in Gannon and von Backström (2000). The convergence tolerance for the boundary layer blockage modelling method in the SUCC is based upon the

RMS value of the change in boundary layer positions along the compressor in the axial direction. It has a default value of 10^{-4}. It was found to be impractical to decrease the size of this tolerance to any degree, as there appeared to be a limit on the accuracy of the boundary layer method not far below this value, particularly for the NACA 10-stage machine, which had a larger number of quasi- orthogonals than any of the other test cases.

The relaxation factor used for most of the MTFM simulations was 0.3, although it was sometimes decreased to 0.1 in order to improve the stability of the process for the NACA 5- and 10-stage simulations, particularly when the number of streamlines in the computational grid was increased from 5 and 7 respectively to 9. The relaxation factor for the boundary layer modelling method was somewhat smaller. A value of 0.1 was usually used, but this was decreased to 0.05 when a large degree of numerical instability was evident. The streamline curvature method did not require an explicitly defined relaxation factor, as it makes use of the numerical damping strategy advocated in Novak (1967) and Aungier (2003).

In all cases, streamlines were initially placed a constant distance apart in the radial direction. This was the method used in the grid generation component of the SUCC, which was not written by the author. It was left unmodified, as it is very simple, and give similar streamline positioning to the approach favoured by Aungier (2003) and Novak (1967), that is, placing streamlines so that equal sectional areas exist between stream tubes in the radial plane.

All simulations were performed on a Pentium 3 733 MHz machine with 256 Mb of RAM. Execution time for the convergence of the solution of the flow field through the NACA 5-stage compressor for one set of operating conditions with five streamlines was recorded to compare performance. It was found that when the MTFM was used without boundary layer blockage modelling, the computation time was approximately 30 seconds, after which time approximately 300 iterations had been performed. The relaxation factor used was 0.3. The computation time for the SCM without blockage modelling was rather lower: approximately 11 seconds, after which time approximately 100 iterations had been performed. When boundary layer blockage was calculated, with a relaxation factor of 0.05 the MTFM (which was once again used with a relaxation factor of 0.3) required over 40 seconds, and performed 426 iterations, whereas the SCM required approximately 45 seconds but performed only 152 iterations. For the NACA 8-stage compressor model with 7 streamlines, and a boundary layer blockage relaxation factor of 0.05, the MTFM required 85 seconds to run 226 iterations, using a relaxation factor of 0.1. The SCM took rather longer to converge, at 140 seconds, and 163 iterations. The reason why the SCM has rather longer run-times, particularly for compressors with a higher number of blade

rows, is probably because an inner iterative loop must be run to convergence on each quasi-orthogonal, and each blade row requires at least two quasi-orthogonals to be adequately defined.

4.2 Experimental data

The experimental data used for comparison with simulation results for test cases was not obtained by this researcher. For this reason, the reader is directed to Kovach and Sandercock (1954), Geye *et al.* (1953) and Budinger and Thompson (1952) for detailed information on the experimental techniques used to obtain performance data for the NACA 5-stage, 8-stage and 10-stage compressors respectively. Roos (1990) and Roos (1995) describe the experimental technique used for the Rofanco compressor test bench. However, as this research was conducted locally, a very brief description of of the techniques used will be provided when this test case is discussed.

4.3 The Rofanco 3-stage compressor

The Rofanco 3-stage compressor is a low speed, low pressure ratio machine. The University of Stellenbosch has one such machine as a test bench. The test bench no longer has the original blades, as these were destroyed in testing some years ago, and have been replaced with NACA-65 profile blades in three repeating stages. In addition, the machine has no inlet guide vanes; consequentially the blades are set in such a way that the reaction of the machine is relatively high, approximately 0.85. The design speed of the machine is 3000 rpm, the nominal total-to-total pressure ratio across the machine is approximately 1.02, and the design massflow rate is approximately 3.5 kg/s It is an appealing first test case, as it has a very simple geometry, and comparatively low flow speeds and Mach-numbers (the Mach-number at the first-stage rotor tip is approximately 0.2). However, the low flow speeds can also introduce low Reynolds-Number effects which can prove difficult to model accurately.

At this point, some explanation of the method by which experimental data was obtained should be presented. Roos (1990) made use of total pressure rakes and static pressure tappings at the compressor inlet and outlet and a venturi flow meter at the compressor outlet. The total pressure rakes consisted of lengths of small diameter tubing with one end sealed, and equally spaced holes drilled in a line along the length, which was approximately equal to the annulus. This rake design records average total pressure across the annulus. Roos (1995) recorded the velocity distributions behind each blade row in the test bench by use of a cobra probe which was traversed across the annulus. The experimental setup was similar to that of Lewis (1989). A HBM pressure transducer was used to record pressures seen by the probe, while an angular potentiometer was used to determine the inclination of the probe. In both cases, a 60-tooth wheel with a magnetic transducer was used to

measure the rotational speed of the shaft.

The computational grid used for this test case is shown in figure 4.1. The grid was created from geometric data obtained by measurements taken on the actual machine by numerous researchers, including Lewis (1989), Roos (1990) and Roos (1995). A quasi-orthogonal was placed at the leading and trailing edge of each rotor and stator blade row. Three quasi-normals were placed between the compressor inlet and the leading edge of the first rotor row, and four between the trailing edge and the last exhaust. Five streamlines were used for this grid, including those on the hub and shroud of the compressor. Because of the simplicity and low flow speeds in this compressor, it was possible to run simulations on it with a considerably larger number of streamlines without loss of stability or a great increase in computational time. This had no noticeable effect on the results obtained.

The SUCC was used to generate total-to-total pressure ratio characteristics for 70%, 80%, 90% and 100% of the design speed. Simulation of the compressor operation was performed using the MTFM and the SCM with and without boundary layer blockage modelling. However, it is known that a boundary layer occupying a small but significant fraction of the annulus area is present even at the inlet, due to preliminary investigations conducted with a five hole probe before a failure of the data capture hardware ended this line of investigation. Consequentially, results obtained without the use of boundary layer blockage modelling were expected to be somewhat unrealistic. This was the case, as the predicted pressure ratios were higher than indicated by the experimental data. Use of blockage modelling decreased the error somewhat, and the MTFM with boundary layer blockage modelling gave reasonably good agreement with compressor characteristics obtained experimentally by Roos (1990). This experimental data was used in preference to that obtained by the

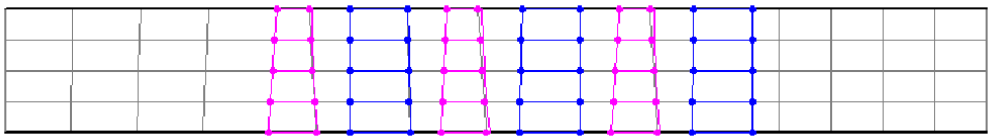

Figure 4.1: Computational grid for the Rofanco 3-stage compressor

author due to the poor quality of the latter.

The blockage area fraction at the inlet was not known, so a trial-and-error approach was used to determine what effect this would have on the accuracy of the prediction. The value eventually used was 1% on hub and shroud. However, the simulation for this machine was found to be highly insensitive to this value, though. The results of the simulations using MTFM and SCM, with boundary layer blockage effects included, are shown in figures 4.2 and 4.3 respectively. The boundary layer blockage model can be seen to introduce a small discontinuity into the characteristics. This was also observed for the NACA 5-stage compressor.

The only stall criterion which indicated stall for this machine was that of de Haller. The experimental stall limit was taken as the point with the highest pressure ratio on each characteristic, as suggested by Aungier (2003). The indicated stall line was slightly conservative, but offered reasonable agreement with experimentally-determined values. The error between the predicted and experimentally determined characteristics was greatest at higher pressure ratios and lower massflow rates on each characteristic. Under these conditions, the simulation predicts a higher pressure ratio than that indicated by the experimental results. It should be noted that it is under these conditions that stall is most likely to occur. The errors appear to be greater on the lower speed characteristics. This may perhaps be due to the low Reynolds number effects which were mentioned previously, and which are not presently included in the SUCC. Fortunately, the error is not very large. Table 4.1 give the percentage error, defined as the normalised difference between the experimental and simulated stall points on each characteristic. The percentage error in the combined column is the square-root of sum of the squares of the percentage errors for the massflow rate and pressure ratio.

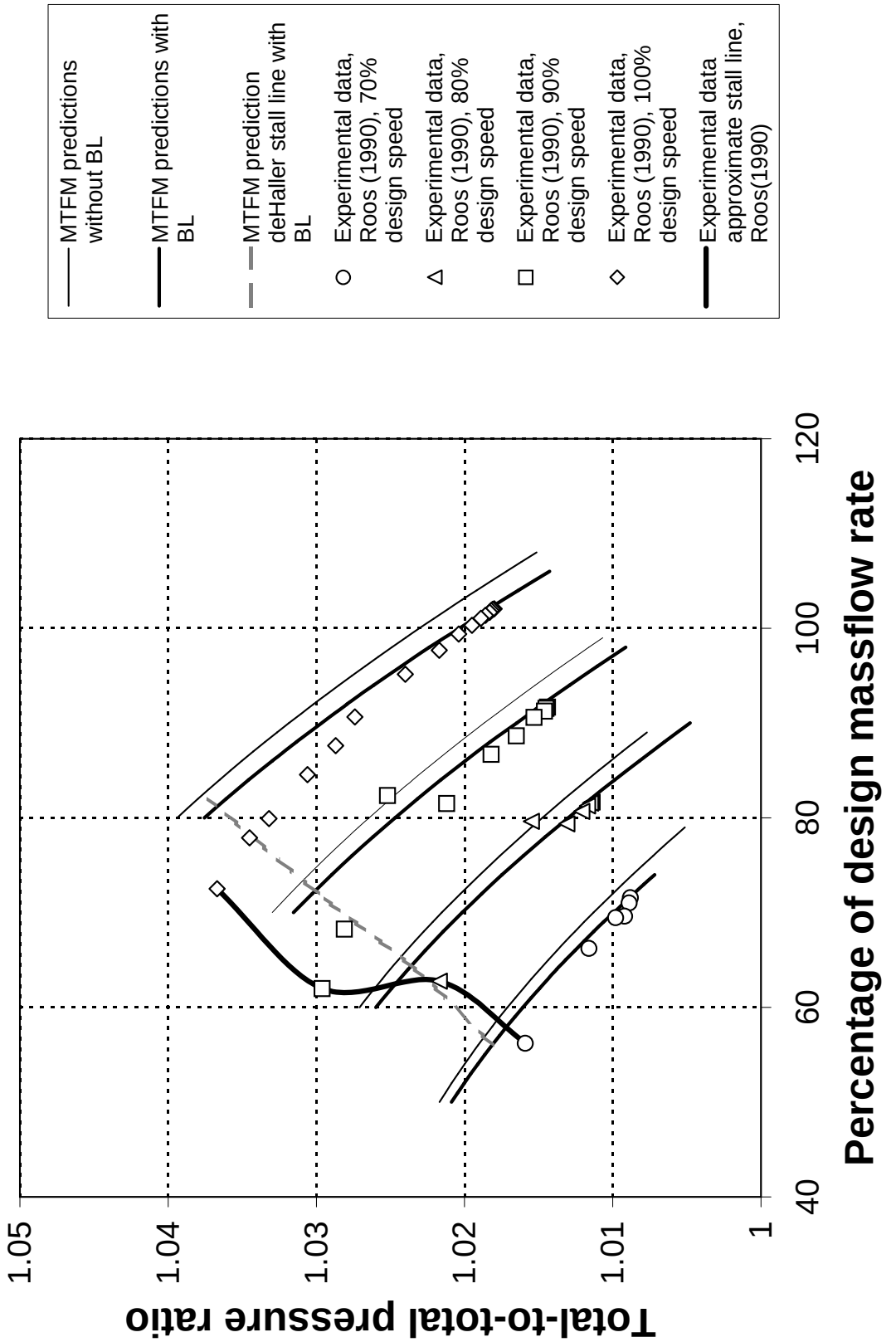

Figure 4.2: Predicted and experimental characteristics for the Rofanco 3-stage compressor with and without boundary layers using MTFM

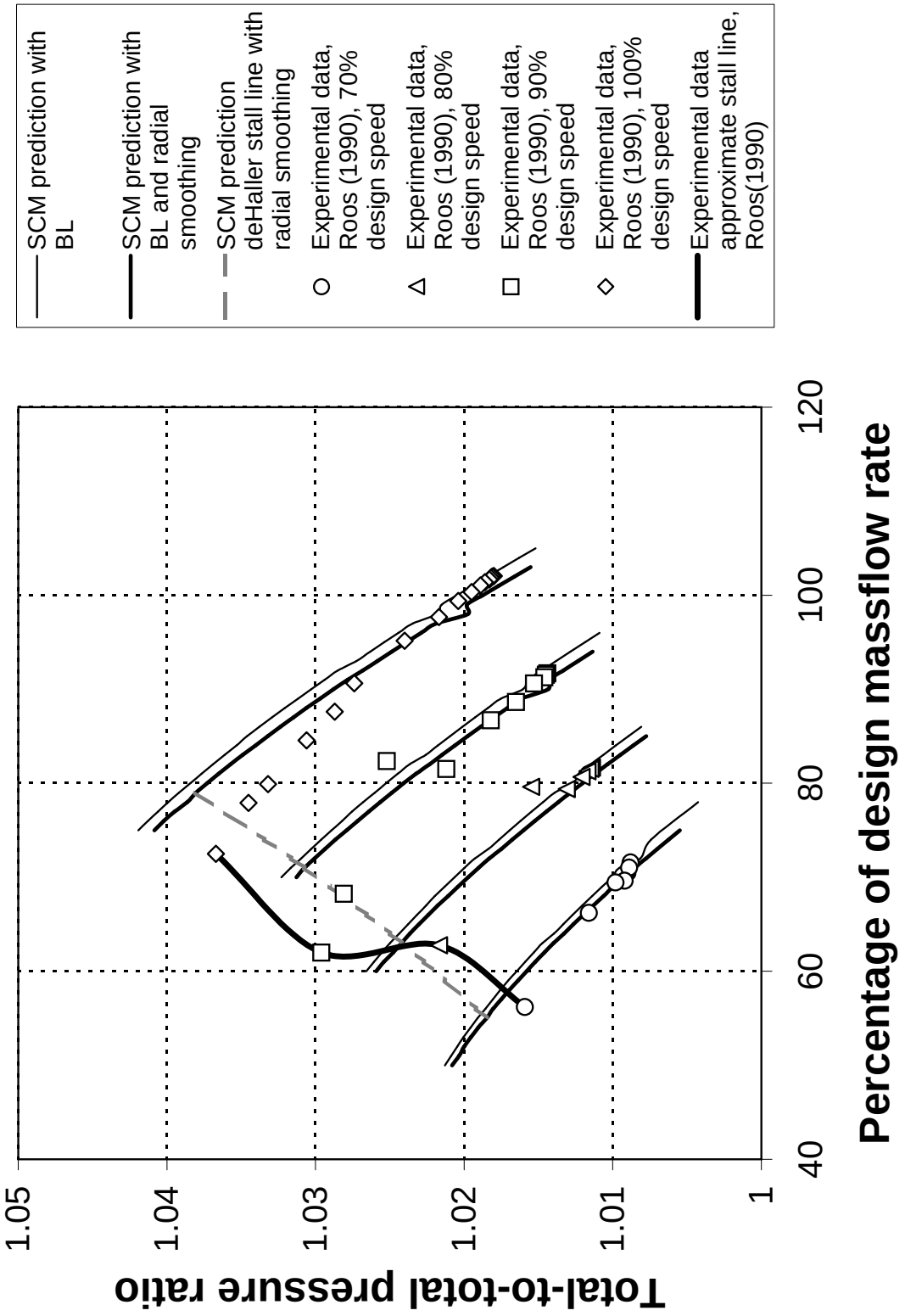

Figure 4.3: Predicted and experimental characteristics for the Rofanco 3-stage compressor using SCM with smooothing

4.4 The NACA 5-stage compressor

The NACA 5-stage compressor was one of the three compressors used by Aungier (2003) as test cases to demonstrate the accuracy of his axial flow compressor simulation strategy, including his stall prediction model. It is a transonic machine, but it has a small number of blade rows, which allows for its simulation within a relatively small amount of time, but it exhibits many properties useful for the testing of a simulation code, namely choke and blockage effects, high Mach-number flow (the relative Mach-number at the tip of the first-stage rotor is approximately 1.2 at design point) and a reasonably high pressure ratio near its operating point. The compressor has no inlet or exit guide vanes, and thus has a high degree of reaction, the stators returning the flow to an approximately axial direction.

The computational grid used for most of the simulations is shown in figure 4.4. Five streamlines were used, including those on the compressor annulus. Seven quasi-normals including the one at the compressor inlet were placed before the leading edge of the first blade row, and six including the one at the compressor exhaust were placed at after the trailing edge of the last blade row. A quasi-normal was placed at the leading and trailing edge of each blade row. These quasi-orthogonals are important because the blade row model is applied on them. They are indicated by the slightly thicker lines with dots on them in figure 4.4.

Total-to-total pressure ratio characteristics for the NACA 5-stage compressor were obtained from 40% to 100% of design-speed, in increments of 10%. However, only the 80%, 90% and 100% characteristics were examined in any detail, as these were the characteristics for which experimental and simulated data were available. Results were obtained using the MTFM and the SCM with and without boundary

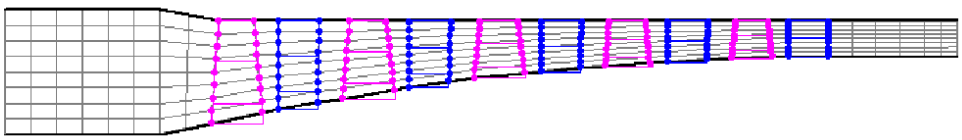

Figure 4.4: Computational grid for the NACA 5-stage compressor

layer blockage modelling. These results are compared with experimental data from Kovach and Sandercock (1954) in figure 4.5. Results obtained by use of the MTFM and SCM, with boundary layer blockage effects, are shown in figures 4.7 and 4.8 respectively. The results with radial smoothing on blade rows are compared with those obtainable without it and the experimental data in figure 4.10, showing how small a change in results is caused by the use of radial smoothing. The effect of increasing the number of streamlines from 5 to 9 is shown in figure 4.9. The result can be seen to be a slight improvement in the agreement between the simulated and the experimental results, both in the shape and position of the characteristics, and in the stall prediction obtained.

Results obtained using the MTFM and SCM without blockage modelling exhibit similar trends to those of the test data, though, of course, the pressure ratios predicted were rather high for the corresponding massflow rate, and thus not of much use for stall prediction. Use of blockage modelling corrected this to a great degree, particularly for the 100% and 80% design speed characteristics. The blockage model did, however introduce some error into simulation, which appears as a small discontinuity on all characteristics. On the 80% characteristic obtained with the MTFM, agreement with the experimental data and Aungier's simulation data was reasonably good, while at design speed slightly better agreement with the experimental data was obtained with the SUCC than was obtained by Aungier. This was not so on the 90% characteristic, however. For that speed Aungier's results agreed well with the experimental data at higher pressure ratios, whereas those generated by the SUCC were somewhat low. It is probably coincidental that the 90% line calculated with the MTFM without boundary layer blockage effects corresponds closely with the experimental data for that speed. It can also be seen that the SCM produces slightly less accurate results than the MTFM for all speeds shown. It is also interesting to note that agreement between experimental data and simulation results obtained by Thomas (2005) was probably worse for the 90% characteristic for both the NACA 5-stage compressor than other characteristics. This could reflect a shortcoming in the blade row loss models or boundary layer loss models used in both simulations.

From figure 4.9 the effect of increasing the number of streamlines from 5 to 9 can be seen to be a slight increase in accuracy. The increase in the computational time associated with this change is, however, quite large. Figure 4.6 shows the predicted efficiencies compared with the experimentally obtained ones. Once again, better agreement is obtained for the 100% and 80% characteristics than for the 90% speed characteristic. The predicted efficiency for that characteristic is considerably lower than that indicated by the experimental data. This suggests that one of the components of the losses, quite possibly that relating to blade row loss mechanisms,

is unrealistically high. A similar error was observed in the total-to-total pressure ratio characteristic for the NACA 10-stage compressor prediction for the 90% line, but not for the efficiency on that line, as will be seen later.

Stall prediction results for this compressor displayed a number of interesting points. Most notable was the extreme conservatism displayed by de Haller's criterion. For the three characteristics discussed, this criterion predicted stall over significant portions of multiple blade rows for the entire operating range modelled. This result would seem erroneous, had it not also been reported by Aungier (2003) for this machine.

The other extreme was displayed by the diffusion factor stall criterion for the characteristic at 100% of design speed. This criterion predicted stall at considerably lower massflow rates and higher pressure ratios than those indicated by the test data. The error involved was not as large as that exhibited by de Haller's criterion, however, and agreement with the experimental points on the 80% line was actually slightly better for this criterion than Aungier's blade row criterion.

Stall as predicted with Aungier's criterion for the MTFM prediction agreed well with both experimental data and Aungier's predictions, particularly at design speed. The stall point for the experimental data may be taken as the point having the highest pressure ratio on each characteristic. The stall prediction for the characteristic at 90% of design speed was as accurate as could be expected, given the error in the prediction of compressor performance near stall at that speed. For the 80% of design speed characteristic, Aungier's criterion gave slightly more conservative results for the onset of stall than those suggested by the experimental data and Aungier's simulation results. However, the accuracy of Aungier's blade row criterion is never significantly less than that of the diffusion factor, and is considerably better for the 100% characteristic.

Stall prediction results were not obtainable with the SCM until radial entropy smoothing was applied on the trailing edges of all blade rows. Once this was done, Aungier's criterion began to detect stall, and the SCM was able to simulate a slightly wider range of operations of the compressor on most characteristics. This was a fairly dramatic argument for the importance of radial mixing models. The stall lines thus obtained were similar to those obtained while using the MTFM at design speed, but were rather conservative on the 80% characteristic.

Of the remaining stall prediction methods implemented, none of the stability-based stall criteria nor the boundary layer stall criterion gave any predictions. The former is easy to explain, as none of the characteristics showed any sort of peak or even any significant flattening. The latter is less easily explained. The most probable explanation is that the form of stall indicated by this criterion simply did

not occur. Aungier makes no mention of any results obtained by the use of this criterion after having mentioned it.

Tables 4.2, 4.3 and 4.4 list the error in the predicted stall point according to each criterion, for each characteristic. All errors are relative to, and as a percentage of the experimentally determined value. The percentage in the combined column represents the square-root of the sum of the squares of the percentage errors for massflow rate and pressure ratio.

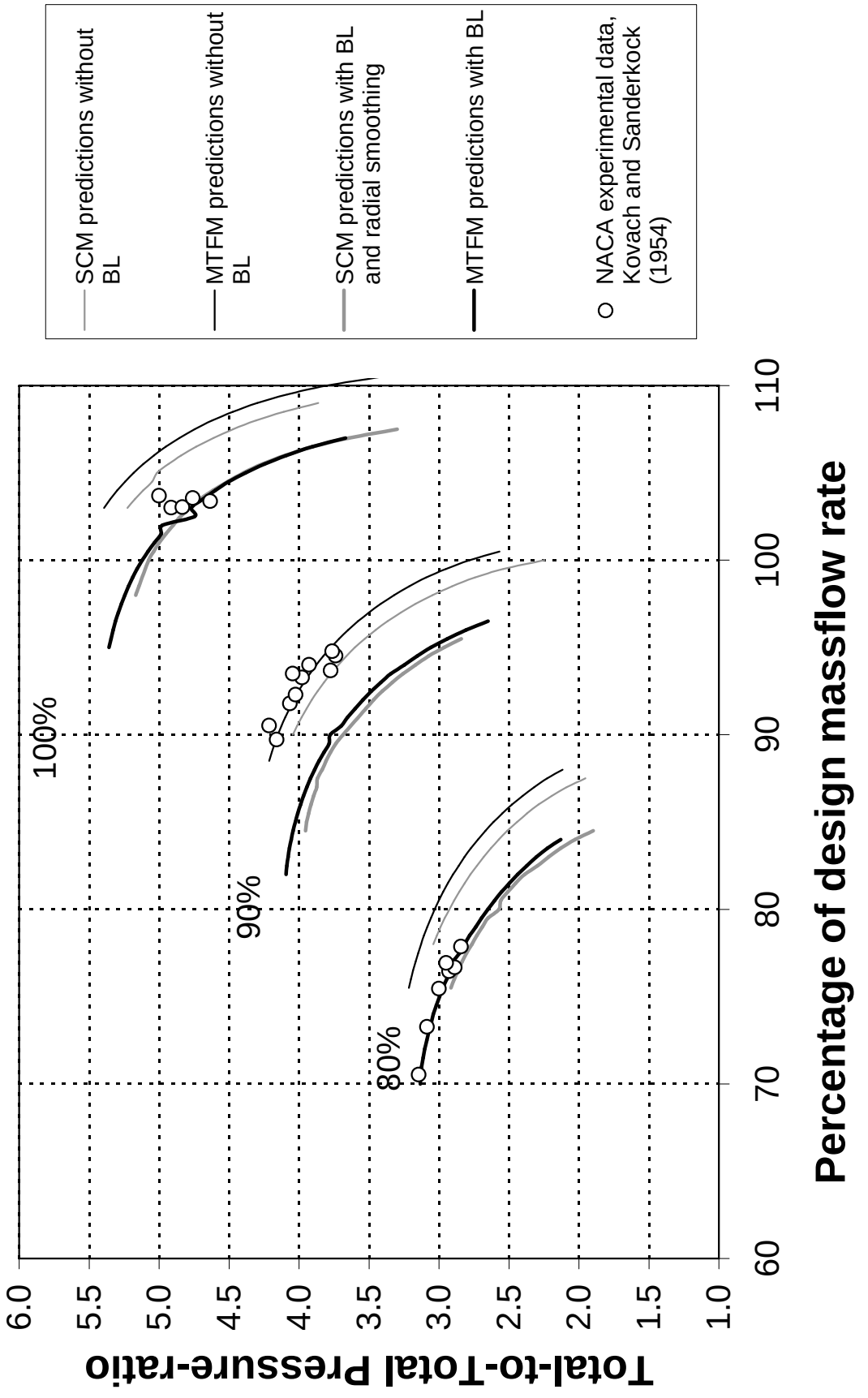

Figure 4.5: Predicted characteristics for the NACA 5-stage compressor with and without boundary layer blockage effects

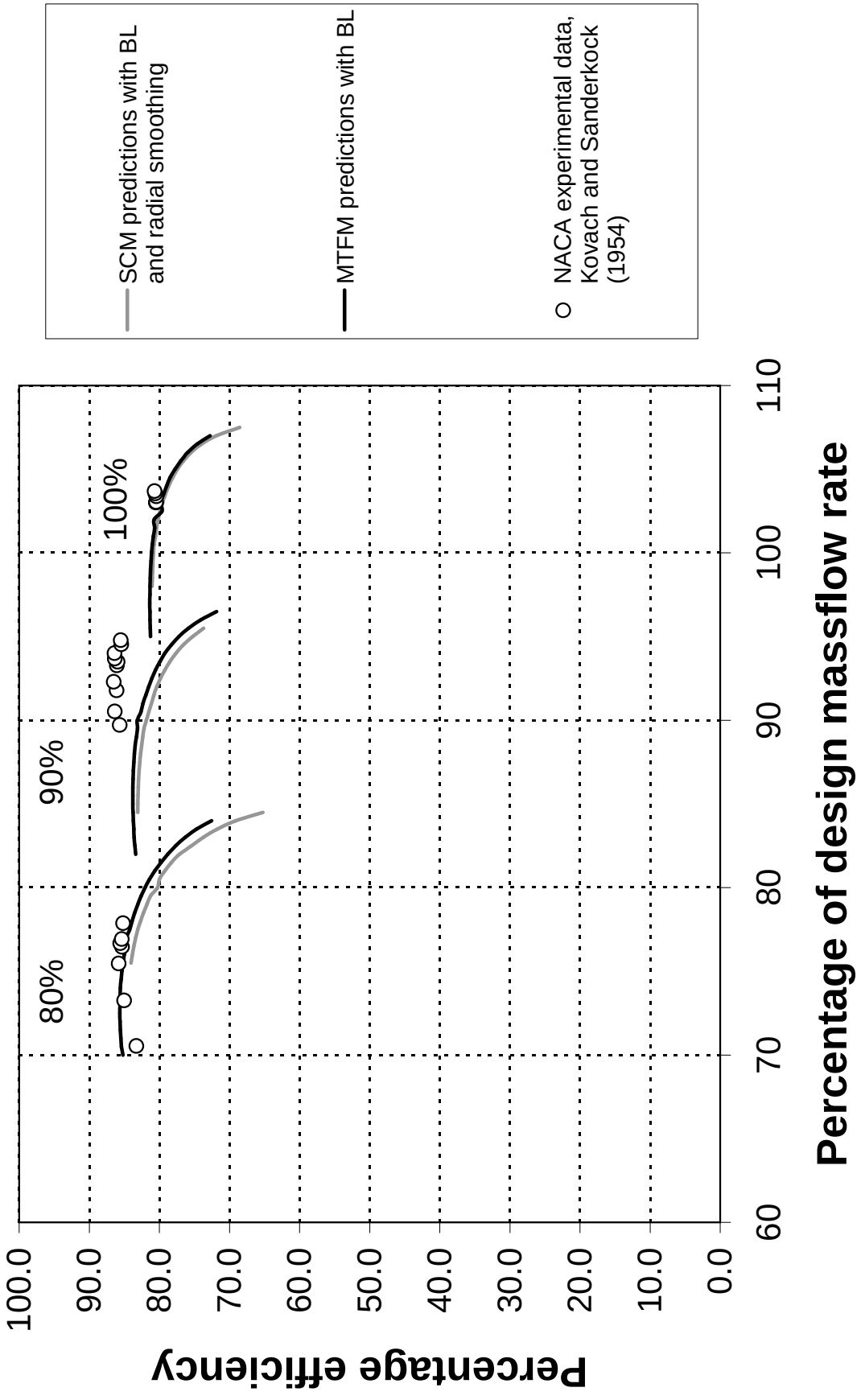

Figure 4.6: Predicted efficiency characteristics for the NACA 5-stage compressor

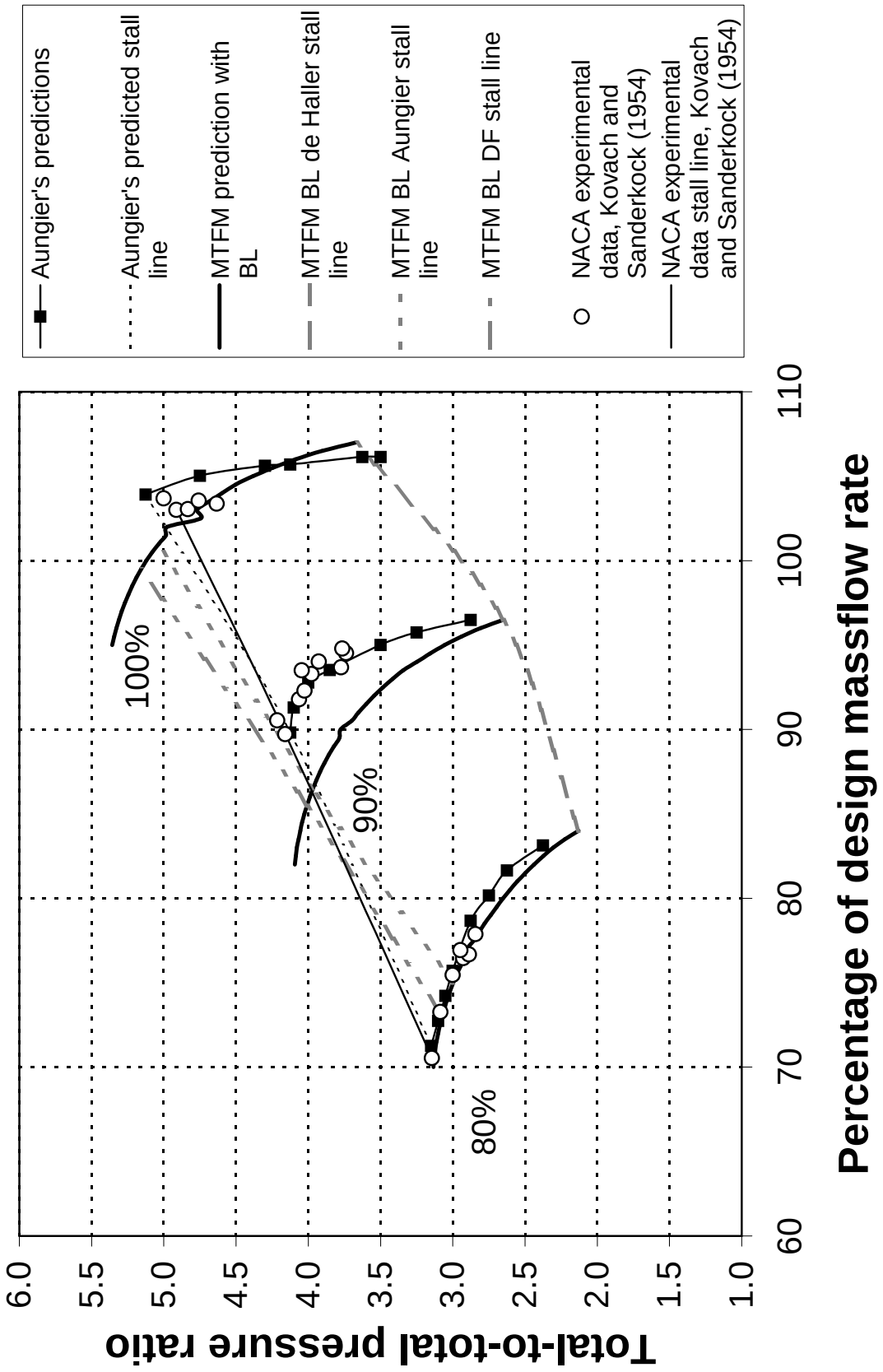

Figure 4.7: Predicted and experimental characteristics for the NACA 5-stage compressor using MTFM

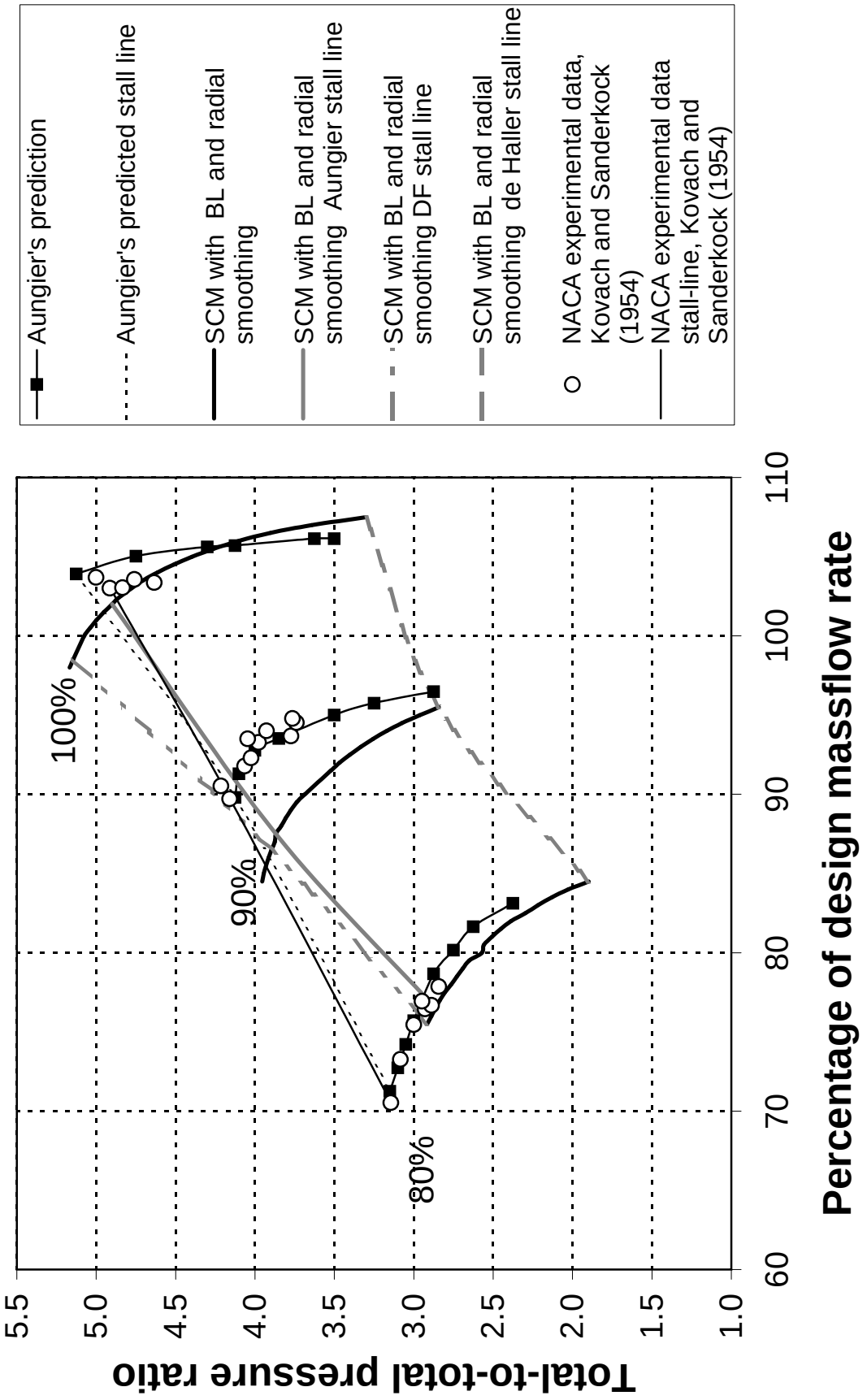

Figure 4.8: Predicted and experimental characteristics for the NACA 5-stage compressor using SCM with radial entropy smoothing

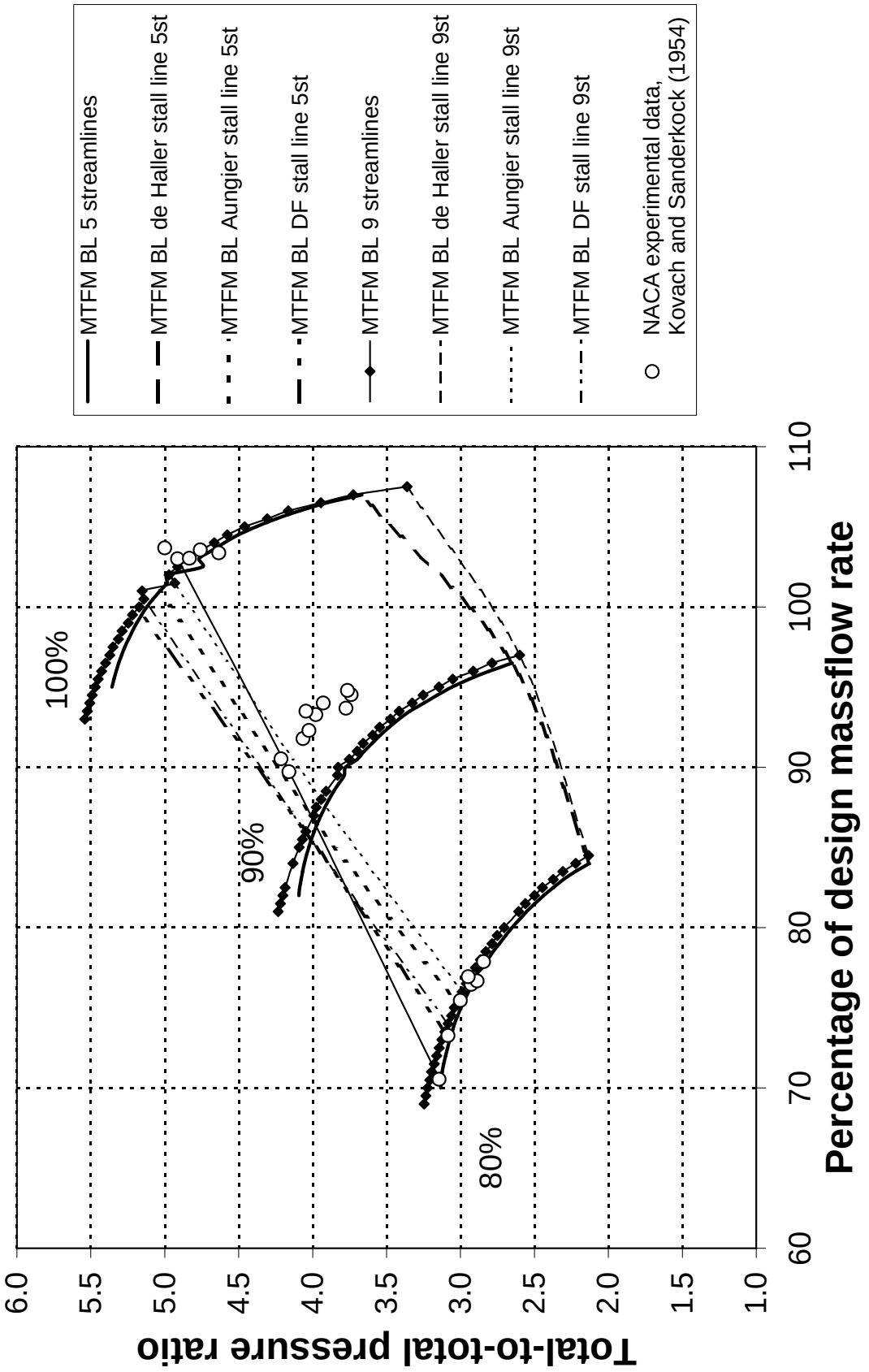

Figure 4.9: Predicted and experimental characteristics for the NACA 5-stage compressor using MTFM with 5 and 9 streamlines

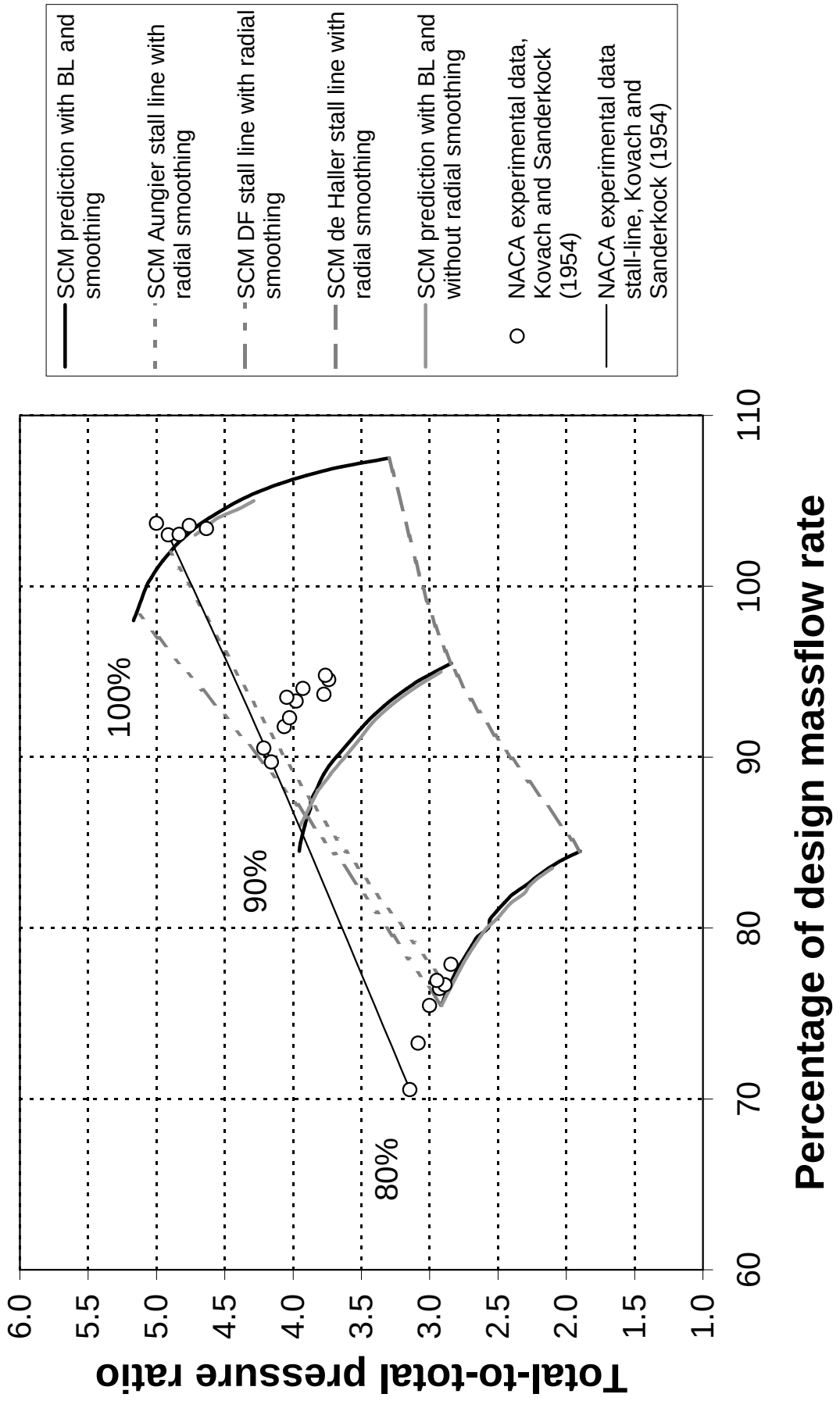

Figure 4.10: Predicted and experimental characteristics for the NACA 5-stage compressor using SCM with and without radial entropy smoothing

4.5 The NACA 8-stage compressor

The NACA 8-stage compressor, like the 5-stage machine discussed in the preceding section, is a transonic machine. No results could be obtained using blockage modelling at any rotational speed, therefore this machine was only simulated without blockage. However, the results thus obtained were remarkably accurate, particularly at and near design speed. There was a somewhat larger error for lower-speed characteristics, and once again, agreement between characteristics predicted with the SUCC MTFM code was worst at high pressure ratios.

Figure 4.11 shows the computational grid used for simulations of this machine. There are five streamlines, and five quasi-normals before the leading edge of the first blade row. Quasi-normals were placed on the leading and trailing edges of each blade row, as with all other test cases. The blade rows are indicated by the thicker lines with dots on the nodes of the computational grid which lie inside the blade rows. This compressor has an exit guide vane row, and initially only one quasi-orthogonal was placed after the trailing edge of that row, at the compressor exhaust. The exit was lengthened and more quasi-normals were added in an attempt to improve the stability of the model. However this appeared to have no effect. It can also be seen that in the grid displayed, there are still multiple quasi-normals inside the outlet guide vane row, these were later removed, and the leading and trailing edge quasi-orthogonals more carefully positioned, which improved numerical stability slightly. The results obtained using the MTFM without boundary layer blockage are shown in figure 4.12. The experimental data was obtained from Geye *et al.* (1953).

De Haller's stall criterion was once again the most conservative, and consequentially the least accurate, although the error in this case was considerably smaller than for the 5-stage compressor. For this machine, the shortcomings of the diffusion factor began to become apparent; while it provided accurate estimations of the stall limit on some characteristics, it failed totally on others. Aungier's stall criterion was comparatively inaccurate when the first occurrence of stall was used as an indicator;

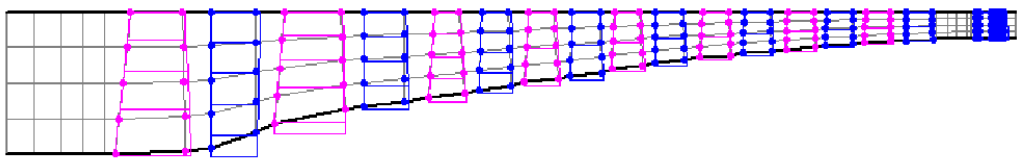

Figure 4.11: Computational grid for the NACA 8-stage compressor

when the "25% of two blade rows" stall line was used, it showed good agreement with the test data, particularly at higher rotational speeds. A similar trend was observed when the NACA 5-stage compressor was simulated. However, these results were rendered superfluous once more accurate results were obtained by application of boundary layer blockage modelling.

No tables of error percentages have been included for this test case as the few results obtained cannot be considered to represent the operation of this compressor realistically, and thus are not meaningful other than that they exhibit similar trends to the more successfully simulated NACA 5-stage compressor.

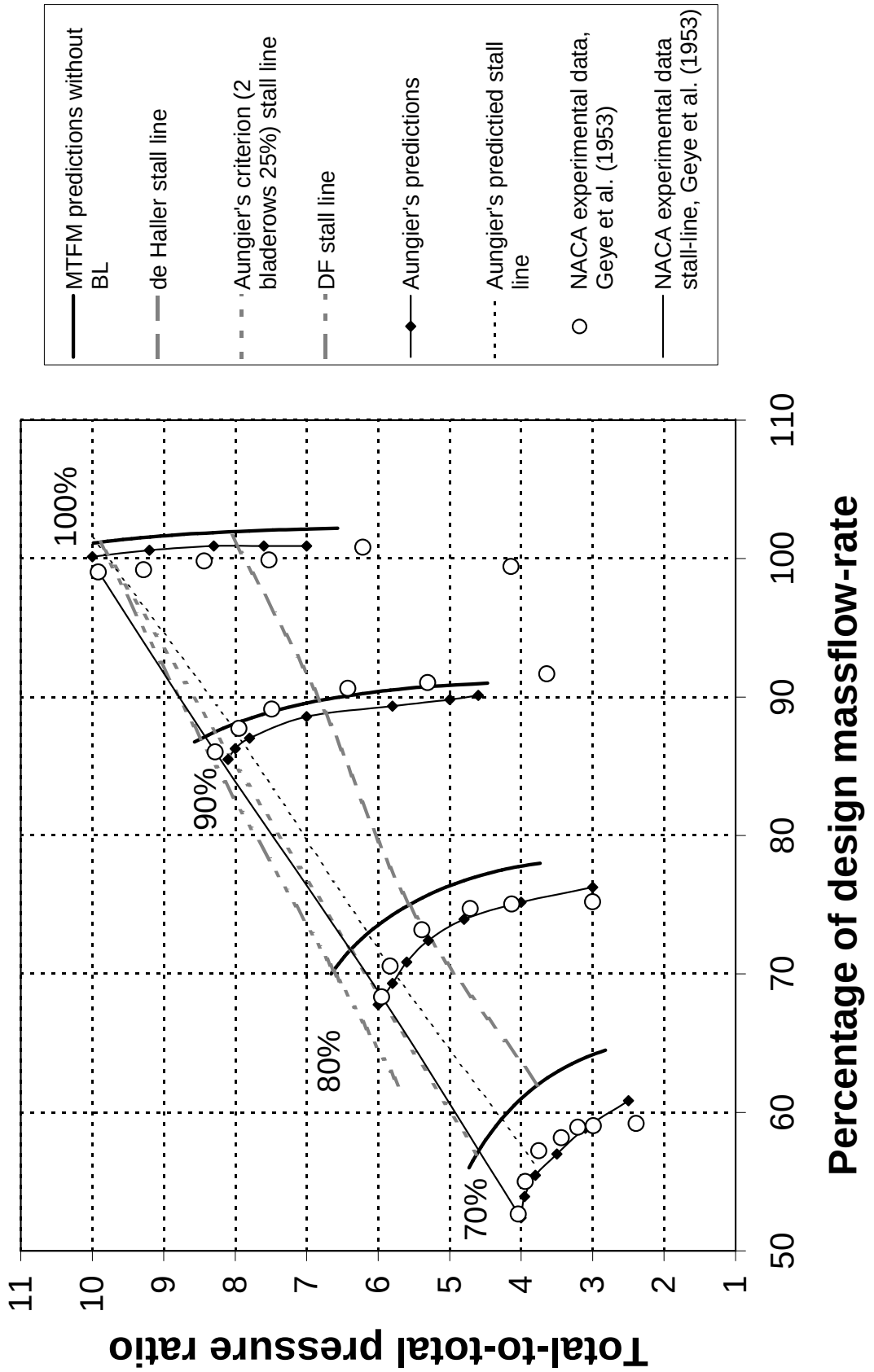

Figure 4.12: Predicted characteristics for the NACA 8-stage compressor without boundary layer blockage effects

4.6 The NACA 10-stage compressor

The NACA 10-stage compressor is the most conservative design of the three NACA compressors examined. It is a subsonic machine (with a relative Mach-number of approximately 0.7 at the tip of the first rotor row when operating at design point), and thus less susceptible to high Mach-number related loss mechanisms which can be difficult to predict accurately. Consequently, one would expect good agreement between simulation results and those obtained experimentally by previous researchers. This is in fact the case.

The computational grid for the NACA 10-stage compressor is displayed in figure 4.13. It can be seen that the machine has a very simple geometry. It should also be noted that this machine has inlet guide vanes, unlike all the preceding test cases. The number of streamlines used in the grid was seven; somewhat higher than that used in the NACA 5- and 8-stage machines. This was possible because of the greater numerical stability of this compressor.

The characteristics for 80%, 90% and 100% of the design speed of approximately 10000 RPM were examined for both the MTFM and the SCM. The experimental data was obtained from Budinger and Thompson (1952). Following the advice of Aungier (2003), the experimental stall limit can be taken as the point with the highest pressure ratio on each characteristic.

As can be seen in figure 4.16, excellent agreement was obtained for the 100% line between the simulation results from SUCC using MTFM and the experimental data available. As with the 5-stage machine discussed in section 4.4, agreement with experimental data was worst on the 90% speed characteristic, though quite good on the 80% line. However, on all characteristics, the difference was smallest near the stall point, which ensured comparatively good stall prediction results. There was a

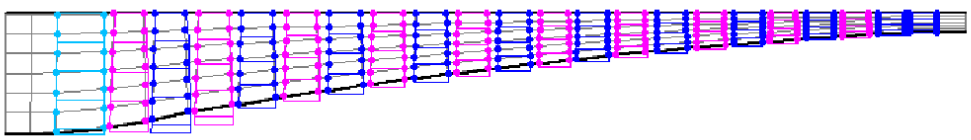

Figure 4.13: Computational grid for the NACA 10-stage compressor

small but noticeable difference between results obtained with the MTFM and those obtained with the SCM. Figure 4.17 reveals that results obtained with the SCM were somewhat less accurate. In figure 4.19, radial smoothing can clearly be seen to have no significant effect, other than to increase the range of operational conditions for which the simulation is numerically stable.

An attempt was also made to determine the effect of refining the grid by increasing the number of streamlines from seven to nine. The results of this effort are shown in figure 4.18. It was not possible to increase the number of streamlines used with the SCM, as the code became unstable when the number of streamlines became too large. The figure therefore only shows results obtained with the MTFM. Somewhat surprisingly, the results appear to be slightly less accurate for the 80% and 100% characteristics, and correspond slightly better with the experimental data for the 90% characteristic. Efficiency predictions for this machine were uniformly somewhat high when compared with experimental values, as shown in figure 4.15. This was also observed by the original creator of the SUCC package, and even occurred on the troublesome 90% characteristic, unlike the efficiency prediction for the NACA 5-stage compressor at 90% of design speed. This can possibly be accounted for by the omission of a model for some secondary loss mechanisms, possibly relating to leakage at the blade tips and stator roots and tips.

Stall prediction results for this machine were remarkably accurate. At design speed de Haller's and Aungier's criterion gave virtually identical results. Aungier's criterion was actually slightly more conservative than de Haller's criterion, although the difference between the two and the error as compared with experimental data was small. Indeed, both methods gave a considerably better estimation of the stall-point on the 80% line than was obtained by Aungier, and with the exception of the 90% line, agreement between the experimental data available and results from the SUCC was generally better than that achieved by Aungier. This is particularly true of the stall prediction for the 80% speed characteristic, of which Aungier comments that his prediction does not agree well with the experimental data. The diffusion factor criterion predicted stall at considerably lower massflow rate and higher pressure ratio than was indicated by the experimental data. The error was proportionally larger than the error for this criterion for the NACA 5-stage compressor. Possible ramifications of this will be discussed in the following chapter.

Tables 4.5, 4.6 and 4.7 list the error in the predicted stall point according to each criterion, for each characteristic. All errors are relative to, and as a percentage of the experimentally determined value. The percentage in the combined column represents the square-root of the sum of the squares of the percentage errors for massflow rate and pressure ratio.

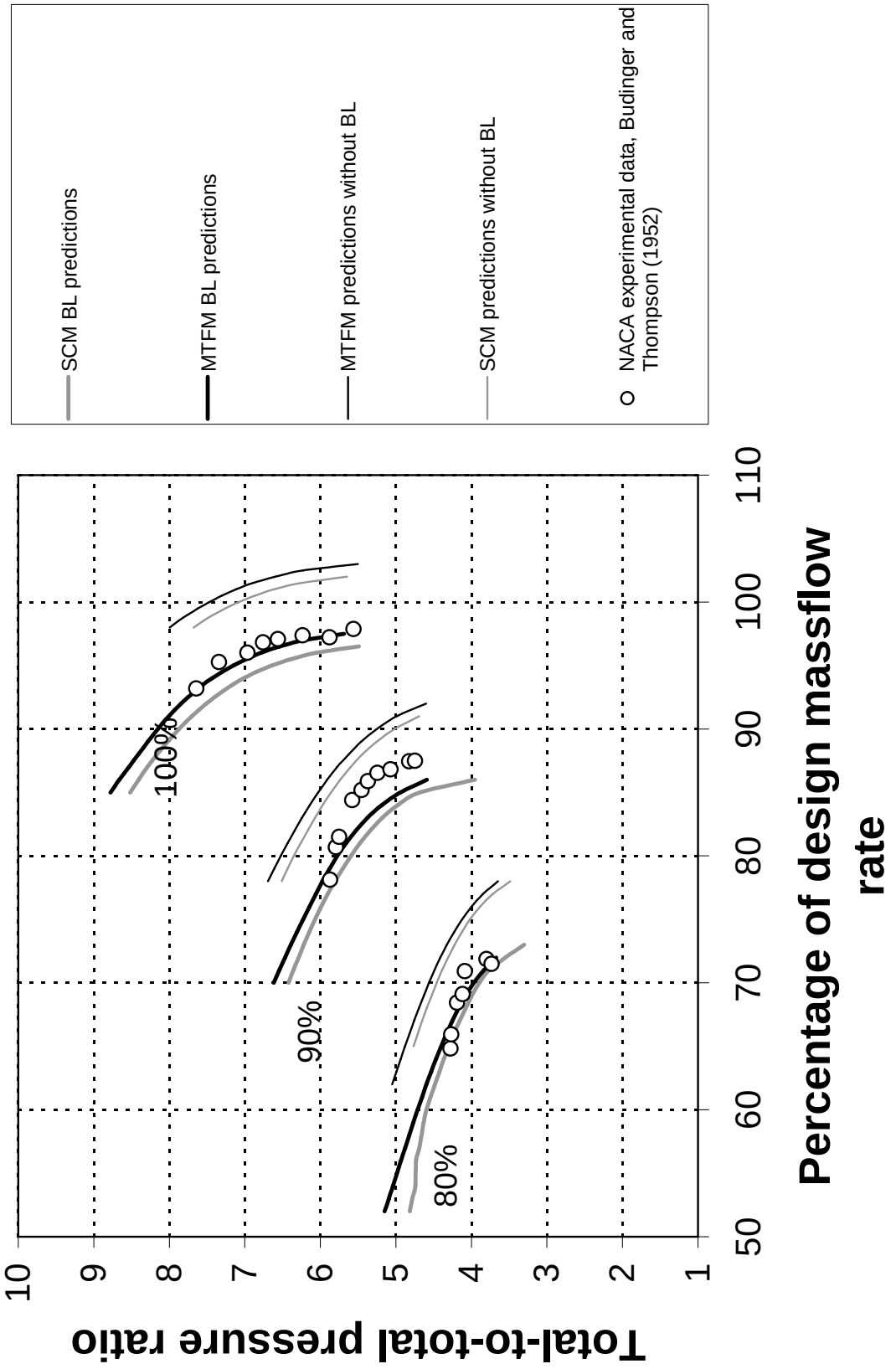

Figure 4.14: Predicted characteristics for the NACA 10-stage compressor with and without boundary layer blockage effects

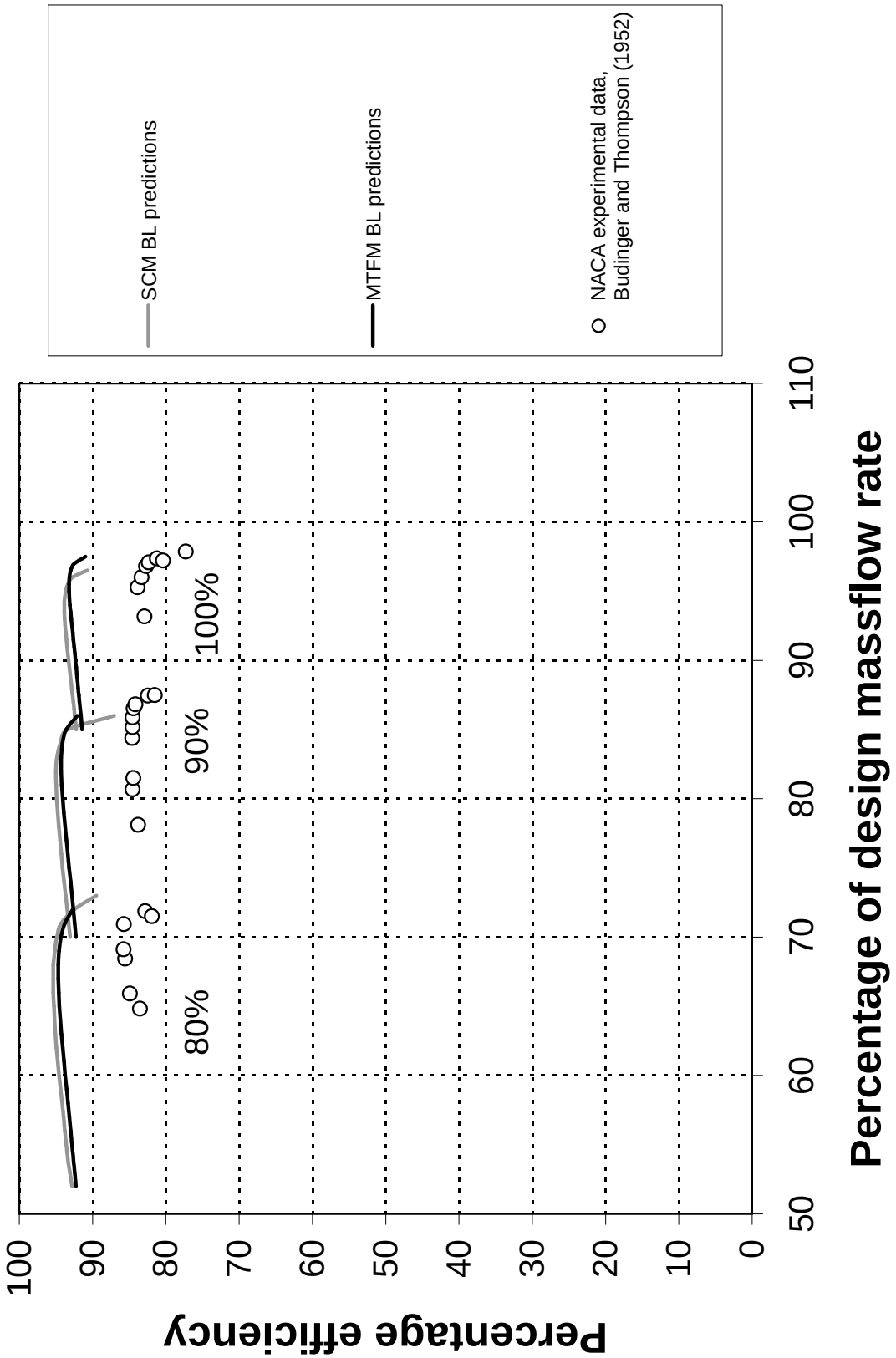

Figure 4.15: Predicted efficiency characteristics for the NACA 10-stage compressor

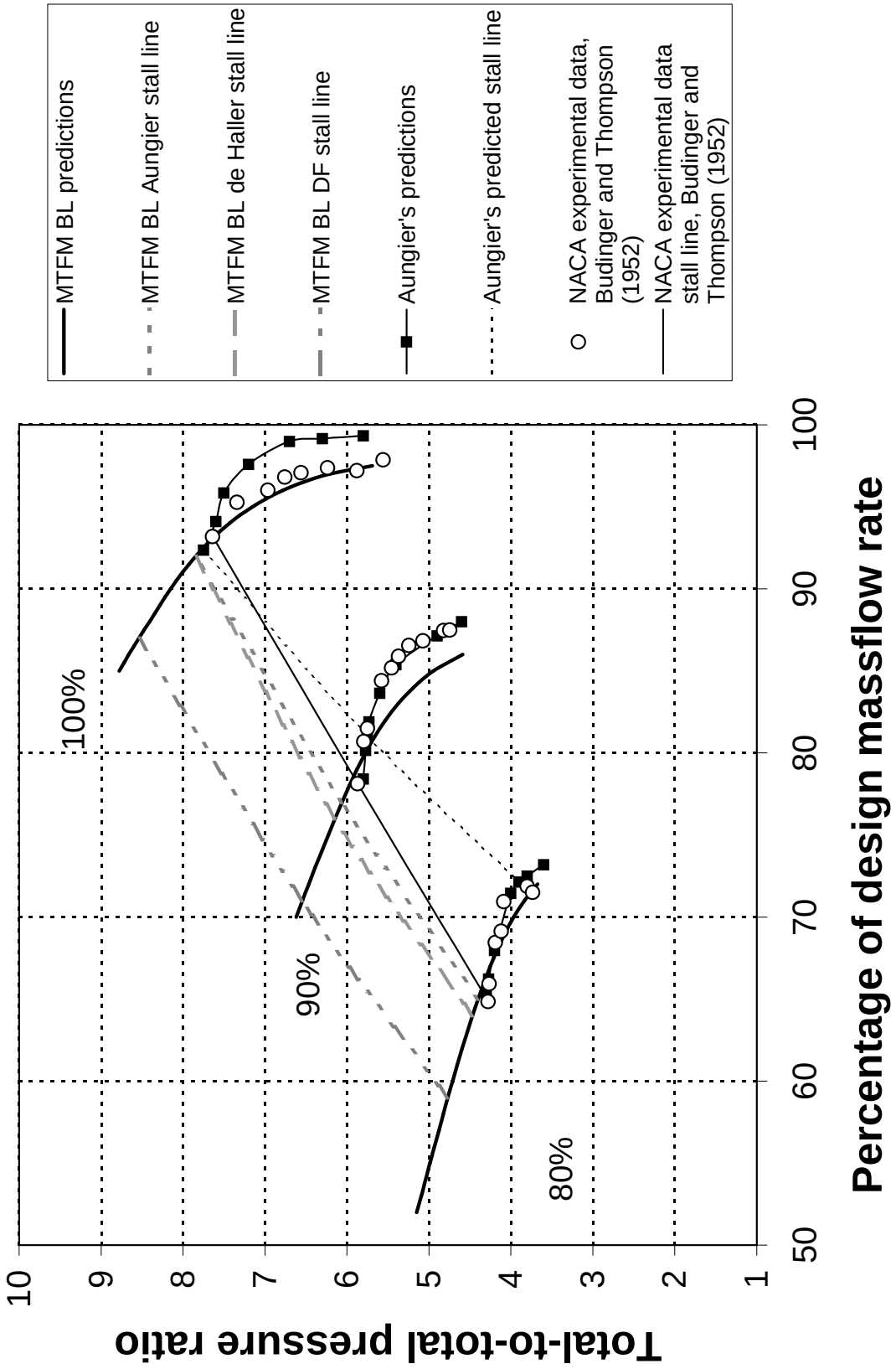

Figure 4.16: Predicted and experimental characteristics for the NACA 10-stage compressor using MTFM

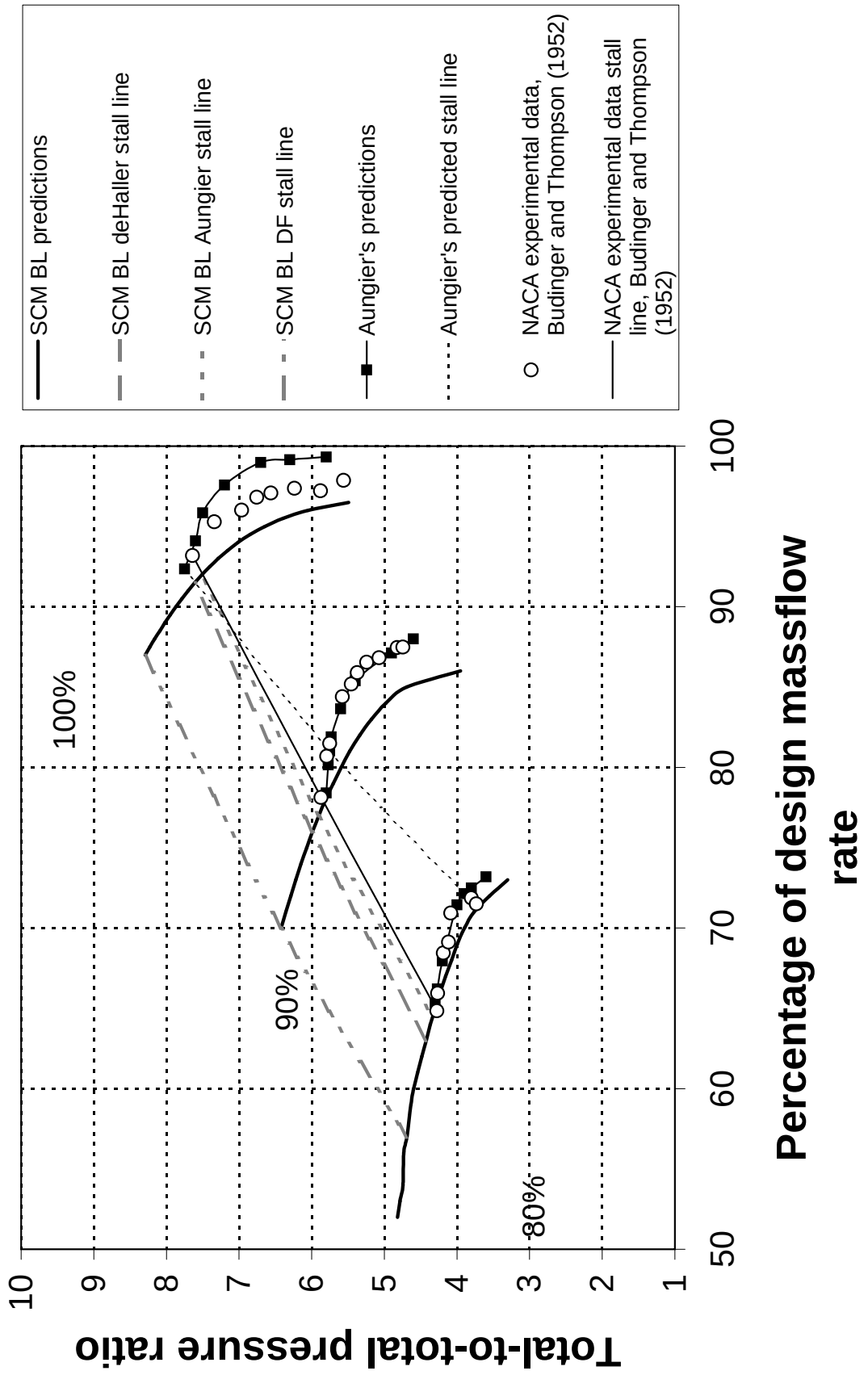

Figure 4.17: Predicted and experimental characteristics for the NACA 10-stage compressor using SCM

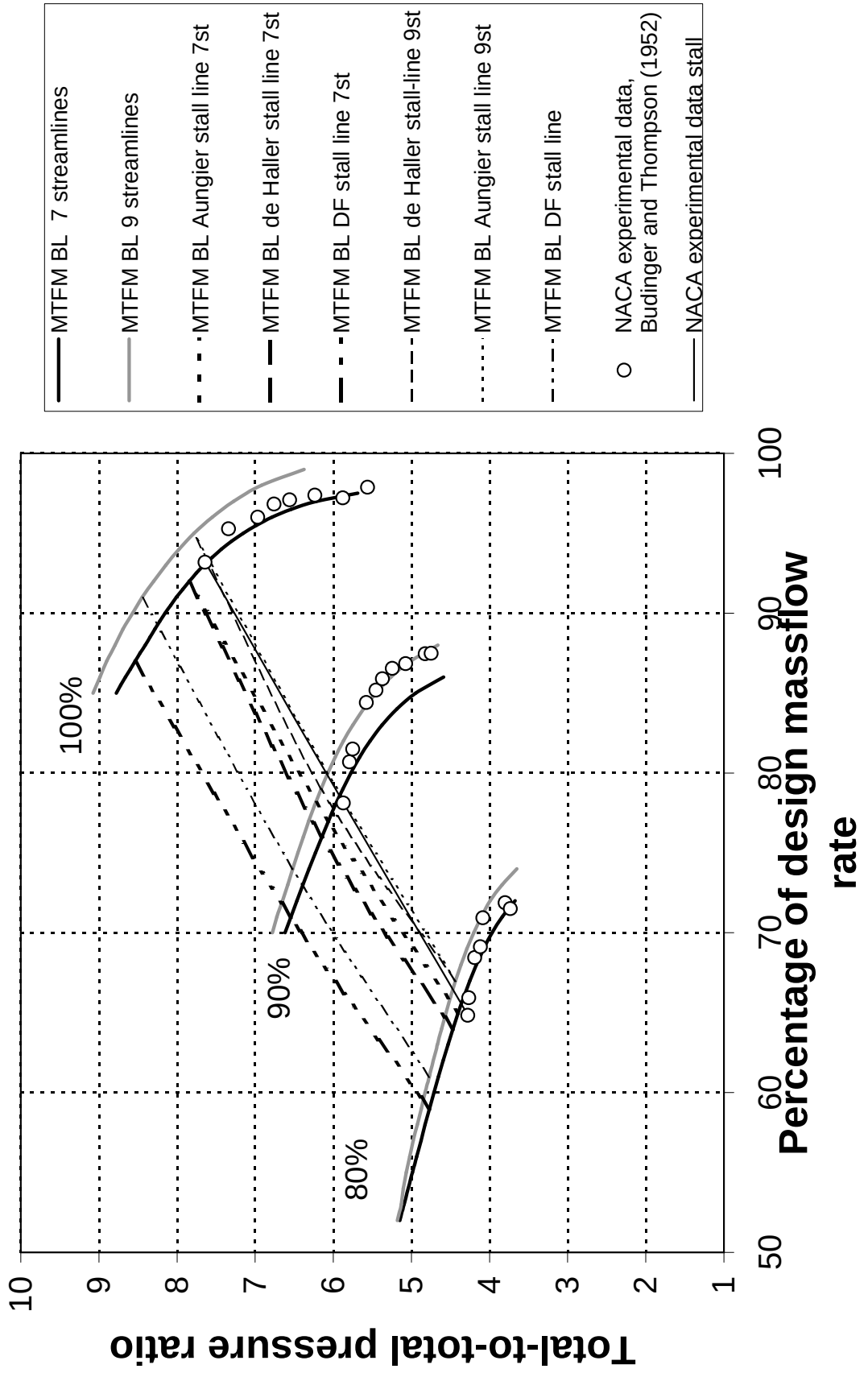

Figure 4.18: Predicted and experimental characteristics for the NACA 10-stage compressor using MTFM with 7 and 9 streamlines

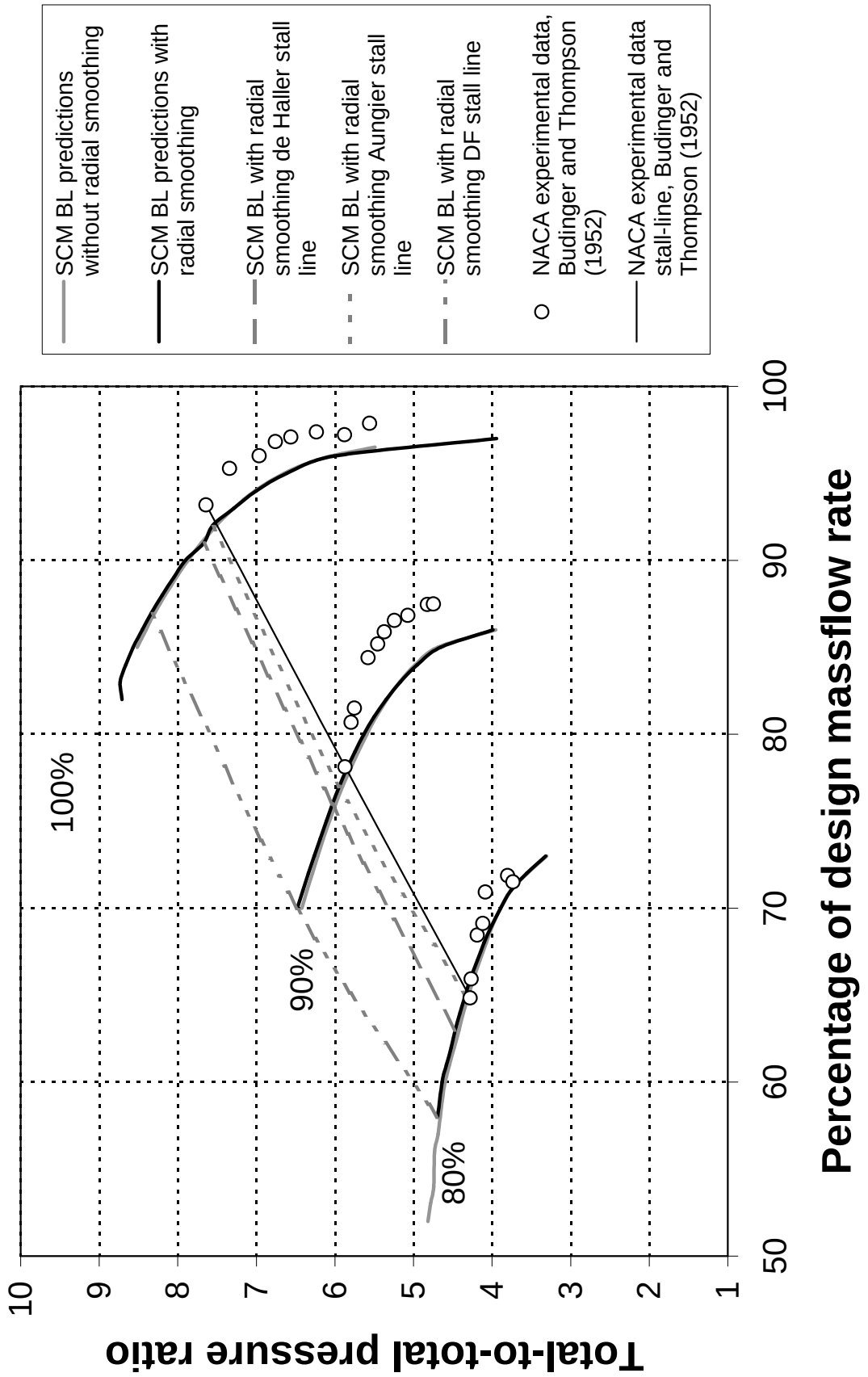

Figure 4.19: Predicted and experimental characteristics for the NACA 10-stage compressor using SCM with radial entropy smoothing

4.7 Summary of results

This chapter has described the results of the simulations of the four test cases used to evaluate the various stall prediction methods. The first test case, the Rofanco 3-stage compressor operated well within the incompressible flow regime, having a relative Mach-number of approximately 0.1 at the first rotor blade row when operating at design conditions. The predicted characteristics agreed relatively well with those obtained by Roos (1990) at high massflow rates and low pressure ratios, but less well at lower massflow rates, probably due to the lack of a model for low Reynolds-number effects in the SUCC. Use of the boundary layer blockage model also introduced a small discontinuity when used in conjuction with the SCM. The only stall prediction criterion to predict stall was that of de Haller. This criterion appeared to give acceptable accuracy for predicting the position of the stall line, although the inclusion of a low Reynolds number effects model would probably improve the accuracy of results. The NACA 5-stage transonic compressor had a relative Mach number of approximately 1.2 at the first rotor blade row at design conditions. For this test case, the characteristics for 80% and 100% of design speed agreed well with experimental data, but that at 90% contained a significant error. This was also clearly observed for the 90% characteristic of the NACA 10-stage subsonic compressor which was also used as a test case. A larger error was also present in the efficiency predictions for the NACA 5-stage compressor at 90% of design-speed, though the error for all characteristics examined for the NACA 10-stage machine were approximately equal, and unfortunately relatively large. The prediction results obtained by Thomas (2005) for the NACA 5-stage compressor also show a larger error for the 90% characteristic than for the other characteristics examined. The code used by Thomas (2005) differed from the SUCC in all but two respects, namely the blade row loss model, which was different but very similar in each code, and the boundary layer blockage model. Both of these models must therefore be examined in more depth so as to determine the cause of this error. For the NACA 5-stage compressor, de Haller's criterion was by far the worst, proving to be hopelessly conservative, as mentioned by Aungier (2003). The diffusion factor method provided a better estimation of the onset of stall, but was somewhat optimistic. The most accurate prediction was obtained by use of Aungier's blade row criterion. For the NACA 10-stage subsonic compressor, which had a relative Mach number of approximately 0.7 at the first rotor blade row, de Haller's and Aungier's criteria both provided equally accurate stall predictions which approximated the experimentally obtained stall conditions well. The diffusion factor criterion provided a less satisfactory stall prediction for this test case. The remaining test case, namely the NACA 8-stage transonic compressor, was not sta-

ble enough to generate any performance predictions when boundary layer blockage modelling was employed. However, results obtained without boundary layer blockage show similar trends to the NACA 5-stage machine, with Aungier's criterion providing the best stall prediction, de Haller somewhat conservative, and the diffusion factor criterion somewhat optimistic. However, these results are not conclusive, as they do not accurately reflect the operational conditions of the compressor. The stability-based methods all functioned very poorly, as virtually no predicted performance characteristics exhibited a point of zero gradient, and in the few cases which did, the point lay a considerable distance beyond the experimentally determined stall line. It was also found that increasing the number of streamlines almost always improved the accuracy of predictions. The stability of the simulations was improved by use of Aungier's radial smoothing model, particularly for the SCM, although the effect of the use of this model on the accuracy of predictions was negligible.

Rofanco compressor, MTFM, with BL, 5 streamlines			
Speed	Percentage error: de Haller criterion		
	Massflow rate	T-T pressure ratio	Combined
70%	-0.397%	14.182%	14.118%
80%	-4.790%	9.756%	10.868%
90%	16.129%	2.297%	16.129%
100%	13.088%	-1.668%	13.194%
Rofanco compressor, SFM, with radial smoothing and BL, 5 streamlines			
Speed	Percentage error: de Haller criterion		
	Massflow rate	T-T pressure ratio	Combined
70%	-2.175%	16.264%	16.409%
80%	-6.278%	11.498%	13.100%
90%	14.516%	3.902%	15.031%
100%	8.950%	3.698%	9.684%

Table 4.1: Errors for stall prediction for the Rofanco compressor

NACA 5-stage compressor, MTFM, with BL, 5 streamlines			
Speed	Percentage Error: de Haller Criterion		
	Massflow rate	T-T pressure ratio	Combined
80%	19.057%	-347.331%	51.023%
90%	6.575%	-48.671%	49.113%
100%	3.863%	-31.811%	32.045%
Speed	Percentage Error: Aungier's Blade Row Criterion		
	Massflow rate	T-T pressure ratio	Combined
80%	6.301%	-6.874%	9.325%
90%	-4.469%	-7.645%	8.855%
100%	-1.961%	3.083%	3.143%
Speed	Percentage error: diffusion factor criterion		
	Massflow rate	T-T pressure ratio	Combined
80%	3.466%	-3.333%	4.809%
90%	-5.573%	-6.370%	8.464%
100%	-3.417%	6.256%	7.128%

Table 4.2: Stall-prediction errors for the NACA 5-stage compressor simulated with 5 streamlines and the MTFM

NACA 5-stage compressor, MTFM, with BL, 9 streamlines			
Speed	Percentage error: de Haller criterion		
	Massflow rate	T-T pressure ratio	Combined
80%	19.766%	-47.103%	51.082%
90%	7.127%	-50.231%	50.734%
100%	4.348%	-39.664%	39.901%
Speed	Percentage error: Aungier's blade row criterion		
	Massflow rate	T-T pressure ratio	Combined
80%	7.718%	-7.205%	10.559%
90%	-2.812%	-8.452%	8.908%
100%	-0.990%	1.502%	1.799%
Speed	Percentage error: diffusion factor criterion		
	Massflow rate	T-T pressure ratio	Combined
80%	4.883%	-2.761%	5.610%
90%	-5.021%	-5.231%	7.251%
100%	-2.446%	5.857%	6.347%

Table 4.3: Stall-prediction errors for the NACA 5-stage compressor with 9 streamlines and the MTFM

NACA 5-stage compressor, SCM, with BL and radial-smoothing, 5 streamlines			
Speed	Percentage error: de Haller criterion		
	Massflow rate	T-T pressure ratio	Combined
80%	19.766%	-58.078%	61.349%
90%	5.471%	-42.702%	43.051%
100%	4.348%	-41.239%	41.468%
Speed	Percentage error: Aungier's blade row criterion		
	Massflow rate	T-T pressure ratio	Combined
80%	8.427%	-13.095%	15.572%
90%	-3.364%	-10.758%	11.272%
100%	-0.990%	-0.332%	1.044%
Speed	Percentage error: diffusion factor criterion		
	Massflow rate	T-T pressure ratio	Combined
80%	7.009%	-10.708%	12.798%
90%	-4.469%	-9.859%	10.824%
100%	-4.388%	5.935%	7.381%

Table 4.4: Stall-prediction errors for the NACA 5-stage compressor with 5 streamlines and the SCM with radial smoothing

NACA 10-stage compressor, MTFM, with BL, 7 streamlines			
Speed	Percentage Error: de Haller Criterion		
	Massflow rate	T-T pressure ratio	Combined
80%	-1.317%	5.830%	5.977%
90%	-2.739%	5.665%	6.293%
100%	-1.290%	3.075%	2.967%
Speed	Percentage error: Aungier's blade row criterion		
	Massflow rate	T-T pressure ratio	Combined
80%	0.225%	3.764%	3.771%
90%	-1.460%	3.932%	4.194%
100%	-1.290%	3.075%	3.334%
Speed	Percentage error: diffusion factor criterion		
	Massflow rate	T-T pressure ratio	Combined
80%	-9.027%	15.018%	14.625%
90%	-9.138%	13.823%	16.570%
100%	-6.655%	13.482%	15.035%

Table 4.5: Stall-prediction errors for the NACA 10-stage compressor with 7 streamlines and the MTFM

NACA 10-stage compressor, MTFM, with BL, 9 streamlines			
Speed	Percentage error: de Haller criterion		
	Massflow rate	T-T pressure ratio	Combined
80%	3.309%	4.864%	5.883%
90%	1.100%	5.900%	6.002%
100%	1.929%	2.128%	2.872%
Speed	Percentage error: Aungier's blade row criterion		
	Massflow rate	T-T pressure ratio	Combined
80%	3.309%	4.864%	5.883%
90%	2.380%	4.100%	4.741%
100%	-1.929%	2.128%	2.872%
Speed	Percentage error: diffusion factor criterion		
	Massflow rate	T-T pressure ratio	Combined
80%	-5.943%	15.125%	13.250%
90%	-5.299%	13.323%	14.338%
100%	-2.363%	12.117%	12.345%

Table 4.6: Stall-prediction errors for the NACA 10-stage compressor with 9 streamlines and the MTFM

NACA 10-stage compressor, SCM, with BL and radial-smoothing, 7 streamlines			
Speed	Percentage error: de Haller criterion		
	Massflow rate	T-T pressure ratio	Combined
80%	-2.839%	5.891%	6.548%
90%	-2.739%	3.340%	4.320%
100%	-2.363%	0.436%	2.403%
Speed	Percentage error: Aungier's blade row criterion		
	Massflow rate	T-T pressure ratio	Combined
80%	0.225%	1.910%	1.923%
90%	-1.460%	1.576%	2.148%
100%	-1.290%	-1.268%	1.809%
Speed	Percentage error: diffusion factor criterion		
	Massflow rate	T-T pressure ratio	Combined
80%	-10.569%	12.758%	16.567%
90%	-10.418%	12.536%	16.300%
100%	-6.655%	10.433%	12.375%

Table 4.7: Stall-prediction errors for the NACA 10-stage compressor with 7 streamlines and the SCM with radial smoothing

Chapter 5

Conclusions and recommendations

The purpose of this chapter is to discuss the implications of the results presented in the previous chapter, and to present guidelines to ensure accurate stall predictions with the SUCC, and similar codes. The strengths and weaknesses of the various stall prediction criteria are discussed. A guideline for the choice of stall criteria appropriate for a given compressor and a possible explanation for the apparent validity of this guideline are proposed. Finally, recommendations for improvements to the SUCC and suggestions for possible future lines of research are presented.

5.1 Factors influencing accuracy of stall predictions

It is obvious that a stall prediction obtained from a axisymmetric compressor simulation can only be accurate if the conditions predicted by that simulation are fairly accurate. However, something should be said about the factors that can positively or negatively affect that accuracy. Here follows a discussion of various factors which must be considered when attempting to obtain an accurate stall prediction using the methods described in this text.

5.1.1 Choice of throughflow method

One of the research questions which this text attempted to answer was the effect of the choice of throughflow method on the accuracy of stall prediction. One would assume that if two throughflow methods were both sufficiently accurate, there should be very little difference, if any, between flow fields and thus stall predictions obtained by application of the matrix throughflow method or the streamline curvature

method. This was confirmed to a large degree by a comparison of the results obtained for test cases using these two methods. It should be stated that the results obtained for the test cases for this implementation of MTFM were more accurate than those obtained for this implementation of the SCM. However, the difference is generally small, and it is not impossible that with some small refinements and tuning, the accuracy of the SCM code could be improved to the point where the small difference between the two methods would disappear altogether. At any rate, the stall predictions obtained by the two throughflow methods are so similar that the choice does not appear to be a significant one.

5.1.2 Effects of boundary layer blockage modelling

The importance of accurate blockage modelling when attempting to simulate axial flow compressor operation cannot be overemphasised. If boundary layer blockage is not taken into account, then velocities calculated for a given mass flow will be unrealistically low. This will affect any loss models that are implemented and make the results obtained from them unrealistic. The result is that higher pressure ratios are predicted than are obtainable for a given massflow rate, and the simulation does not indicate choke when the compressor would experience it. Consequentially, a performance characteristic obtained with a simulation not including boundary layer blockage will be shifted somewhat to the right and top of an actual compressor characteristic at the indicated speed and massflow rate, although the shape of the incorrect characteristic will resemble a 'scaled-up' version of the actual characteristic in most cases.

With errors such as the ones described in the shape of the characteristic obtained from such a simulation, it can already be seen that stall results thus obtained will not be satisfactory. However, neglecting boundary layer blockage introduces yet another error into an attempt to predict the onset of stall. As is stated previously, such a simulation predicts throughflow velocities which are somewhat low, due to the increase in available flow area. This in turn affects the incidence angle seen by the blade rows in the compressor, increasing it somewhat. Now although it has been established that a high incidence angle in a compressor blade row is not necessarily the only factor influencing compressor stall, it will certainly encourage it. Thus a compressor simulation not including boundary layer blockage will indicate that the compressor is more susceptible to stall than is actually the case. For the NACA 5- and 8-stage machines, the stall line indicated from the simulations sans boundary layers were far too conservative when compared with experimental data, and it was not until a line was plotted representing the stall of two blade rows over

a significant portion of their area (approximately 25%) that some agreement was obtained between the position of the lines (of course, the actual predicted points still did not coincide with the actual stall points, as there was a large offset between the predicted and experimental characteristics, as has been explained here).

While the preceding argument assumes the fairly drastic case of the total omission of boundary layer blockage, an incorrect estimation of the degree of blockage will have a similar, though probably smaller effect, and also cause erroneous stall prediction results.

5.1.3 Effects of computational grid layout

For the SUCC at least, the preparation of the computational grid for a given compressor appears to be rather important. The accurate placement of quasi orthogonals on the leading and trailing edges of blade rows, for instance, appears to be of considerable importance to the stability and accuracy of both the MTFM and the SCM. It is also important that, wherever possible, only one quasi-orthogonal be used to define the leading or trailing edge of a blade row, particularly if the SCM is the computational method to be used.

The number of quasi-orthogonals should be kept as small as possible; this not only appears to increase the stability of the computational methods somewhat, but it also obviously results in a saving of computation time. The placement of large numbers of quasi-orthogonals within a blade row, where properties can at best be very imprecisely estimated through some mechanism such as interpolation, is known to have a seriously detrimental effect on the accuracy and stability of the simulation, at least for the methods implemented in the SUCC. Novak (1967) provides guidelines for extending the streamline curvature method to provide flow predictions within a blade row with some confidence, while Aungier (2003) gives an explanation on how to solve the flow field within the blade row using the matrix throughflow method. However, such methods have not been implemented in the SUCC at present, and are of questionable desirability.

Conversely, a larger number of streamlines or quasi-streamlines will improve accuracy, although it may increase the computation time somewhat, and in the case of the SCM, create some instability in the computational method. Experimentation has shown that approximately seven streamlines seem to be sufficient to ensure reasonable accuracy, without increasing computation time and decreasing numerical stability to an unacceptable level.

5.1.4 Effect of blade row loss model and radial mixing on blade rows

The blade row model advocated by Aungier (2003) is that of Lieblein, and it was this model which was used in the SUCC simulations to determine the outlet angle and loss coefficients. The limit on loss coefficients advocated by Aungier (2003), $\omega \leq 0.5$, had been incorporated into the SUCC by the original creator of the package.

The need for a mixing model was especially apparent with the SCM, which was initially unable to converge to a solution for operating conditions such as those encountered in the NACA 5-stage compressor simulation.

The effect of the use of radial entropy smoothing was quite dramatic. Although the results which were obtained using the SCM without radial entropy smoothing were virtually identical to those obtained by utilising it, the SCM was far more numerically stable when radial smoothing was employed, and it was possible to obtain results for massflows and pressure ratios not previously accessible due to numerical instability. This holds true for all the test cases investigated. One slightly undesirable side-effect of the smoothing process which was only apparent for the NACA 5-stage compressor was that all stall prediction methods produced more conservative results than had previously been the case for the 80% and 90% characteristics for Aungier's blade row criterion.

5.2 Choice of stall prediction criteria

Based upon the results of the test cases, some conclusions may be reached as to which stall prediction criteria are most appropriate for estimating the stall conditions for a given compressor.

For compressors operating in the transonic regime, Aungier's criterion appears to be by far the most accurate, as can clearly be seen by examining the NACA 5-stage simulation results ($M = 1.2$ at the tip of the rotor row under design conditions). For such conditions, de Haller's criterion is usually much too conservative to be useful. Also to be noted is the fact that for transonic machines operating at high speeds, the diffusion factor method, although inaccurate, is considerably less so than de Haller.

On machines operating in the subsonic regime, such as the NACA 10-stage compressor, ($M = 0.7$ at the tip of the rotor row under design conditions) the difference between the prediction obtained for de Haller's criterion and Aungier's blade row criterion is considerably smaller. Indeed, for the case cited, there is very little to choose from between the two criteria. The error for the diffusion factor stall criterion is much greater, and this criterion suggests that stall occurs much later than it does

in reality.

On a very low speed, low pressure ratio machine such as the Rofanco 3-stage compressor, de Haller's criterion is the only stall criterion to give useful results.

When one considers the nature of these three criteria, a plausible reason for this behaviour suggests itself. De Haller's criterion examines the ratio between the outlet and inlet velocities of a blade row to use as an indicator of stall resulting from endwall boundary layer separation. In order to do this, the blade row is regarded as something approximating an ideal diffuser. The diffusion factor criterion regards maximum blade loading as the limiting factor. Aungier's criterion attempts to take both models into account. It seems reasonable to assume blade loading would have a more significant effect on flow through a blade row at high relative Mach-numbers than at low ones. However, the blade row still acts something like a diffuser, though not an ideal one. Thus only a stall criterion taking into account both blade loading effects and diffuser-related effects will predict stall with any accuracy. At lower speeds, the blade loading effects become less pronounced, and the diffuser-related and endwall boundary layer related effects are dominant, and thus are the controlling factor in determining stall. This explains why either Aungier's or de Haller's criterion can be used interchangeably for a machine like the NACA 10-stage compressor. On a very low speed, low Mach-number machine such as the Rofanco 3-stage compressor, the blade rows behave very much like an ideal diffuser, therefore de Haller's criterion is the best indication of the onset of stall.

The preceding explanation is no doubt somewhat simplistic, and attention should perhaps be paid to dimensionless groups other than the Mach-number in attempting to explain why the various criteria provide accurate or inaccurate predictions for a given machine.

System stability criteria such as Dunham's criterion are only useful when a clearly defined peak or point of zero gradient occurs on the characteristic used to determine stability. Aungier (2003) does comment at the beginning of his discussion of stall criteria for use with axisymmetric throughflow methods that gradient-based stability criteria are not the most suitable criteria for such purposes, as such methods will not always provide solutions for compressor operation far enough into the unstable region to form a clearly defined peak. He also comments that the simple radial mixing model which he advocates affects the position of the peak in a simulation. This researcher has found that it was virtually impossible to obtain a characteristic which peaked without the use of mixing models, and that the peak thus predicted was rather an inaccurate indicator of the onset of compressor stall. An examination of the 100% speed predicted characteristic in figures 4.17 and 4.19 will show such a peak which was obtained when radial smoothing was applied, but not obtained without

it. It can therefore be stated with relative certainty that such methods are probably most useful when applied to a more complex model, possibly one regarding the flow system to which the compressor is connected, such as that described in Moore and Greitzer (1986*a*) or to a characteristic curve-fitted to actual experimentally obtained compressor performance data. It is, however, possible that the implementation of a more complex and accurate model for radial mixing, such as those advocated by Cumpsty (1989) and described in section 2.2.6 would improve the performance of this criterion.

Aungier's boundary layer stall criterion also did not yield any stall predictions. Aungier comments that it was not useful for the three test cases he made use of, and rarely occurs in most other compressors he has encountered, and it is therefore reasonable to assume that this is not a useful criterion, at least for the present code and boundary layer modelling method, with the present test cases. It is also possible that the lack of success of this criterion may be due to some inadequacy in the boundary layer model applied.

5.3 Recommendations for further work

The SUCC has now been extended so as to include the streamline curvature method, radial loss smoothing on blade rows and a number of stall prediction criteria. These have collectively been tested and evaluated using four test cases, of which three produced useful results. A number of issues have arisen during the course of the testing of the new portions of the code. A list of these follows:

- The method used for calculating D_{eq} as outlined in chapter 3 is somewhat crude. A better formulation, such as that of Aungier (2003), should be implemented.
- The numerical stability of the streamline curvature method should be improved.
- A shock loss model must be implemented for the leading edges of blade rows of transonic compressors.
- Provision should be made for bleed flows in the SCM (provision has been made for bleed flows in the MTFM).
- The STFM should be implemented in the SUCC.

In addition, a number of issues in the original code of the SUCC were discovered during the testing process. They are as follows:

- The boundary layer blockage model is unreliable and should be improved to improve the overall stability of the SUCC.
- All the test cases investigated showed a marked discrepency between predicted and experimental performance for the characteristic at 90% of design speed. The reason for this must be determined.
- The reason for the failure of the NACA 8-stage compressor model must be determined.

Finally, there are a number of possible improvements which might be made to the SUCC, which, while not of great importance, would make it easier to use:

- It should be possible to set the convergence tolerances for the throughflow method and the boundary layer blockage method in the user-input file of a simulation.
- A better initial estimate of thermodynamic properties would improve the chances of a simulation converging to a solution.

In addition to the preceding points, there are a number of topics which are not directly related to developing or improving the SUCC. For instance the SUCC should be used to obtain a performance and stall prediction for the T-56 compressor.

It is also possible that Aungier's blade row stall criterion could be improved slightly. At present, the criterion is based upon functions obtained by fitting curves to experimental data for 2-dimensional diffuser peak static pressure recovery as a function of diffuser area ratio and velocity ratio. However, some compressor blade rows have an area ratio that does not fall within the range of the experimental data. This means that the curve-fitted function can not be used with any confidence for these cases. Aungier (2003) overcomes this problem by imposing a limit on the area ratio. However, it should be possible to obtain additional data which would allow the range of the correlation to be extended to include a larger range of equivalent area ratios in compressor blade rows. This data could be obtained by practical investigation, possibly using blade cascades instead of a two-dimensional diffuser, or by means of a CFD analysis. Alternatively, both approaches could be used to obtain greater certainty of the accuracy of the resulting data and correlation.

Finally, the effect of the use of an alternative, and possibly more accurate radial mixing model on the overall accuracy of compressor performance and stall predictions could be investigated. The method currently implemented, based upon that described in Aungier (2003), has the benefit of being extremely simple. However,

it is rather crude, and does not have as solid a theoretical basis as the other two methods described in Chapter 2.

List of References

Adkins, G. and Smith, L. (1982). Stall inception in axial flow compressors. *Trans ASME Journal of Engineering for Power*, vol. 104, p. 97.

Aungier, R.H. (2003). *Axial-flow Compressors: a Strategy for Aerodynamic Design and Analysis*. New York, ASME Press.

Bernadé, J. (1986 October). *The Development of an Impulse-Type Compressor Blade Cascade*. Master's project, University of Stellenbosch, Faculty of Engineering.

Bernd Höss, D.L. and Fottner, L. (2000). Stall inception in the compressor system of a turbofan engine. *Journal of Turbomachinery*, vol. 122, pp. 32–44.

Budinger, R. and Thompson, A. (1952). Investigation of a 10-stage subsonic axial-flow compressor; II–preliminary analysis of overall performance. NACA Research Memorandum RME52C04, NACA, Washington DC.

Cumpsty, N.A. (1989). *Compressor Aerodynamics*. Longman.

Day, I.J. (1993). Stall inception in axial flow compressors. *Journal of Turbomachinery*, vol. 115, pp. 1–9.

Day, I.J. and Camp, T.R. (1997). A study of spike and modal stall phenomena in a low-speed axial compressor. *Journal of Turbomachinery*, vol. 120, pp. 393–401.

Gallimore, S. and Cumpsty, N. (1986). Spanwise mixing in multistage axial flow compressors part (ii). *Journal of Turbomachinery*, vol. 108, pp. 2–9.

Gannon, A.J. and von Backström, T.W. (2000). Comparison of streamline throughflow and streamline curvature methods. *International Journal of Turbo and Jet Engines*, vol. 17, pp. 161–170.

Geye, R., Budinger, R. and Voit, C. (1953). Investigation of a high pressure-ratio eight-stage axial-flow research compressor with two transonic inlet stages; II–preliminary analysis of overall performance. NACA Research Memorandum RME53J06, NACA, Washington DC.

Grüber, B. and Carstens, V. (2001). The impact of viscous effects on the aerodynamic damping of vibrating transonic compressor blades – a numerical study. *Journal of Turbomachinery*, vol. 123, pp. 409–417.

Howell, A. (1945). Design of axial compressors. *Proceedings of the Institution of Mechanical Engineers, United Kingdom*, vol. 153.

Inoue, M., Kuroumaru, M., Tanino, T., Yoshida, S. and Furukawa, M. (2001). Comparative studies on short and long length-scale stall cell propagating in an axial compressor rotor. *Journal of Turbomachinery*, vol. 123, pp. 24–32.

Johnsen, I. and Bullock, R. (1954). Aerodynamic design of axial flow compressors. NACA SP-36, NACA, Washington DC.

Koch, C.C. (1981). Stalling pressure rise capability of axial flow compressor stages. *Trans. ASME,Journal of Engineering for Power*, vol. 103, pp. 645–656.

Kovach, K. and Sandercock, D. (1954). Experimental investigation of a five-stage axial-flow compressor with transonic rotors in all stages; II–compressor overall performance. NACA Research Memorandum RME54G01, NACA, Washington DC.

Lewis, K. (1989 July). *Prediction of Stall Inception in an Axial Flow Compressor*. Master's project, University of Witwatersrand, Faculty of Engineering.

McDougall, N.M., Cumpsty, N.A. and Hynes, T.P. (1990). Stall inception in axial compressors. *Journal of Turbomachinery*, vol. 112, pp. 116–124.

Moore, F.K. and Greitzer, E.M. (1986*a*). A theory of post-stall transients in axial compression systems: Part I–development of equations. *ASME Journal of Engineering for Gas Turbines and Power*, vol. 108, pp. 68–76.

Moore, F.K. and Greitzer, E.M. (1986*b*). A theory of post-stall transients in axial compression systems: Part II–application. *ASME Journal of Engineering for Gas Turbines and Power*, vol. 108, pp. 231–239.

Novak, R.A. (1967). Streamline curvature computing procedures for fluid-flow problems. *ASME Journal of Engineering for Power*, vol. 89, pp. 478–490.

Ottavy, X., Trébinjac, I. and Vouillarmet, A. (2001). Analysis of the interrow flow field within a transonic axial flow compressor. *Journal of Turbomachinery*, vol. 123, pp. 49–63.

Pampreen, R.C. (1993). *Compressor Surge and Stall*. Concepts ETI, Inc. Norwich, Vermont, USA 05055.

Pratap, A., Mata, S. and Geetha, P. (2005). Improvement of a multi-stage transonic compressor using cfd. *ISABE Procedings, ISABE 2005-1267*.

Reneau, L., Johnston, J. and Kline, S. (1967). Performance and design of straight two-dimensional diffusers. *Trans. Journal of Basic Engineering, ASME*, vol. 89, pp. 141–150.

Rogers, D.F. and Adams, J.A. (1976). *Mathematical Elements for Computer Graphics.* McGraw-Hill Book Company.

Roos, T. (1990 November). Reblading and testing of the rofanco low speed axial flow compressor. Undergraduate final year project, Faculty of Engineering, University of Stellenbosch.

Roos, T. (1995 March). *A Prediction Method for Flow in Axial Flow Compressors.* Master's project, University of Stellenbosch, Faculty of Engineering.

Thiart, G.D. (2004). The Stellenbosch University Compressor Code. Private communication.

Thiart, G.D. (2005). Turbomachinery simulations - axisymmetric flow. Private communication.

Thomas, K.D. (2005 April). *Blade Row and Blockage Modelling in an Axial Compressor Througflow Code.* Master's project, University of Stellenbosch, Faculty of Engineering.

Appendix A

Derivation and implementation of the MTFM

Nomenclature

Symbols

c	velocity component
C_p, C_{p_n}	constant-pressure heat capacity, constant-pressure heat capacity coefficient
F, $\boldsymbol{F}$	body force component, body force vector
h	enthalpy
l	co-ordinate along streamline
n	index
p	absolute pressure
$\boldsymbol{q}$	meridional velocity vector
r	radial co-ordinate
R	ideal gas constant
s	entropy
T	absolute temperature
V	total velocity magnitude
z	axial co-ordinate
β	angle of streamline w.r.t. axial direction
ρ	density
ω	rotational speed
Ω	vorticity component
ψ	stream function
θ	circumferential co-ordinate

Special subscripts

$_0$	stagnation value
$_n$	in a direction normal to a streamline in the meridional plane
$_{\text{ref}}$	reference value

A.1 Governing equations

A.1.1 Throughflow equation

The throughflow equation is derived from the energy equation,

$$Tds = dh - \frac{dp}{\rho} \tag{A.1}$$

which can be written as follows in terms of the stagnation enthalpy $h_0 = h + \frac{1}{2}V^2$:

$$\frac{dp}{\rho} = dh_0 - Tds - d\left(\tfrac{1}{2}V^2\right) \tag{A.2}$$

We now consider the meridional components of this expression, under the assumption of axisymmetric flow (i.e. all gradients w.r.t. θ vanish):

$$\frac{1}{\rho}\frac{\partial p}{\partial z} = \frac{\partial h_0}{\partial z} - T\frac{\partial s}{\partial z} - c_z\frac{\partial c_z}{\partial z} - c_r\frac{\partial c_r}{\partial z} - c_\theta\frac{\partial c_\theta}{\partial z} \tag{A.3}$$

$$\frac{1}{\rho}\frac{\partial p}{\partial r} = \frac{\partial h_0}{\partial r} - T\frac{\partial s}{\partial r} - c_z\frac{\partial c_z}{\partial r} - c_r\frac{\partial c_r}{\partial r} - c_\theta\frac{\partial c_\theta}{\partial r} \tag{A.4}$$

The pressure gradients can be eliminated from these expressions by utilization of the meridional components of the momentum equation, i.e.

$$\frac{1}{\rho}\frac{\partial p}{\partial z} = F_z - c_z\frac{\partial c_z}{\partial z} - c_r\frac{\partial c_z}{\partial r} \tag{A.5}$$

$$\frac{1}{\rho}\frac{\partial p}{\partial r} = F_r - c_z\frac{\partial c_r}{\partial z} - c_r\frac{\partial c_r}{\partial r} + \frac{c_\theta^2}{r} \tag{A.6}$$

The resultant expressions are as follows:

$$\frac{\partial h_0}{\partial z} - T\frac{\partial s}{\partial z} - F_z = c_r\Omega_\theta + c_\theta\frac{\partial c_\theta}{\partial z} \tag{A.7}$$

$$\frac{\partial h_0}{\partial r} - T\frac{\partial s}{\partial r} - F_r = -c_z\Omega_\theta + c_\theta\frac{\partial c_\theta}{\partial r} + \frac{c_\theta^2}{r} \tag{A.8}$$

In these two expressions Ω_θ denotes the θ-component of vorticity, i.e.

$$\Omega_\theta = \frac{\partial c_r}{\partial z} - \frac{\partial c_z}{\partial r} \tag{A.9}$$

Multiplying Eq. (A.7) by c_r and Eq. (A.8) by c_z and subtracting the products, we obtain the following expression for this vorticity component:

$$\Omega_\theta = \frac{1}{c_z^2 + c_r^2}\left[c_r\left(\frac{\partial h_0}{\partial z} - T\frac{\partial s}{\partial z} - F_z - c_\theta\frac{\partial c_\theta}{\partial z}\right) - c_z\left(\frac{\partial h_0}{\partial r} - T\frac{\partial s}{\partial r} - F_r - \frac{c_\theta}{r}\frac{\partial (rc_\theta)}{\partial r}\right)\right] \tag{A.10}$$

This expression can be rewritten in terms of stream function derivatives (see section A.3):

$$\Omega_\theta = \frac{c_z F_r - c_r F_z}{c_z^2 + c_r^2} - \rho r\left[\frac{\partial h_0}{\partial \psi} - T\frac{\partial s}{\partial \psi} - \frac{c_\theta}{r}\frac{\partial (rc_\theta)}{\partial \psi}\right] \tag{A.11}$$

Also, using the relationship between the stream function and the meridional velocity components,

$$\frac{\partial \psi}{\partial r} = \rho r c_z \quad \text{and} \quad \frac{\partial \psi}{\partial z} = -\rho r c_r \tag{A.12}$$

we obtain the throughflow equation:

$$\frac{\partial}{\partial z}\left(\frac{1}{\rho r}\frac{\partial \psi}{\partial z}\right) + \frac{\partial}{\partial r}\left(\frac{1}{\rho r}\frac{\partial \psi}{\partial r}\right) = \frac{\partial c_z}{\partial r} - \frac{\partial c_r}{\partial z} = -\Omega_\theta \tag{A.13}$$

Note that two alternative versions of the expression for Ω_θ (as given by equation A.11) are often used for axial flow and radial flow machines respectively. For axial flow machines, the formulation for Ω_θ is taken directly from equation A.8, i.e. equation A.7 is ignored, giving the axial flow version for vorticity formulation:

$$\Omega_\theta = \frac{1}{c_z}\left[\frac{\partial h_0}{\partial r} - T\frac{\partial s}{\partial r} - F_r - \frac{c_\theta}{r}\frac{\partial (rc_\theta)}{\partial r}\right] \tag{A.14}$$

Likewise, for radial flow machines, the formulation for Ω_θ is taken directly from equation A.7, i.e. equation A.8 is ignored, giving the radial flow version for vorticity formulation:

$$\Omega_\theta = \frac{1}{c_r}\left[\frac{\partial h_0}{\partial z} - T\frac{\partial s}{\partial z} - F_z - \frac{c_\theta}{r}\frac{\partial (rc_\theta)}{\partial z}\right] \tag{A.15}$$

A.1.2 Swirl equation

The governing equation for swirl is the θ-component of the momentum equation, i.e.

$$F_\theta = c_z\frac{\partial c_\theta}{\partial z} + \frac{c_r}{r}\frac{\partial}{\partial r}(rc_\theta) \tag{A.16}$$

Note that this expression can be written in the form

$$rF_\theta \;=\; \boldsymbol{q}\cdot\boldsymbol{\nabla}(rc_\theta) \tag{A.17}$$

where $\boldsymbol{q}$ denotes the meridional velocity, i.e. $\boldsymbol{q}= c_z\boldsymbol{e_z}+c_r\boldsymbol{e_r}$. If $F_\theta = 0$, then $\boldsymbol{q}\cdot\boldsymbol{\nabla}(rc_\theta) = 0$, which means that, since the direction of $\boldsymbol{q}$ is identical to that of the streamlines in the meridional plane, the quantity rc_θ is constant along streamlines in the meridional plane.

A.1.3 Stagnation enthalpy variation

The change in stagnation enthalpy in the direction along a streamline (denoted by l) is that given by the Euler turbomachinery equation:

$$\frac{\partial h_0}{\partial l} \;=\; \omega\,\frac{\partial(rc_\theta)}{\partial l} \tag{A.18}$$

A.1.4 Entropy variation

Elimination of Ω_θ from Eqs. (A.7) and Eq. (A.8) yields the following expression:

$$c_z\left[\frac{\partial h_0}{\partial z} - T\,\frac{\partial s}{\partial z} - F_z - c_\theta\,\frac{\partial c_\theta}{\partial z}\right] + c_r\left[\frac{\partial h_0}{\partial r} - T\,\frac{\partial s}{\partial r} - F_r - \frac{c_\theta}{r}\,\frac{\partial(rc_\theta)}{\partial r}\right] \;=\; 0 \tag{A.19}$$

Note that this expression can be written in the form

$$\boldsymbol{q}\cdot\left[\boldsymbol{\nabla}h_0 - T\boldsymbol{\nabla}s - \boldsymbol{F} - \frac{c_\theta}{r}\,\boldsymbol{\nabla}\left(rc_\theta\right)\right] \;=\; 0 \tag{A.20}$$

It is clear that, since the direction of $\boldsymbol{q}$ is identical to that of the streamlines in the meridional plane, the streamline-direction component of the quantity in the square brackets must be zero, i.e.

$$\frac{\partial s}{\partial l} \;=\; \frac{1}{T}\left[\frac{\partial h_0}{\partial l} - F_l - \frac{c_\theta}{r}\,\frac{\partial(rc_\theta)}{\partial l}\right] \tag{A.21}$$

The stagnation pressure gradient in this expression can be eliminated using equation A.18:

$$\frac{\partial s}{\partial l} \;=\; \frac{1}{T}\left[\left(\omega - \frac{c_\theta}{r}\right)\frac{\partial(rc_\theta)}{\partial l} - F_l\right] \tag{A.22}$$

A.1.5 Equations of state

The enthalpy of the fluids generally used in turbomachines can be expressed in terms of the temperature as

$$dh = C_p dT \tag{A.23}$$

where C_p, the constant-pressure heat capacity, is a polynomial function of temperature, i.e.

$$C_p = \sum_{n=0}^{N} C_{p_n} T^n \tag{A.24}$$

Fluid density can be taken as constant, i.e. incompressible flow, or can be expressed in terms of pressure and temperature by means of the ideal gas law, i.e.

$$\rho = \frac{p}{RT} \tag{A.25}$$

A.2 Simulation procedure

In this section, a procedure for simulating the flow through an axisymmetric turbomachine by means of the formulation presented in section A.1 is proposed. A numerical solution procedure is adopted, i.e. the flow domain is "covered" with a suitable computational grid, and all variables are stored at all grid points. One assumption w.r.t. the influence of blade rows is introduced: the meridonial component of the body force produced by the blade row is assumed to be aligned with the meridional streamlines, i.e. the meridional component is equal to F_l, and $F_r = F_l \sin\beta_l$ and $F_z = F_l \cos\beta_l$, where β_l denotes the angle of the meridional streamline w.r.t. the axial direction. The proposed procedure is as follows:

Step 1: Start with approximate values for all dependent variables at all grid points. For the first iteration, these values are obtained from interpolation of the inlet conditions throughout the computational domain, and/or from specified initial conditions. For subsequent iterations, the values determined during the previous iteration are used.

Step 2: Determine new distributions of c_θ, h_0 and s throughout the computational domain. Between the inlet and the first blade row, and between blade rows, rc_θ, h_0 and s are constant along streamlines, so that some interpolation procedure can be used to set the values of the three variables. Within blade rows, the variation of c_θ is prescribed by the blade row model, and therefore the variation of h_0 can be determined by means of equation A.18. The variation of s must also be prescribed

by means of the blade row model, either directly or indirectly[1].

Step 3: Compute grid point values of F_r and/or F_z, as outlined in section A.4, and thereafter grid point values of Ω_θ, as represented by equation A.11, A.14 or A.15, as appropriate. The currently available temperature values are used in this step.

Step 4: Solve the throughflow equation (equation A.13) to determine the new stream function distribution at all grid points.

Step 5: Compute new distributions of radial and axial velocity components, using equation A.12 with the currently available density values.

Step 6: Update the enthalpy values at all grid points, using the definition $h = h_0 - \frac{1}{2}V^2$.

Step 7: Update the static temperature values using the equation of state, as outlined in section A.5.

Step 8: Update the static pressure values by integrating equation A.1 along streamlines, as outlined in section A.5.

Step 9: If the fluid under consideration is compressible, update the density values using the equation of state.

Step 10: Check if the solution has converged, if not, return to step 2.

Step 11: Compute the stagnation temperature values from the stagnation enthalpy values using the equation of state, as outlined in section A.5.

Step 12: Compute the stagnation pressure values from the static pressure values as well as the static and stagnation temperatures, as outlined in A.5.

A.3 Stream function derivatives

A stream function derivative of a function ϕ at a point is computed by taking the derivative of ϕ in a direction perpendicular to the streamline (denoted by n) through the point:

$$\frac{\partial\phi}{\partial\psi} = \left(\frac{d\phi}{d\psi}\right)_n = \frac{(\partial\phi/\partial r)(dr)_n + (\partial\phi/\partial z)(dz)_n}{(\partial\psi/\partial r)(dr)_n + (\partial\psi/\partial z)(dz)_n} \tag{A.26}$$

The meridional velocity vector is everywhere parallel to streamlines, therefore

$$\left(\frac{dr}{dz}\right)_l = \frac{c_r}{c_z} = -\frac{\partial\psi/\partial z}{\partial\psi/\partial r} \tag{A.27}$$

[1] A typical procedure can be that a drag coefficient is calculated by means of the blade row model; this can be converted to a value of F_l that is valid along the streamline between the leading edge and the trailing edge of the blade row; then equation A.21 can be used to determine the variation of s, using the available variations of c_θ and h_0

Now, since $(dr/dz)_n = -1/(dr/dz)_l$, it follows from Eqs. (A.26) and (A.27) that

$$\frac{\partial\phi}{\partial\psi} = \frac{(\partial\phi/\partial r)(\partial\psi/\partial r) + (\partial\phi/\partial z)(\partial\psi/\partial z)}{(\partial\psi/\partial r)^2 + (\partial\psi/\partial z)^2} \tag{A.28}$$

Note that this expression can also be written as follows, in terms of physical quantities:

$$\frac{\partial\phi}{\partial\psi} = \frac{c_z(\partial\phi/\partial r) - c_r(\partial\phi/\partial z)}{\rho r(c_z^2 + c_r^2)} \tag{A.29}$$

A.4 Evaluation of F_r and F_z

From the assumption that the meridional component of the body force is aligned with the meridional streamlines, it follows that

$$F_r = F_l \times \frac{c_r}{\sqrt{c_r^2 + c_z^2}} \tag{A.30}$$

$$F_z = F_l \times \frac{c_z}{\sqrt{c_r^2 + c_z^2}} \tag{A.31}$$

The value from F_l is determined from equation A.21:

$$\begin{aligned} F_l &= \frac{\partial h_0}{\partial l} - T\frac{\partial s}{\partial l} - \frac{c_\theta}{r}\frac{\partial(rc_\theta)}{\partial l} \\ &= \left[\frac{\partial h_0}{\partial r} - T\frac{\partial s}{\partial r} - \frac{c_\theta}{r}\frac{\partial(rc_\theta)}{\partial r}\right]\frac{\partial r}{\partial l} + \left[\frac{\partial h_0}{\partial z} - T\frac{\partial s}{\partial z} - \frac{c_\theta}{r}\frac{\partial(rc_\theta)}{\partial z}\right]\frac{\partial z}{\partial l} \\ &= \left[\frac{\partial h_0}{\partial r} - T\frac{\partial s}{\partial r} - \frac{c_\theta}{r}\frac{\partial(rc_\theta)}{\partial r}\right] \times \frac{c_r}{\sqrt{c_r^2 + c_z^2}} + \\ &\quad \left[\frac{\partial h_0}{\partial z} - T\frac{\partial s}{\partial z} - \frac{c_\theta}{r}\frac{\partial(rc_\theta)}{\partial z}\right] \times \frac{c_z}{\sqrt{c_r^2 + c_z^2}} \end{aligned} \tag{A.32}$$

A.5 Evaluation of pressure and temperature values

A.5.1 Static temperature

The static temperature values are found from the enthalpy values; from equations A.23-A.24 it follows that

$$h - h_{\text{ref}} = \int_{T_{\text{ref}}}^{T} C_p\, dT = \sum_{n=1}^{N} \frac{C_{p_n}}{n+1}\left(T^{n+1} - T_{\text{ref}}^{n+1}\right) \tag{A.33}$$

Note that the static temperature values have to be found by means of an iterative procedure, except in special cases such as for a constant C_p value or for a linear

dependency of C_p on T.

A.5.2 Static pressure

The static pressure values are obtained by integration of equation A.1 along streamlines, starting from the inlet boundary, and utilizing the appropriate equation of state in the process:

Incompressible fluid:

$$\begin{aligned} dp &= \rho(dh - Tds) \\ \Rightarrow \quad p_2 &= p_1 + \rho \int_1^2 (dh - Tds) \\ &\approx \rho \left[(h_2 - h_1) - \tfrac{1}{2}(T_1 + T_2)(s_2 - s_1) \right] \end{aligned} \tag{A.34}$$

Ideal gas:

$$\begin{aligned} \frac{dp}{p} &= \frac{1}{R}\left(\frac{dh}{T} - ds\right) \\ \Rightarrow \quad p_2 &= p_1 \left(\frac{T_2}{T_1}\right)^{C_{p_0}/R} \left[\sum_{n=1}^{N} \frac{C_{p_n}}{n} (T_2^n - T_1^n) - (s_2 - s_1) \right] \end{aligned} \tag{A.35}$$

where the subscripts "1" and "2" indicate upstream and downstream conditions respectively.

A.5.3 Stagnation temperature

The stagnation temperatures are computed in a similar fashion as the static temperatures:

$$h_0 - h = \int_T^{T_0} C_p \, dT = \sum_{n=1}^{N} \frac{C_{p_n}}{n+1} \left(T_0^{n+1} - T^{n+1} \right) \tag{A.36}$$

Note that here also the stagnation temperature values have to be found by means of an iterative procedure.

A.5.4 Stagnation pressure

The stagnation pressure values are computed from equation A.1 with $ds = 0$:

Incompressible fluid:

$$\begin{aligned} dp &= \rho dh \\ \Rightarrow \quad p_0 &= p + \rho\,(h_0 - h) \end{aligned} \tag{A.37}$$

Ideal gas:

$$\begin{aligned} \frac{dp}{p} &= \frac{dh}{RT} \\ \Rightarrow \quad p_0 &= p \exp\left(\frac{1}{R}\int_T^{T_0} \frac{C_p\,dT}{T}\right) = p\left(\frac{T_0}{T}\right)^{C_{p_0}/R} \sum_{n=1}^{N} \frac{C_{p_n}}{n}\left(T_0^n - T^n\right) \end{aligned} \tag{A.38}$$

Appendix B

Implementation of Aungier's SCM algorithm

The algorithm used to implement the streamline curvature method for the SUCC is based upon the algorithm given by Aungier (2003), which is in turn based upon the method of Novak (1967). It is not the purpose of this appendix to provide a complete derivation of the governing equations of the method. This appendix represents a brief explanation of the meaings and origin of the major equations and the manner in which they are used.

B.1 The computational grid

The compressor flowfield is divided up into a grid composed of quasi-orthogonals (also called quasi-normals) and streamlines. The coordinate system used for calculation is composed of meridional coordinates (symbol m), or the distance along a streamline from the compressor flow field inlet (coordinate z_0), and quasi-orthogonal coordinates (symbol y), or the distance along a quasi-normal from the hub.

The equations to convert from axisymmetric(r-z) coordinates to this coordinate system are given by equations (B.1) and(B.2) below.

$$m = \int_{z_0}^{z} \left[1 + \left(\frac{\partial r}{\partial z} \right)^2 \right] dz \tag{B.1}$$

$$y = \sqrt{(r - r_0)^2 + (z - z_0)^2} \tag{B.2}$$

This leads to the definition of three angles, namely the stream surface slope angle ϕ, (which is the angle between the streamline and the axial direction), the angle

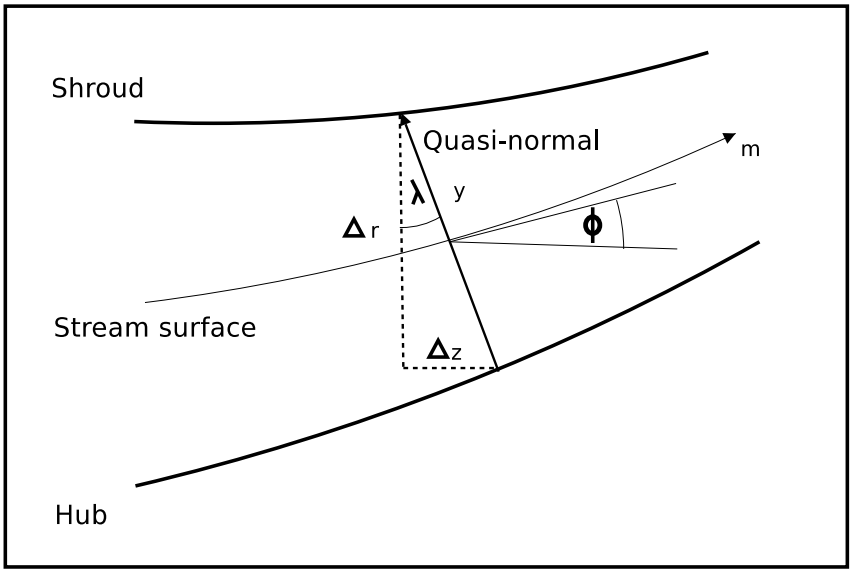

Figure B.1: The positioning of quasi-normals and streamlines on a compressor annulus

between a quasi-normal and the stream surface ϵ, and the angle between a quasi-orthogonal and a true orthogonal $\lambda = \phi - \epsilon$. Figure B.1 illustrates the positioning of a quasi-normal with respect to the compressor annulus, and the various associated angles and coordinate systems.

For the purposes of developing the governing equations, it is sometimes necessary to be able to express a derivative with respect to a true normal coordinate in terms of the quasi-normal and meridional coordinats. Aungier (2003) provides the relation for this purpose in equation B.3.

$$\frac{\partial}{\partial n} = \frac{1}{\cos\epsilon}\left[\frac{\partial}{\partial y} - \sin\epsilon\frac{\partial}{\partial m}\right] \tag{B.3}$$

Having now defined the computational grid, the equations on which the method is based can be formulated.

B.2 Governing equations

The SCM centers around the solution of the meridional flow field on a single quasi-normal. Aungier begins his development of the governing equations with those for the conservation of mass and momentum along a quasi-normal. The mass-balance across a quasi-normal is expressed as in equation B.4.

$$\dot{m} = 2\pi \int_0^{y_s} W_m \rho r \cos\epsilon dy \tag{B.4}$$

The axisymmetric, time-steady, inviscid momentum equations for the normal and tangential components of the meridional flow are given in equations (B.5) and (B.6).

$$\kappa_m W_m^2 + \frac{W_\theta}{r}\frac{\partial\left(rW_\theta + \omega r^2\right)}{\partial n} + W_m\frac{\partial W_m}{\partial n} = \frac{\partial I}{\partial n} - T\frac{\partial s}{\partial n} \tag{B.5}$$

$$\frac{\partial\left(rW_\theta + \omega r^2\right)}{\partial m} = \frac{\partial rC_\theta}{\partial m} = 0 \tag{B.6}$$

In equation (B.5), the term

$$W_m\frac{\partial W_m}{\partial n}$$

represents the substantive acceleration of the flow. The term $\kappa_m W_m^2$ is the centripetal acceleration of the flow following a curved streamline. The streamline curvature

$$\kappa_m = \frac{1}{r_m} = -\frac{\partial\phi}{\partial m}$$

is the inverse of the radius of curvature of the streamline. The term in W_θ is an expression of the merional acceleration component resulting from the swirl velocity component. The term

$$\frac{\partial I}{\partial n} - T\frac{\partial s}{\partial n}$$

is an alternative way of expressing the relative static pressure gradient with respect to the normal direction.

The assumption is then made that

$$\frac{\partial I}{\partial n} = 0$$

and

$$\frac{\partial s}{\partial n} = 0$$

that is the gradients of rothalpy and entropy in the normal direction are zero. These expressions, together with equation (B.6) are substituted into equation (B.5). The result is then rewritten in terms of the quasi-normal coordinate system by the application of equation (B.3), and further manipulated until it can be written in the form shown in equation (B.7).

$$\frac{\partial W_m}{\partial y} = f_1(y)\,W_m + f_4(y) \tag{B.7}$$

The terms in equation (B.7) are collected into the functions $f_1(y)$ and $f_4(y)$ in order to facilitate the solving of the differential equation. The function $f_4(y)$ is

given in equation (B.8):

$$f_4(y) = \frac{1}{W_m}\left(\frac{\partial I}{\partial y} - T\frac{\partial s}{\partial y} - \frac{W_\theta}{r}\frac{\partial (rC_\theta)}{\partial y}\right) \tag{B.8}$$

and the quantity $F(y)$ is expressed in equation (B.15):

$$f_1(y) = -\kappa_m \cos\epsilon + \frac{\sin\epsilon}{W_m}\frac{\partial W_m}{\partial m} \tag{B.9}$$

Alternative formulations for equations (B.8) and (B.9) for use on blade row trailing edges are defined in terms of β', the relative flow angle. Expressing equation (B.15) and equation (B.8) in terms of β' yields equations (B.10) and (B.11) respectively:

$$f_1(y) = \cos^2\beta'\left(-\kappa_m\cos\epsilon - \frac{\tan\beta'}{r}\frac{\partial (r\tan\beta')}{\partial y} + \frac{\sin\epsilon}{W_m}\frac{\partial W_m}{\partial m}\right) \tag{B.10}$$

$$f_4(y) = \cos^2\beta'\frac{1}{W_m}\left(\frac{\partial I}{\partial y} - T\frac{\partial s}{\partial y}\right) \tag{B.11}$$

It is evident that the partial derivative of the meridional velocity in the meridional direction is required for the calculation of equation (B.9) or (B.10). This complicates the solution of the differencial equation (B.7), so Aungier (2003) cites the method to remove this difficulty suggested in Novak (1967). This is done by using the differential form of the axisymmetric, time-steady, continuity equation in the meridional direction, equation (B.12) the expression for the curvature of a true normal, κ_n:

$$\kappa_n = \frac{\partial \phi}{\partial n}$$

$$\frac{\partial r\rho W_m}{\partial m} + \kappa_n r\rho W_m = 0 \tag{B.12}$$

This expression is then also rewritten in terms of the quasi-normal coordinate system, and manipulated algebraically, resulting in equation (B.13).

$$\frac{\partial W_m}{\partial m} = \frac{W_m}{1-M_m^2}\left(-\left(1+M_\theta^2\right)\frac{\sin\phi}{r} - \frac{1}{\cos\epsilon}\frac{\partial\phi}{\partial y} - \kappa_m\tan\epsilon\right) \tag{B.13}$$

Equation (B.13) is used in preference to a finite differencing scheme because it allows the partial derivative to be evaluated independently of the solution of the flow field on other quasi-orthogonals, which should make the solution of these equations somewhat more stable. However,it must be used subject to two constraints, namely that the Meridional Mach-number $M_m < 1$, and that the meridional velocity $W_m \neq 0$. If either of these conditions is not satisfied, equation(B.13) becomes singular

because of the resulting zero-terms in the denominator, in which case it is peferable to use a finite differencing scheme, where it is not necessary to divide by zero.

The solution for the differencial equation (B.7) can now be obtained analytically, and is shown in equation (B.14)

$$W_m(y) = W_m(0) F(y) + F(y) \int_0^y \frac{f_4(y)}{F(y)} dy \tag{B.14}$$

$$F(y) = \exp\left[\int_0^y f_1(y)\, dy\right] \tag{B.15}$$

This equation is solved after discretizing the derivatives and numerically approximating the integrals.

The meridional velocity at the hub, W_{m0}, serves as the constant of intergration in equation (B.14). This is, however, not initially known. It must therefore be estimated, the values of W_m solved across the quasi-normal, the conservation of mass across the quasi-normal as given in equation (B.4) applied through numerical integration, and the value of W_{m0} adjusted to decrease the discrepancy between the calculated and known massflow through the machine.

B.3 Simulation procedure

The implementation of the SCM as described in the previous section reuses a great deal of the code originally written for the MTFM. The overall simulation procedure is thus nearly identical to that described in section A.2 of appendix A. The only differences are that the SCM algorithm requires the calculation of rothalpy across the flow field in addition to the other thermodynamic properties required for the MTFM, and that steps 3, 4 and 5 of section A.2 are replaced by the process which follows.

1. Calculate values for ϕ, ϵ and κ_m based on present streamline positions. The partial derivatives needed to calculate these quantities were approximated using 2- and 3-point finite differencing schemes based on Taylor series, as suggested by Aungier (2003), as this apparently offers better numerical stability than other methods such as a spline or polynomial curve-fit.

2. Solve the meridional flow field $W_m(y)$ on each successive quasi-orthogonal, starting with the first one at the compressor inlet. This is done in the following way:

- The value of the meridional velocity at the compressor hub W_m is estimated, often calculated from the massflow rate through the entire machine.
- Starting at the streamline closest to the hub, the meridional velocity component is calculated by means of equation (B.14), in which y is the meridional coordinate at the point of calculation.
- The maximum change in meridional velocity is noted.
- The massflow is computed for the newly calculated flow field, by a numerical approximation of equation (B.4).
- The value of $W_m(0)$ is adjusted so as to cause the calculated massflow rate for the next iteration to better approximate the actual (known) massflow rate. A relaxation factor x is used in the manner shown in equation (B.16).

$$W_m(0)_{new} = W_m(0)_{old}\left[1 - x\left(\dot{m}_{calc} - \dot{m}_{exact}\right)/\dot{m}_{exact}\right] \tag{B.16}$$

- The entire process is repeated until the maximum change in meridional velocity at any streamline and the error in the calculated massflow rate are less than a preset tolerance.

3. Interpolate the new positions of the streamlines based on the assumption of massflow between stream surfaces remaining constant.
4. Adjust the position of the streamlines by the difference between the old positions and the new positions as calculated in the previous step, multiplied by a relaxation factor to ensure numerical stability.
5. Repeat the entire process until the maximum change of position of a streamline at any point is less than a specified tolerance.

B.4 Radial mixing

The radial mixing model implemented in SUCC was essentially that advocated by Aungier (2003). The only modification was that the entropy s was substitued for the total pressure loss $\Delta P_t'$ in equations (2.15) to (2.17). This was necessary because in the SUCC, the pressure losses are not calculated directly, as is advocated by Cumpsty (1989) and Aungier (2003). Instead, the entropy is the first thermodynamic property calculated, from which all other thermodynamic properties

are subsequently calculated. The algorithms for the calculation of thermodynamic properties in the SUCC are described fully in Thiart (2004) and Appendix A.

Appendix C

Additions to the SUCC

A list of features added to the SUCC during the course of this project is given below.

- The module StallModel was added to the SUCC. This contained implementations of the following stall criteria:
  - diffusion factor stall criterion
  - de Haller's stall criterion
  - Aungier's blade row stall criterion
  - Aungier's boundary layer stall criterion
  - Dunham's stability criterion
  - Aungier's stability criterion
  - A static-to-static stability criterion.

  It also contains a function to calculate the diffusion factor over a blade row. If a criterion detects that stall has occurred, the name of the criterion, the massflow rate and pressure ratio and the axial and radial coordinates are appended to a text file. In the case of the stability criteria, the coordinates are set to 0.

- The module StreamlineCurvature was added to the SUCC. This contains subroutines to allow the flow field to be solved using the SCM. This required the addition of a field for the flow exit angle to the type psitable in the Module Compressorbladerows.

- The Module MiscMaths was added to the SUCC. The functions and subroutines in this module should probably eventually be included in the MiscUtilities module. This contains the implementations of the following general-purpose mathematical tools:

  - spline fitting for natural and clamped 3-dimensional cubic splines.
  - Taylor series based numerical integration for unevenly spaced 2-D data
  - Finite difference numerical differentiation for unevenly spaced 2-D data
  - Finite Difference numerical second derivative calculation for unevenly spaced 2-D data *There may be some duplication with existing methods here.*
  - Thomas algorithm solver for tridiagonal matrices

- Subroutines for the calculation of rothalpy have been added to the FlowVariables module.
- The Subroutine AungierModel in the module Compressorbladerows has been modified to allow optional radial entropy smoothing.
- A number of functions returning information about a specified blade row have been added to the Compressorbladerows module. These do not modify any of the original internal variables of the module in any way.
  - The design RPM for a specified blade row
  - The RPM of a specified blade row for the current simulation
  - The quasi-orthogonal associated the leading and trailing edges of a specified blade row
  - The number of the blade row (if any) associated with a specified quasi-orthogonal. If no blade row exists at the quasi-orthogonal, then a value of 0 is returned.

In addition, a number of minor changes such as the addition of boolean 'flag' variables or calls to subroutines in the new modules have been added to the Compressorbladerows and the ComputationalMethod module and the SuccSolv program. Nothing has been removed from the original program, and wherever possible, no modifications were made to existing subroutines or modules.

Appendix D

Sample calculations for Aungier's blade row stall criterion

Sample calculations are presented here for Aungier's blade row stall criterion. Sample calculations for other criteria are not included because they are either trivial (such as de Haller's criterion, or the diffusion factor criterion), or because they require the solution of simultaneous equations for the purposes of spline fitting (such as the stability criteria). The data used were obtained from one of the simulations of the NACA 5-stage compressor.

Aungier's blade row stall criterion is based on the inequality given in equation(3.4), repeated here for convenience:

$$W_{RE} < \begin{cases} \left[(0.15 + 11t_b/c) \,/\, (0.25 + 10t_b/c)\right] \,/ \\ \left[1 + 0.4\left[\theta\sigma/\left[2\sin(\theta/2)\cos\gamma\right]\right]^{0.65}\right] & \text{if } D_{eq} \leq 2.2 \\ \left(\left[(2.2/D_{eq})^{0.6}\right](0.15 + 11t_b/c) \,/\, (0.25 + 10t_b/c)\right) \,/ \\ \left(1 + 0.4\left[\theta\sigma/\left(2\sin(\theta/2)\cos\gamma\right)\right]^{0.65}\right) & \text{if} D_{eq} > 2.2 \end{cases}$$

while imposing the limit given by the inequality in equation(3.5), also repeated here:

$$\theta\sigma/\left[2\sin(\theta/2)\cos\gamma\right] \geq 1.1$$

First, calculate the value of W_{RE}:

$$W_{RE} = \sqrt{\frac{P_{02,rel} - P_2}{P_{01_rel} - P_1}}$$

Substituting in values extracted from SUCC:

$$W_{RE} = \sqrt{\frac{317594.94 - 284129.84}{317632.08 - 277768.04}} = 0.91$$

Now, calculate the right hand side of the inequality shown in (3.5).

$$\theta\sigma/\left[2\sin\left(\theta/2\right)\cos\gamma\right] = 0.9 \cdot 1.338/\left[2\sin\left(0.9/2\right)\cos\left(0.1885\right)\right] = 1.194 \geq 1.1$$

It can be seen that the limit imposed by this inequality is not active for this case. The value of D_{eq} was extracted directly from SUCC:

$$D_{eq} = 1.828 < 2.2$$

This means that the simpler version of equation (3.4) will be the active one.

The value of the ratio of maximum profile thickness to chord length is then calculated.

$$\frac{t_b}{c} = \frac{0.001}{0.0517} = 0.193$$

Now the right hand side of (3.4) can be evaluated:

$$\frac{\left(0.15 + 11t_b/c\right)/\left(0.25 + 10t_b/c\right)}{1 + 0.4\left[\theta\sigma/\left[2\sin\left(\theta/2\right)\cos\gamma\right]\right]^{0.65}} = \frac{\left(0.15 + 11 \cdot 0.193\right)/\left(0.25 + 10 \cdot 0.193\right)}{1 + 0.4\left[1.194\right]]^{0.65}}$$

$$= 0.720 < W_{RE} = 0.91$$

This indicates that the compressor is not stalled at the blade row and radius examined.

Appendix E

Sample input for SUCC code

This chapter contains the content for the input files for the NACA 5-stage compressor model. Details on interpreting the input file can be found in Thiart (2004).

```
NACA 5-stage AA0AT.def

! Naca 5-stage compressor
! - Deviation and primary loss model: Aungier
! - Secondary loss model: None
! - Cp: temperature-dependent
! - Boundary layers: default (Aungier)

! Compressor definition: annulus

FILE c:\andrewgill\fiddlewithsucc\Succ\Applications\
Naca5Stage\Naca5Stage_Annulus.txt

! Compressor definition: bleeds (no bleeds)

! Compressor definition: blade rows

BLADEROWS
! Stage 1
ROTOR 1 12605 23 AUNGIER AUNGIER CONSTANT 0.0LE Station05 DCA TABLE
FILE c:\andrewgill\fiddlewithsucc\Succ\Applications\
Naca5Stage\Naca5Stage_Rotor01.txt
STATOR 1 33 MIRROR AUNGIER AUNGIER CONSTANT 0.0 LE Station07 DCA TABLE
FILE c:\andrewgill\fiddlewithsucc\Succ\Applications\
Naca5Stage\Naca5Stage_Stator01.txt
! Stage 2
```

```
ROTOR 2 12605 27 AUNGIER AUNGIER CONSTANT 0.0 LE Station09 DCA TABLE
FILE c:\andrewgill\fiddlewithsucc\Succ\Applications\
Naca5Stage\Naca5Stage_Rotor02.txt
STATOR 2 39 MIRROR AUNGIER AUNGIER CONSTANT 0.0 LE Station11 DCA TABLE
FILE c:\andrewgill\fiddlewithsucc\Succ\Applications\
Naca5Stage\Naca5Stage_Stator02.txt
! Stage 3
ROTOR 3 12605 28 AUNGIER AUNGIER CONSTANT 0.0 LE Station13 DCA TABLE
FILE c:\andrewgill\fiddlewithsucc\Succ\Applications\
Naca5Stage\Naca5Stage_Rotor03.txt
STATOR 3 37 MIRROR AUNGIER AUNGIER CONSTANT 0.0 LE Station15 NACA65 TABLE
FILE c:\andrewgill\fiddlewithsucc\Succ\Applications\
Naca5Stage\Naca5Stage_Stator03.txt
! Stage 4
ROTOR 4 12605 25 AUNGIER AUNGIER CONSTANT 0.0 LE Station17 DCA TABLE
FILE c:\andrewgill\fiddlewithsucc\Succ\Applications\
Naca5Stage\Naca5Stage_Rotor04.txt
STATOR 4 36 MIRROR AUNGIER AUNGIER CONSTANT 0.0 LE Station19 NACA65 TABLE
FILE c:\andrewgill\fiddlewithsucc\Succ\Applications\
Naca5Stage\Naca5Stage_Stator04.txt
! Stage 5
ROTOR 5 12605 23 AUNGIER AUNGIER CONSTANT 0.0 LE Station21 DCA TABLE
FILE c:\andrewgill\fiddlewithsucc\Succ\Applications\
Naca5Stage\Naca5Stage_Rotor05.txt
STATOR 5 35 MIRROR AUNGIER AUNGIER CONSTANT 0.0 LE Station23 NACA65 TABLE
FILE c:\andrewgill\fiddlewithsucc\Succ\Applications\
Naca5Stage\Naca5Stage_Stator05.txt

! Operating conditions: stagnation pressure & temperature, and mass flow

CONSTANT 101325 288.16 30.617485

! Operating conditions: boundary layer thickness (optional)

BLB 0.001 0.001

! Thermodynamic properties

IDEALGAS 287.05
POLYNOMIAL 1.048763e3 -3.838892e-1 9.45603e-4 -5.486731e-7 7.907137e-11
DEFAULT

! Computational grid: quasi-streamlines
```

```
CONSTANT 3

! Computational grid: quasi-orthogonals (optional)

CONSTANT Station01 1
CONSTANT Station02 1
CONSTANT Station03 1
CONSTANT Station04 1
CONSTANT Station06 0
CONSTANT Station08 0
CONSTANT Station10 0
CONSTANT Station12 0
CONSTANT Station14 0
CONSTANT Station16 0
CONSTANT Station18 0
CONSTANT Station20 0
CONSTANT Station22 0
CONSTANT Station24 0
CONSTANT Station25 0
CONSTANT Station26 0
CONSTANT Station27 0
CONSTANT Station28 0
CONSTANT Station29 0

! Computational method: throughflow method

MTFM FV MSI 0.3

! Computational method: boundary layer blockage method (optional)

DEFAULT 0.05

! Compressor map

SPEED
LINE 80 70 90 0.5
LINE 90 80 100 0.5
LINE 100 98 108 0.5

! Initial conditions

STRATEGIC
```

```
FILE c:\andrewgill\fiddlewithsucc\Succ\Applications\Naca5Stage\Naca5Stage_ICs.txt

Naca5Stage_Rotor01.txt

0.0000  0.0655   8.90   0.00  Rotor101  58.4  0.080000
0.2000  0.0663  22.40   0.00  Rotor102  40.3  0.069834
0.6000  0.0678  40.20   0.00  Rotor103  19.9  0.056966
1.0000  0.0681  49.70   0.00  Rotor104  11.7  0.050000

Naca5Stage_Stator01.txt

0.0000  0.0514   5.50   0.00  Stator104   45.0  0.080000
0.4000  0.0514  11.20   0.00  Stator103   42.4  0.075870
0.8000  0.0514  16.80   0.00  Stator102   43.8  0.069573
1.0000  0.0514  19.80   0.00  Stator101   45.6  0.065000

Naca5Stage_Rotor02.txt

0.0000  0.0681  17.40   0.00  Rotor201  52.1  0.080000
0.2000  0.0683  26.30   0.00  Rotor202  40.0  0.061570
0.6000  0.0691  39.60   0.00  Rotor203  23.7  0.058560
1.0000  0.0693  48.00   0.00  Rotor204  14.8  0.050000

Naca5Stage_Stator02.txt

0.0000  0.0521  12.70   0.00  Stator204   47.3  0.080000
0.4000  0.0521  16.20   0.00  Stator203   47.7  0.075345
0.8000  0.0521  19.70   0.00  Stator202   50.1  0.069054
1.0000  0.0521  22.20   0.00  Stator201   50.4  0.065000

Naca5Stage_Rotor03.txt

0.0000  0.0726  27.90   0.00  Rotor301  42.4  0.080000
0.2014  0.0729  33.70   0.00  Rotor302  34.1  0.053888
0.6007  0.0732  43.20   0.00  Rotor303  21.7  0.060135
1.0000  0.0744  49.80   0.00  Rotor304  13.8  0.050000

Naca5Stage_Stator03.txt

0.0000  0.0519  11.90   0.00  Stator303   55.7  0.100000
0.4980  0.0519  16.20   0.00  Stator302   54.5  0.095724
1.0000  0.0519  20.70   0.00  Stator301   54.4  0.090000
```

Naca5Stage_Rotor04.txt

```
0.0000  0.0726  37.80   0.00  Rotor401  26.8  0.080000
0.1982  0.0726  41.10   0.00  Rotor402  23.1  0.052335
0.5991  0.0726  46.70   0.00  Rotor403  17.3  0.060271
1.0000  0.0726  51.10   0.00  Rotor404  13.0  0.050000
```

Naca5Stage_Stator04.txt

```
0.0000  0.0519  11.70   0.00  Stator403   54.4  0.100000
0.4975  0.0519  15.30   0.00  Stator402   53.1  0.095583
1.0000  0.0519  18.90   0.00  Stator401   52.7  0.090000
```

Naca5Stage_Rotor05.txt

```
0.0000  0.0688  42.30   0.00  Rotor501  22.4  0.080000
0.2011  0.0688  44.80   0.00  Rotor502  19.7  0.054051
0.5978  0.0688  49.00   0.00  Rotor503  15.4  0.060632
1.0000  0.0688  52.50   0.00  Rotor504  12.0  0.050000
```

Naca5Stage_Stator05.txt

```
0.0000  0.0517  10.80   0.00  Stator503   51.6  0.100000
0.4971  0.0517  13.90   0.00  Stator502   50.8  0.095508
1.0000  0.0517  17.20   0.00  Stator501   50.3  0.090000
```

Naca5Stage_Annulus.txt

```
Station01  0.113323  -0.254000   0.267600  -0.254000  12605   0
Station02   0.113323  -0.190500   0.267600  -0.190500
Station03   0.113323  -0.127000   0.267600  -0.127000
Station04   0.113323  -0.063500   0.267600  -0.063500
Station05   0.127000  0.000000  0.254000  0.009736
Station06   0.140677  0.063500  0.254000  0.0530
Station07   0.144780  0.082550  0.254000  0.082550
Station08   0.152908  0.131  0.254000  0.133
Station09   0.157480  0.161925  0.254000  0.170476
Station10   0.168226  0.225425  0.254000  0.216
Station11   0.171450  0.244475  0.254000  0.244475
Station12   0.179090  0.293  0.254000  0.295275
Station13   0.183388  0.323850  0.254000  0.331582
Station14   0.189445  0.386  0.254000  0.378
Station15   0.191262  0.406400  0.254000  0.406400
```

```
Station16   0.195326  0.455  0.254000  0.456
Station17   0.197612  0.485775  0.254000  0.489440
Station18   0.201613  0.540  0.254000  0.535
Station19   0.202946  0.561975  0.254000  0.561975
Station20   0.205710  0.611  0.254000  0.612
Station21   0.207264  0.641350  0.254000  0.645798
Station22   0.208927  0.691  0.254000  0.686
Station23   0.209550  0.711200  0.254000  0.711200
Station24   0.209550  0.760  0.254000  0.760
Station25   0.209550  0.790575  0.254000  0.790575
Station26   0.209550  0.819150  0.254000  0.819150
Station27   0.209550  0.849150  0.254000  0.849150
Station28   0.209550  0.879150  0.254000  0.879150
Station29   0.209550  0.899150  0.254000  0.899150
Station30   0.209550  0.919150  0.254000  0.919150
```

Naca5Stage_ICs.txt

```
Station02   101325  288.16  BLB 0.002 0.002
Station03   101325  288.16  BLB 0.003 0.003
Station04   101325  288.16  BLB 0.004 0.004
Station05   101325  288.16  BLB 0.005 0.005
Station06   101325  288.16  BLB 0.006 0.006
Station07   101325  288.16  BLB 0.007 0.007
Station08   101325  288.16  BLB 0.008 0.008
Station09   101325  288.16  BLB 0.009 0.009
Station10   101325  288.16  BLB 0.010 0.010
Station11   101325  288.16  BLB 0.011 0.011
Station12   101325  288.16  BLB 0.012 0.012
Station13   101325  288.16  BLB 0.013 0.013
Station14   101325  288.16  BLB 0.014 0.014
Station15   101325  288.16  BLB 0.015 0.015
Station16   101325  288.16  BLB 0.016 0.016
Station17   101325  288.16  BLB 0.017 0.017
Station18   101325  288.16  BLB 0.018 0.018
Station19   101325  288.16  BLB 0.019 0.019
Station20   101325  288.16  BLB 0.020 0.020
Station21   101325  288.16  BLB 0.021 0.021
Station22   101325  288.16  BLB 0.022 0.022
Station23   101325  288.16  BLB 0.023 0.023
Station24   101325  288.16  BLB 0.024 0.024
Station25   101325  288.16  BLB 0.025 0.025
Station26   101325  288.16  BLB 0.026 0.026
```

```
Station27   101325  288.16  BLB 0.027 0.027
Station28   101325  288.16  BLB 0.028 0.028
Station29   101325  288.16  BLB 0.029 0.029
Station30   101325  288.16  BLB 0.030 0.030
```